

ODOR-EVOKED MODULATION OF THE OLFACTORY
BULB BY PROJECTIONS FROM THE HORIZONTAL
LIMB OF THE DIAGONAL BAND OF BROCA

Dissertation zur Erlangung
des Doktorgrades (Dr. rer. nat.)
der Mathematisch-Naturwissenschaftlichen Fakultät
der Rheinischen Friedrich-Wilhelms-Universität Bonn

Vorgelegt von

Monika Müller

aus Duisburg, Deutschland

Bonn 2021

Angefertigt mit Genehmigung der Mathematisch-Naturwissenschaftlichen
Fakultät der Rheinischen Friedrich-Wilhelms Universität Bonn

1. Gutachter: Prof. Dr. Martin Fuhrmann
2. Gutachter: Prof. Dr. Walter Witke

Tag der Promotion: 21.05.21

Erscheinungsjahr: 2021

Guten Tag“, sagte der kleine Prinz.

„Guten Tag“, sagte der Händler.

Es war ein Händler, der durststillende Pillen verkaufte.

Man schluckt eine Pille pro Woche und hat kein Bedürfnis mehr zu trinken.

„Warum verkaufst du das?“, sagte der kleine Prinz.

„Das bringt eine große Zeitersparnis“, sagte der Händler.

„Experten haben dies berechnet. Man kann dreiundfünfzig Minuten pro Woche einsparen.“ „Und was macht man mit diesen dreiundfünfzig Minuten?“

„Man macht damit, was man will ...“

„Ich würde“, sagte der kleine Prinz,

„wenn ich mir dreiundfünfzig Minuten erspart hätte,

gemütlich zu einem Brunnen gehen ...“

- Der kleine Prinz -

(Antoine de Saint-Exupéry)

Danke, Mama

PREVIOUS PUBLICATION

Partial work of this dissertation has been published in:

Schwarz, I.*, **Müller, M.***, Pavlova, I., Schweihoff, J., Musacchio, F., Mittag, M., Fuhrmann, M.*, and Schwarz, M.K.* (2020).

The diagonal band of broca continually regulates olfactory-mediated behaviors by modulating odor-evoked responses within the olfactory bulb.

bioRxiv, doi: <https://doi.org/10.1101/2020.11.07.372649>.

*equal contribution of first and last authors

ACKNOWLEDGEMENT

First of all, I would like to thank my “*Doktorvater*” Prof. Dr. Martin Fuhrmann for giving me the opportunity to prepare my dissertation in his group at the DZNE. I am grateful for all the discussions and the independence he granted me during the last years.

My gratitude also extends to all other members of my committee for taking part in the final steps of my PhD work: Prof. Dr. Witke, Prof. Dr. Schoch-McGovern und Prof. Dr. Mass.

As continuous companion throughout my PhD work, I would like to thank my collaborators Dr. Martin K. Schwarz, Inna Schwarz, and especially the other half of this project Irina Kim (née Pavlova) for the great collaboration and all the encouraging discussions. Especially Irina made me feel less alone in our research field throughout the conduction of this project.

Furthermore, I would like to thank the animal research facility (ARF) and light microscopy facility (LMF) of the DZNE for all their support and patience during the last years.

My particular thanks goes to my colleagues in the AG Fuhrmann, which supported me in and outside of the lab. Especially, Julia Steffen and Andrea Baral supported me not only with their tireless work in the lab, but also by being the good souls of this group. The analysis of my data would not have been possible without Fabrizio Musacchio and Manuel Mittag. I would like to thank Steffi Poll for patiently reading this dissertation and always helping me with good advice and her irrefutable positive attitude. Also, Eleonora Ambrad and Sophie Crux supported me and this project with many -sometimes late- discussions and always helpful input. But above all, I am thankful for the friendships and care that members of my work group offered me during the last year. Especially, the adventures with Nora aka Kartoffelkind, Manu aka Manule, Sophie aka lemon girl and Felix aka lettuce boy will never be forgotten. The last years would have been a lot less fun without all of you!

Also, all the other friends I made during the journey of my PhD deserve my heartfelt thanks. I wish to thank Tomke, Gio, Telma, Steffi, Babbi, and Gigi for welcoming me in Bonn, lots of scientific and non-scientific discussions,

encouragement during hard times and more delicious meals than I can count. Nelli, Hana and Steffi I would like to thank for their support during the drafting of this dissertation, the fun during numerous hikes and many empty wine bottles.

And most of all I want to thank my whole family and friends at home. Without their constant support and encouragement, I would never have made it through the hard times. I am especially grateful for my parents, that always believed in me even when I stopped.

ZUSAMMENFASSUNG

Olfaktorische Information enthält essentielle Hinweise über die Umwelt und beeinflusst adaptierte verhaltensbiologische Reaktionen. Demzufolge ist das olfaktorische System sehr komplex und involviert verschiedene Hirnareale, welche die Informationen auf unterschiedlichen Ebenen verarbeiten. Der *bulbus olfactorius* (OB) bildet mit seinen zahlreichen Mikroschaltkreisen die erste Verarbeitungsstation olfaktorischer Informationen. Die efferenten Neurone des OB leiten die prozessierten Informationen an andere Hirnregionen weiter und prägen so das Verhalten des Organismus. Verschiedene Kerngebiete des Gehirns modulieren die Repräsentation der Geruchsinformation innerhalb des OB. Eines dieser Areale ist der horizontale Ast des diagonalen Bandes von Broca (HDB), dessen cholinerge, GABAerge sowie möglicherweise glutamaterge Projektionen in den OB reichen. Diese innervierenden Fasern modulieren spontane sowie sensorisch erregte Aktivität verschiedenster Neurone des OB und beeinflussen so die an andere Hirnareale weitergeleiteten Informationen. Mit dem Ziel neue Erkenntnisse über die Funktionsweise der Modulationen zu erlangen wurde die neuronale Aktivität dieser Projektionen aus dem HDB innerhalb des OB untersucht. Die Verwendung der *in vivo* Zwei-Photonen-Mikroskopie von Kalziumsensoren in wachen, kopffixierten Mäusen erlaubte die Erforschung axonaler Reaktionen auf die Applikation von Duftstoffen. Dadurch wurde die sensorisch erregte Aktivität in einem Großteil der Axone der HDB Neurone in der glomerulären Schicht untersucht. Diese Antworten sind geruchssensitiv und zeigen erhöhte oder unterdrückte Aktivitätsmuster. Die Analyse spezifisch mit dem Kalziumsensor GCaMP6s markierter cholinergischer und GABAerger Axone zeigte erhöhte Aktivitätsmuster in cholinergen und überwiegend verminderte Aktivitätsmuster in GABAergen Projektionen. Diese charakteristische Antwort auf olfaktorische Stimulation weist auf eine bimodale Modulation der sensorisch erregten Aktivität in efferenten Neuronen des OB hin. Die bimodale Modulation hebt die Repräsentation bestimmter Gerüche gegenüber anderen hervor. Somit, sind einige Gerüche besonders verstärkt, welches vermutlich die Differenzierung von Gerüchen steigert.

ABSTRACT

Olfactory input encodes essential information about the environment and shapes adapted behavioral reactions. Hence, the olfactory system is complex with diverse brain areas processing the sensory input on different levels. The olfactory bulb (OB), with its numerous microcircuits, is the first processing station of olfactory input. The OB output neurons transmit the processed information to other brain areas shaping the organism's behavior. Top-down modulations from a variety of brain regions regulate the representation of odor information in the OB. Among those is the horizontal limb of the diagonal band of Broca (HDB), which neurons send cholinergic, GABAergic and potentially glutamatergic projections into the OB. These innervations modulate the spontaneous and sensory-evoked activity of a variety of bulbar neurons and ultimately shape the output relayed to other brain areas. Monitoring the neuronal activity of these HDB projections within the OB aimed to gain further insight into the effect of the top-down modulations. The use of two-photon *in vivo* Ca²⁺-imaging in awake head-fixed mice enabled the investigation of axonal responses to odor stimulation. This approach revealed sensory-driven activity in a majority of HDB axons in the glomerular layer. These responses are odor-specific and exhibit enhanced as well as suppressed activity patterns. Monitoring cholinergic and GABAergic fibers labeled with the Ca²⁺-indicator GCaMP6s indicated enhanced response patterns in cholinergic and predominantly suppressed response patterns in GABAergic fibers. This characteristic presumably mediates a bimodal modulation of sensory-driven responses in bulbar output neurons emphasizing certain odors over others. Thus, the representation of some odors is accentuated, which might promote odor discrimination.

CONTENTS

Table of content

Table of content	1
List of figures	3
1. Introduction.....	1
1.1. Olfaction	1
1.2. Olfactory bulb	1
1.2.1. Structure and Microcircuits of the olfactory bulb	2
1.2.2. Centrifugal projections to the olfactory bulb	10
1.3. HDB	12
1.3.1. Anatomical aspects of the HDB	12
1.3.2. Connectivity and functional aspects of the HDB	13
1.3.3. Modulation of the olfactory system.....	15
1.4. Aim of the study.....	19
2. Methods.....	20
2.1. Transgenic mice	20
2.2. Stereotactic injection	20
2.3. Cranial window implantation.....	21
2.4. Two-Photon in vivo Ca ²⁺ -imaging.....	22
2.4.1. Two-Photon imaging principles	22
2.4.2. Ca ²⁺ -imaging principles	23
2.5. Two-Photon microscope.....	24
2.5.1. Two-Photon imaging, awake.....	25
2.5.2. Odor stimulation	25
2.6. Perfusion	26
2.7. Post-mortem tissue evaluation	26
2.7.1. Tissue sectioning	26
2.7.2. Confocal image acquisition	26
2.7.3. Quantification of GCaMP6s expression	27
2.8. Ca ²⁺ -imaging data analysis	27
2.8.1. ROI detection and fluorescence change extraction	27
2.8.2. Trace detection and time-lapse parameter extraction.....	28
2.9. Statistics	28

3. Results	29
3.1. Post-mortem analysis of GCaMP6s expression in brain sections....	29
3.2. Cell type-unspecific odor-tuned HDB axons in the OB.....	30
3.3. Cholinergic odor-tuned HDB axons in the OB.....	36
3.4. GABAergic odor-tuned HDB axons in the OB	39
3.5. Reduced glomerular activity upon HDB silencing with tetanus toxin	42
4. Discussion	45
4.1. GCaMP6s expression after stereotactic AAV-injection	49
4.2. Odor-evoked activity in HDB axons.....	50
4.3. Neuron type-specific innervation and differences in activity patterns	57
4.4. HDB mediated modulation of glomerular activity	62
4.5. Conclusion and future experiments.....	65
5. Appendix	68
5.1. Abbreviations.....	68
5.2. Material.....	71
5.2.1. Consumables for surgeries	71
5.2.2. Equipment for surgeries	71
5.2.3. Equipment for tissue sectioning	72
5.2.4. Equipment for in vivo imaging.....	72
5.2.5. Microscopes	72
5.2.6. Reagents.....	73
5.2.7. Anesthesia and medication	73
5.2.8. AAVs	73
5.2.9. Software	74
5.3. Contributions	75
6. References	76

List of figures

FIGURE 1.1. Structure and neurons in the OB..... 2

FIGURE 1.2. Connectivity in the GL. 3

FIGURE 1.3. Connectivity in the EPL. 5

FIGURE 1.4. Connectivity in the GCL..... 8

FIGURE 1.5: Anatomical location of the HDB, VDB, MS and OB..... 13

FIGURE 1.6. Cholinergic and GABAergic HDB projections of the OB. 15

FIGURE 3.1. GCaMP6s expression after stereotactic AAV-injection. 30

FIGURE 3.2. Experimental procedure of monitoring of Ca²⁺-levels in HDB axons. 31

FIGURE 3.3. Analytical procedure for data obtained during recording of Ca²⁺-levels in HDB
axons. 32

FIGURE 3.4. Cell type-unspecific odor-tuned projections from the HDB..... 35

FIGURE 3.5. Cholinergic odor-tuned projections from the HDB. 38

FIGURE 3.6. GABAergic odor-tuned projections from the HDB. 41

FIGURE 3.7. HDB silencing with tetanus toxin affects odor-evoked Ca²⁺-response in the OB.
..... 44

FIGURE 4.1. Hypothesized bimodal HDB modulation of M/T cell activity. 62

1. Introduction

1.1. Olfaction

As organisms living in a complex environment, we are dependent on distinguishing food sources and mates from potential threats and predators. Interpreting our surroundings is governed by processing of sensory information incorporated with our senses. We see, feel, hear, taste and smell the world around us. For a diverse array of animals, the sense of smell – or olfaction – provides crucial sensory input translated into adapted behavioral output.

Olfaction describes the detection and processing of odor information in the central nervous system. Odor molecules excreted from objects and organisms reach the nasal epithelium in the nasal cavity. Here, the odorant activates olfactory receptors located on dendrites of sensory olfactory receptor neurons (ORN). The action potential travels along the axons of ORNs, which constitute the olfactory nerve (Cranial nerve I), and is transmitted to neurons in the olfactory bulb (OB). In the OB odor information is processed and converged with top-down modulation before being relayed to higher brain regions as the olfactory cortex. The olfactory cortex includes the Piriform cortex (PC), anterior olfactory nucleus (AON), the olfactory tubercle (OT), the cortical nucleus of the amygdala (CoA) and the entorhinal cortex (EC). These brain regions further process the stimulus and shape the behavioral output in accordance to the received odor information (for review see (Li et al., 2019)).

1.2. Olfactory bulb

Information received by ORNs are relayed to the OB, the first odor processing station in the brain. Here, the sensory neurons synapse on Mitral- and Tufted cells (M/T cells) – the principal neurons in the OB. The dendrites of M/T cells intermingled with ORN axons form circular structures termed glomeruli. These are densely packed on the surface of each OB hemisphere. Each glomerulus receives input from up to 5000 receptor neurons, all expressing the same odorant specific receptor. ORNs with the same receptor all converge in one or two glomeruli within the OB (Mombaerts et al., 1996). This anatomical characteristic causes each glomerulus to be activated in an odor-specific

manner. The activated glomeruli represent a specific spatial pattern, so-called odor maps, consistent across individuals as was shown by electrical recordings (Clark, 1951; Levetau and MacLeod, 1966) and tracing studies (Astic and Saucier, 1986) early on. Intrinsic imaging techniques (Rubin and Katz, 1999) as well as the use of voltage- and calcium-sensitive dyes confirmed this odotopic representation in several species as the salamander (Kauer, 1991; Wachowiak and Cohen, 2001) and the mouse (Fried et al., 2002; Wachowiak and Cohen, 2001). These imaging techniques furthermore revealed that structurally similar odor molecules often activate glomeruli in the same spatial region. Moreover, glomerular activity is concentration-dependent, with complex spatial representation of different odor concentrations (Rubin and Katz, 1999). However, regulation of glomerular activity is ensured not only by the sensory input but also by a complex system of bulbar interneurons. These interneurons are organized in microcircuits, which shape the activity of M/T cells, the OB output neurons.

1.2.1. Structure and Microcircuits of the olfactory bulb

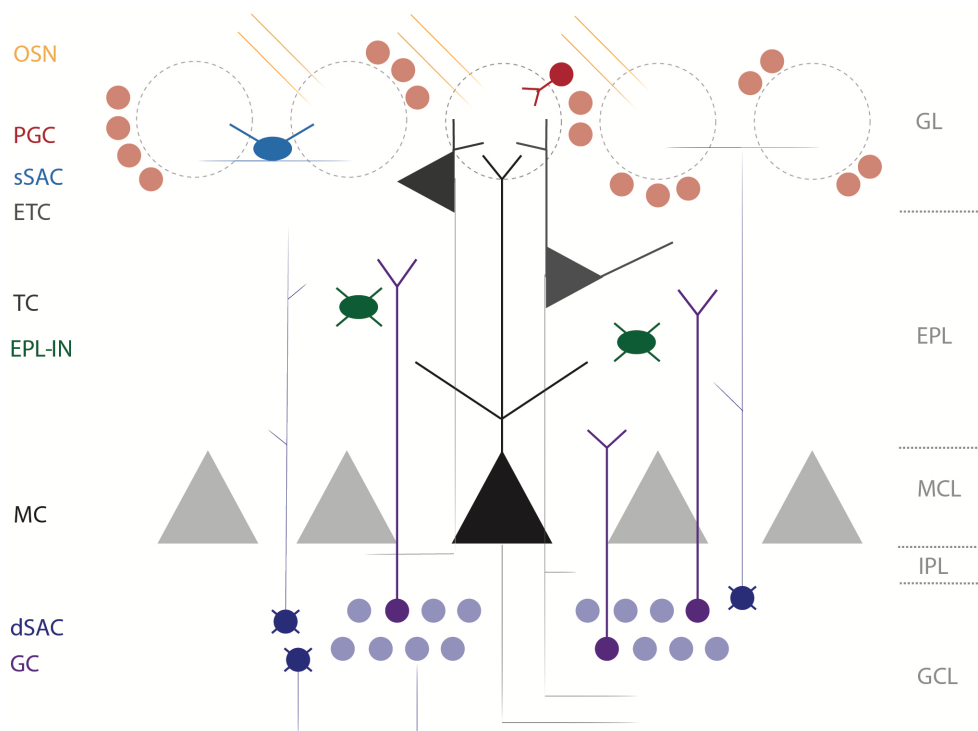


FIGURE 1.1. Structure and neurons in the OB. Schematic illustration of the laminar structures and cell types in the OB. Olfactory sensory neurons (OSN); periglomerular cells (PGC); superficial short-axon cells (sSAC); external tufted cells (ETC); tufted cells (TC); external plexiform layer interneurons (EPL-IN); mitral cells (MC); deep short-axon cells (dSAC); granule cells (GC); glomerular layer (GL); external plexiform layer (EPL); mitral cell layer (MCL), the internal plexiform layer (IPL) and the granule cell layer (GCL). Modified from (Burton, 2017).

The bulbar interneurons and thus microcircuits are structured in anatomical layers of the OB (FIG. 1.1). The OB is a highly organized laminar structure with five layers from outside to inside: the glomerular layer, the external plexiform layer, the mitral cell layer, the internal plexiform layer and the granule cell layer. These layers built an irregular spherical structure in the most anterior part of the rodent brain.

Odor information is received in the **glomerular layer (GL)** and transmitted to M/T cells, the OB output neurons (FIG. 1.2). The GL is shaped by densely packed glomeruli formed from M/T cell dendrites and ORN axons. In the interglomerular space reside interneurons reaching into the glomeruli and modulating M/T cell activity. Interneurons in the GL can be classified in three groups: periglomerular cells (PGC), superficial short-axon cells (sSAC) and external tufted cells (ETC), often summarized as juxtglomerular cells (JGC).

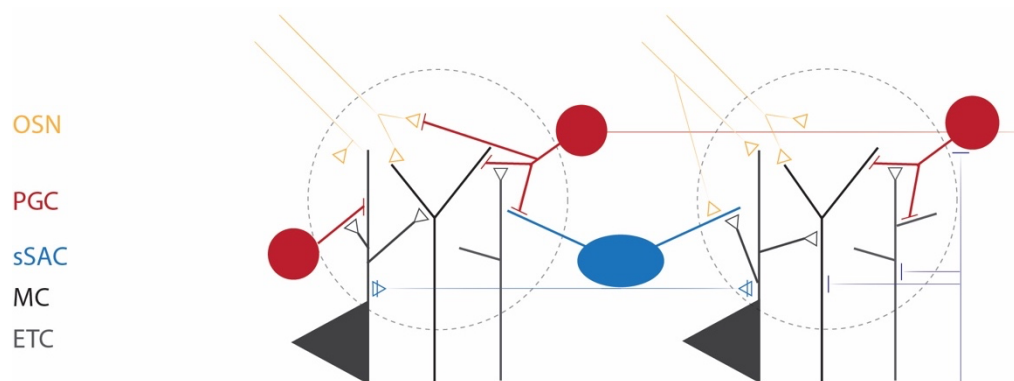


FIGURE 1.2. Connectivity in the GL. Schematic illustration of the microcircuit in the glomerular layer in the OB. Olfactory sensory neurons (OSN); periglomerular cells (PGC); superficial short-axon cells (sSAC); external tufted cells (ETC); mitral cells (MC); open triangles illustrate excitatory synapses, lines illustrate inhibitory synapses, triangles with lines illustrate co-release of GABA and dopamine. Modified from (Burton, 2017).

ETCs have the largest soma among JGCs (Pinching and Powell, 1971a). Their extensive dendritic arborization ramifies through a single, or in few cases throughout two different glomeruli. Here, the excitatory ETCs receive direct sensory driven input from OSN (Hayar et al., 2004). Sensory information is received with a higher sensitivity to weak OSN input compared to mitral cells (MC) and forwarded to the principal neurons (De Saint Jan et al., 2009). Activation of a single ETC induces responses in all MCs connected to the corresponding glomerulus (De Saint Jan et al., 2009). It is hypothesized that this forward excitation is the regular path of sensory-evoked activity in MCs,

which are often not responding directly to OSN input (Gire et al., 2012). ETCs form dendro-dendritic synapses with PGCs and sSACs and provide excitatory input to these inhibitory interneurons (Hayar et al., 2004). Certain ETCs with cell bodies located in the deep GL or even superficial EPL, send secondary (basal) dendrites into the EPL. This group of ETCs extends axons across one bulbar hemisphere or even into the AON pars externa (AONpe). Somata and axons of ETCs not bearing secondary dendrites are exclusively found within the GL (Macrides et al., 1982; Schoenfeld et al., 1985).

PGCs are GABAergic interneurons forming dendro-dendritic synapses with M/T cells and ETCs within a restricted part of a single glomerulus (Pinching and Powell, 1971a; Ribak et al., 1977). Axons of this neuron class span the length of up to six glomeruli and terminate in the interglomerular space (Pinching and Powell, 1971a). Approximately two-thirds of PGCs receive excitatory input from ETCs after sensory-evoked stimulation (Najac et al., 2011). Another PGC fraction receives direct sensory information from OSN (Hayar et al., 2005). Activation of PGCs inhibits M/T cell and ETC responses to OSN input (Aungst et al., 2003; Hayar et al., 2005). This microcircuit provides feedforward inhibition towards M/T cells within one glomerulus regulating OSN stimulation driven activity of the OB output neurons (Najac et al., 2011). Furthermore, PGC provide feedback inhibition mediated by presynaptic GABA_B receptors on the axon terminals of OSN (Bonino et al., 1999; Keller et al., 1998; Nickell et al., 1994). Thus, periglomerular cells play an important role in shaping sensory-evoked activity in GL microcircuits.

The dendritic ramifications of GABAergic sSACs are rather small and extend into few glomeruli (Pinching and Powell, 1971a, b). The axonal projections of sSACs are extensive and reach 5-12 glomeruli or in some cases even interconnect up to hundreds of very distant (up to 1 mm) glomeruli (Aungst et al., 2003; Kiyokage et al., 2010). The group of sSACs bearing very long axons is immunoreactive for not solely GABAergic but also dopaminergic (DA) markers (Kiyokage et al., 2010; Kosaka et al., 1985). These sSACs co-release GABA and dopamine onto ETCs causing GABA_A receptor-mediated inhibitory response followed by DA-D₁-like receptor-mediated excitatory response in ETCs. Thus, sSACs first mediate inhibition followed by excitation of ETCs through activation of GABAergic and DAergic receptors (Liu et al., 2013).

Furthermore, sSACs mediate weak excitation of ETCs and strong excitation of M/T cells via gap junctions electrically connecting these neurons (Banerjee et al., 2015; Liu et al., 2016). Most DAergic sSACs receive excitatory odor-evoked input from ETCs, while others are directly innervated by OSN (Banerjee et al., 2015; Hayar et al., 2004; Kiyokage et al., 2010). The first subgroup of sSACs shows concentration-dependent responses upon odor stimulation innervating ETCs, which leads to a suppression of M/T cell odor responses (Banerjee et al., 2015). To summarize, PGCs and sSACs provide inhibitory innervation of ETCs within GL microcircuits and consequently reduce sensory-evoked activity in M/T cells (FIG. 1.2). Here, PGCs provide lateral inhibition restricted to one glomerulus whereas sSACs facilitate interglomerular connectivity.

The information processed in the glomerular microcircuits propagates inwards through the **external plexiform layer (EPL)** to tufted cell somata and further to mitral cell somata in the MCL (FIG. 1.3).

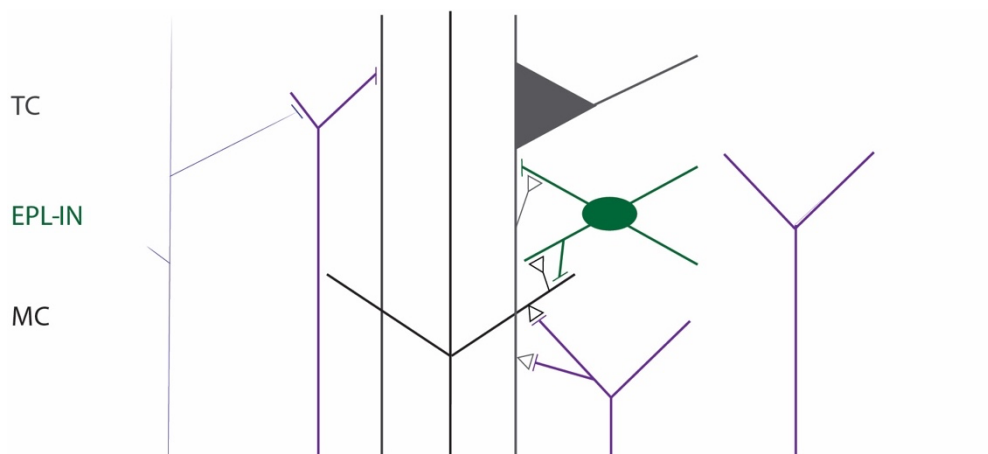


FIGURE 1.3. Connectivity in the EPL. Schematic illustration of the microcircuits in the external plexiform layer in the OB. Tufted cells (TC); external plexiform layer interneurons (EPL-IN); mitral cells (MC); open triangles illustrate excitatory synapses; lines illustrate inhibitory synapses. Modified from (Burton, 2017).

The EPL is composed of secondary dendritic fibers of M/T cells, apical dendrites of granule cells and cell bodies of glutamatergic tufted cell (TC). TC somata are located in the superficial EPL and extend their dendrites laterally within the superficial EPL and into the GL. In contrast, mitral cells stretch secondary dendrites into the deep EPL (Mori et al., 1983). The EPL also comprises a diverse set of GABAergic interneurons, which constitute the predominant cell type in this layer. The interneurons found in the EPL are

classified as Van Gehuchten, inner multipolar, inner horizontal and intermediate short-axon (iSAC) cells (Kosaka et al., 1994; Schneider and Macrides, 1978). These cells are all axonless except for iSACs, which extend their axons within the EPL (Kosaka and Kosaka, 2008). EPL interneurons express a variety of calcium-binding proteins like parvalbumin (PV) (Kosaka et al., 1994), vasoactive intestinal peptide (VIP) (Crespo et al., 2002), calbindin (CB) (Brinon et al., 1992; Kosaka and Kosaka, 2010), Calretinin (CR) (Jacobowitz and Winsky, 1991) as well as the peptide hormone somatostatin (SST) (Lepousez et al., 2010), and the corticotropin-releasing hormone (CRH) (Huang et al., 2013). PV-positive SST-positive as well as CRH-expressing EPL interneurons reciprocally interact with numerous M/T cells providing lateral inhibition and interconnecting cells of different glomeruli (Huang et al., 2013; Lepousez et al., 2010; Toida et al., 1994). Following OSN stimulation, EPL interneurons display activity, probably caused by M/T cell excitation (Hamilton et al., 2005; Huang et al., 2013). Though insufficiently investigated, the interaction between EPL interneurons and principal cells suggests the involvement of a variety of EPL interneurons in an inhibitory circuit modulating odor processing in the EPL (Kato et al., 2013).

The **mitral cell layer (MCL)**, which is located medial to the EPL, contains densely packed mitral cell (MC) and granule cell (GC) somata. The glutamatergic MCs together with TCs are frequently combined and named as M/T cells. These two groups are the principal neurons of the OB and transmit output to other brain regions. M/T cells receive input via excitatory synapses from OSN within the glomeruli and thus, are second order odor processing neurons. M/T cell primary dendrites reach into the GL and arborize in a single glomerulus (Mori et al., 1983). One glomerulus on the other hand connects to various M/T cells. Those M/T cells terminating in a common glomerulus are electrically coupled through gap junctions, which supports synchronization of their firing activity (Christie et al., 2005; Schoppa and Westbrook, 2002). However, MCs and TCs have distinct anatomical and functional characteristics. Anatomically, they are discriminated by their dendritic morphology and soma location: MC somata are densely packed in the MCL, whereas the smaller TC somata are sparsely dispersed in the superficial EPL. MCs extend secondary

dendrites into deeper parts of the EPL compared to TCs, which reach secondary dendrites into the superficial part of EPL (Mori et al., 1983; Orona et al., 1984). MCs and TCs can also be separated functionally. TCs show higher excitability and peak firing rates compared to MCs as well as faster responses to stimulation with a wide range of odor concentrations, whereas MCs have a larger latency in response across odor concentrations. Additionally, TCs are more sensitive to lower odor concentrations compared to MCs, which only respond to high odor concentrations (Burton and Urban, 2014; Igarashi et al., 2012). Furthermore, responsiveness across different odors separates the neuron classes, with TCs being more broadly tuned to various odors. Neighboring MCs often respond to the same set of odors (Kikuta et al., 2013). The activity of both cell types is locked to the sniffing cycle, but with a phase shift to opposing phases of the respiratory cycle. MC activity is delayed in regard to the sniff cycle, which probably is caused by lateral inhibition within the OB (Fukunaga et al., 2012; Igarashi et al., 2012). These facts indicate a dependency of MC activity on lateral inhibition from interneurons in the microcircuits in different OB layers (Kikuta et al., 2013).

After processing in the OB, M/T cells forward the odor information to olfactory cortical areas passing the lateral olfactory tract (LOT). MCs innervate the anterior (APC) as well as posterior part of the piriform cortex (PPC), lateral entorhinal cortex (LEC), lateral olfactory tract (LOT), olfactory tubercle (OT), tenia tecta (TT), anterior (aCoA) and posterolateral (pCoA) cortical amygdala, dorsal anterior olfactory nucleus (dAON) and nucleus of the lateral olfactory tract (NLOT). TCs project to the AON pars externa, posteroventral AON, cap part of the olfactory tubercle and the APC (Haberly and Price, 1977; Igarashi et al., 2012; Nagayama et al., 2010). Summarizing, MC and TC projections appear to build two distinct pathways relaying odor information to the olfactory cortex. TCs potentially are involved in fast odor responses and olfactory behavior, whereas MCs in slower odor responses probably distinguishing complex odor input after processing of the odor information in OB circuits (Fukunaga et al., 2012; Igarashi et al., 2012).

The **internal plexiform layer (IPL)** contains axonal projections from M/T cells and granule cell (GC) dendrites. These dendrites also extend into the MCL and originate from GC somata in the GCL.

The **granule cell layer (GCL)** is the deepest OB layer in the middle of the dorsoventral axis of the circular OB and comprises densely packed GABAergic GCs (FIG. 1.4). Another population of this most abundant type of interneurons in the OB resides in the MCL and outnumbers even MCs within the MCL (Parrish-Aungst et al., 2007).

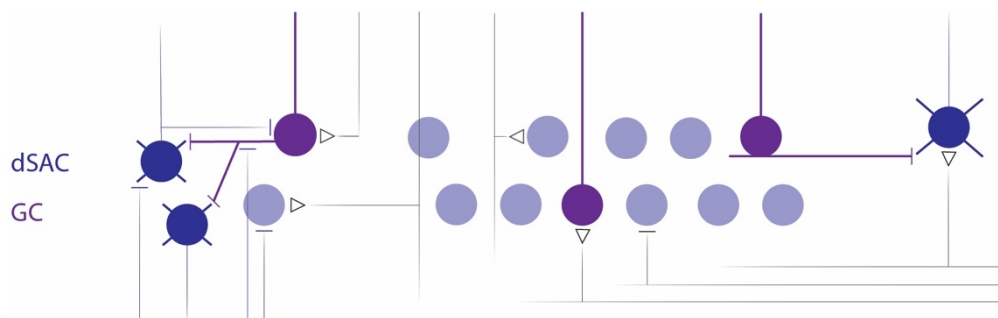


FIGURE 1.4. Connectivity in the GCL. Schematic illustration of the microcircuits in the granule cell layer in the OB. Deep short-axon cells (dSAC); granule cells (GC); open triangles illustrate excitatory synapses; lines illustrate inhibitory synapses. Modified from (Burton, 2017).

The axonless GCs sparsely branch basal dendrites into the GCL (Price and Powell, 1970d). Their apical dendrites extend extensively into the EPL, where they form dendro-dendritic synapses with M/T cells. GC dendritic spines contact M/T cell dendrites forming reciprocal chemical synapses providing feedback inhibition to the principal neurons. Each GC innervates several M/T cells mediated through dendro-dendritic synapses. (Price and Powell, 1970d; Rall et al., 1966). Sensory-evoked excitation of dendro-dendritic GC-M/T cell synapses leads to glutamate release from M/T cell dendrites activating GCs mediated through NMDA and AMPA receptors located on GCs spines. Consequent GABA-release from GCs at the reciprocal dendro-dendritic synapses mediates lateral inhibition of M/T cells (Balu et al., 2007; Isaacson and Strowbridge, 1998; Schoppa et al., 1998). This reciprocal chemical interaction of M/T cells and GCs furthermore drives network synchrony in the OB (Schoppa, 2006). Additional input to GCs is provided by axodendritic synapses in the IPL and GCL originating from ET cells and M/T respectively (Orona et al., 1984). Centrifugal fibers from other brain regions provide further

innervation of GCs (Price and Powell, 1970b). Proximal excitatory input to GC from afferent cortical fibers show fast kinetics and are mediated by NMDA and AMPA receptors (Balu et al., 2007). Inhibitory input to GCs is provided by deep short-axon cells (dSAC) (Price and Powell, 1970e) and centrifugal GABAergic projections from the basal forebrain (BF) (Gracia-Llanes et al., 2010). *In vivo* odor stimulation elicits action potentials in GCs, upon strong odor-evoked excitatory input (Cang and Isaacson, 2003). Incorporating diverse inputs GCs facilitate interglomerular lateral inhibition via M/T cell lateral dendrites.

The second class of GABAergic interneurons in the GCL is named dSACs. These cells show different forms of dendritic morphologies within the GCL and extensive axonal arborization towards various layers of the OB (Eyre et al., 2008; Price and Powell, 1970e; Schneider and Macrides, 1978). Recent literature classifies dSACs according to the area of axon termination (Eyre et al., 2008). The first class of dSACs reaches into the GL (GL-dSACs) innervating PGCs and thus disinhibiting M/T cells. Few axonal branches of these cells are also located in the EPL. The second class of dSACs extends axonal projections primarily to the EPL (EPL-dSACs) innervating dendritic shafts and spines of GCs. Only few axon branches extend into the IPL and superficial GCL. The third class of dSAC axons ramify within the GCL (GCL-dSACs) synapsing on proximal dendrites and somata of GCs. Interestingly, these cells also project axons to cortical regions forming a new output route from the OB. All types of dSACs receive inhibitory input from GABAergic GCs or other SACs (Eyre et al., 2008). Further input originates in M/T cells and electrical stimulation of glomeruli leads to activation of dSACS resulting in feedforward inhibition onto GCs (Burton and Urban, 2015). The class of GL-dSACs additionally directly inhibits apical dendrites of ETCs, TCs, and PGCs across multiple glomeruli (Burton et al., 2017). Thus, GL-dSACs interconnect multiple glomeruli and modulate segregated glomerular microcircuits. Moreover, the inhibitory interneurons receive centrifugal input and are the favored target of fibers originating in the cortex (Boyd et al., 2012). Especially cholinergic centrifugal fibers connect to GL-dSACs (Burton et al., 2017). This makes these neurons essential distributors of cortical modulation within the olfactory bulb. The olfactory cortex is one of the main centrifugal areas providing regulation of sensory-evoked activity within the OB (Shiple and Adamek, 1984).

1.2.2. Centrifugal projections to the olfactory bulb

The **olfactory cortex**, especially the APC and AON, provides centrifugal input to the OB. Pyramidal neurons in the APC directly innervate GCs and PGCs in the ipsilateral OB and drive feedforward inhibition onto M/T cells. However, the primary target for APC feedback projections are superficial and deep SACs in the ipsilateral GL and GCL inhibiting PGCs and GCs respectively. This leads to subsequent disinhibition of M/T cells and ETCs (Boyd et al., 2012). The APC is a target of bulbar output and receives olfactory input from MCs. Odor-evoked activation of principal cells in the APC reflects odor identity in the ensemble of activated neurons in a concentration-independent manner (Roland et al., 2017). Axonal boutons of APC neurons in the GCL showed odor-evoked responses in awake head-fixed mice. These responses fell into two categories: enhanced and suppressed boutons. Moreover, the sensory-evoked responses often outlasted odor stimulation. Muscimol-induced silencing of APC input to the OB resulted in increased odor-evoked amplitudes and number of odor-responding MCs supplemented by a loss of odor selectivity. In comparison, TCs were only mildly affected. Summarizing, this observation suggests that the APC modulates TC activity to a lower extent than MC activity and plays a role in separating the two OB output channels (Otazu et al., 2015). The AON, similar to the APC, innervates PGCs and GCs in the ipsilateral and to a lesser extent in the contralateral OB. Additionally, AON principal neurons directly activate MCs and ETCs (Markopoulos et al., 2012). *In vivo* activation of both the APC and AON results in suppression of odor-evoked M/T cell firing rates caused by GC mediated feedforward inhibition (Boyd et al., 2012; Markopoulos et al., 2012; Oswald and Urban, 2012). The two cortical regions attenuate odor responses in M/T cells via feedforward inhibition presumably promoting odor separation and discrimination. Furthermore, neurons in the anterior olfactory nucleus pars externa (AONpE) show excitatory responses to odors detected with the ipsilateral nostril and inhibitory response to contralaterally located odors. This enables the rodent AONpE to distinguish the position of an odor source relative to the nose by comparing input information from the two nostrils (Kikuta et al., 2010).

The OB also receives **neuromodulatory input** from noradrenergic, serotonergic and cholinergic neurons. Noradrenergic (NE) projections originate in the locus coeruleus (LC), a nucleus in the brainstem involved in arousal, attention and stress. NE modulates the detection and discrimination of odorants in subthreshold concentrations (Escanilla et al., 2010). NE axons preferentially terminate in the GCL, EPL and IPL, less frequently in the MCL and rarely in the GL (McLean et al., 1989). Electrical LC stimulation results in the suppression of M/T cell spontaneous activity and an overall increase in signal-to-noise ratio in M/T cells (Manella et al., 2017). Additionally, increased NE level in the OB reduces inhibitory output from GCs causing disinhibition in M/T cells, which in turn enhances gamma oscillation in the principal cells (Pandipati et al., 2010). Furthermore, NE β -receptor activation increases ET excitability and strengthens rhythmic bursting (Zhou et al., 2016). These modulatory effects are probably the basis for the involvement of NE in olfactory learning (Pandipati et al., 2010).

Serotonergic projections to the OB start in the raphe nuclei (de Olmos et al., 1978), which are involved in regulation of emotion, anxiety, sleep-wake cycle, reward and other aspects. The serotonergic afferents terminate predominantly in the GL, but also the EPL, IPL, and GCL (de Olmos et al., 1978). In the OB serotonin (5-HT) excites ETCs through activation of 5-HT_{2A} receptors and increases ETC bursting activity (Liu et al., 2012). Consequently, MCs, SACs, and PGCs are activated by feedforward excitation through ETCs. Direct serotonergic innervation of sSACs drives GABA release resulting in increased inhibition of PGCs (Brill et al., 2016). These serotonergic modulations of glomerular circuits give rise to 5-HT_{2A} receptor mediated excitation in MCs (Huang et al., 2017). *In vivo* optogenetic stimulation of the raphe nuclei potentiated odor-evoked responses in PGCs and sSACs (Brunert et al., 2016). TC odor responses are increased and odor-evoked MC activity bidirectionally modulated enhancing odor discrimination. This dissimilar effect in TCs and MCs is probably caused by the different innervation of inhibitory interneurons onto the two cell types (Kapoor et al., 2016). Serotonin afferents not only modulate odor processing within the OB, but also directly at the OSN. The serotonergic 5-HT_{2C} receptor weakens glutamatergic OSN transmission and

odor-evoked responses in glomeruli. Interestingly, lower responses were less sensitive to raphe modulation (Petzold et al., 2009).

Cholinergic centrifugal fibers to the OB primarily originate in the ipsilateral horizontal limb of the diagonal band of Broca (HDB) (Price and Powell, 1970c). This acetylcholine (ACh) transmitting nucleus in the basal forebrain is associated with the sleep-wake-cycle, attention, learning, and memory. Manipulating ACh levels within the OB or neuronal activity in the HDB affects cellular activity in the OB as well as odor-driven behavior (Bendahmane et al., 2016; Chaudhury et al., 2009; Liu et al., 2015; Ma and Luo, 2012; Mandairon et al., 2006; Nunez-Parra et al., 2013; Rothermel et al., 2014; Smith et al., 2015). The complex influence of cholinergic HDB afferents on cellular activity and microcircuits in the olfactory bulb will be discussed in more detail below.

1.3. HDB

Many studies do not distinguish between HDB and the magnocellular preoptic nucleus (MCPO). Thus, these two regions will be regarded as one coherent region termed HDB below.

1.3.1. Anatomical aspects of the HDB

The diagonal band of Broca (DBB) is a basal forebrain structure prolonging the medial septum towards anterior and ventral and extending posterior and dorsal towards the amygdala. The anterior medial part is defined as the vertical limb of the diagonal band of Broca (VDB) and sometimes regarded as a single functional structure with the medial septum (MSDB). The bilateral horns extending posterior and dorsal from the VDB are defined as the horizontal limb of the diagonal band of Broca (HDB) (FIG. 1.5). The HDB is comprised of cholinergic, GABAergic (Záborszky et al., 1986), and glutamatergic neurons (Manns et al., 2001). Cholinergic neurons are located in the medial part of the anterior HDB as well as in the dorsal part of the posterior HDB. GABAergic neurons are located in the lateral posterior and ventral parts of the HDB (Brashear et al., 1986; Kiss et al., 1990). The amount of OB projecting GABAergic neurons exceeds cholinergic neurons (Záborszky et al., 1986).

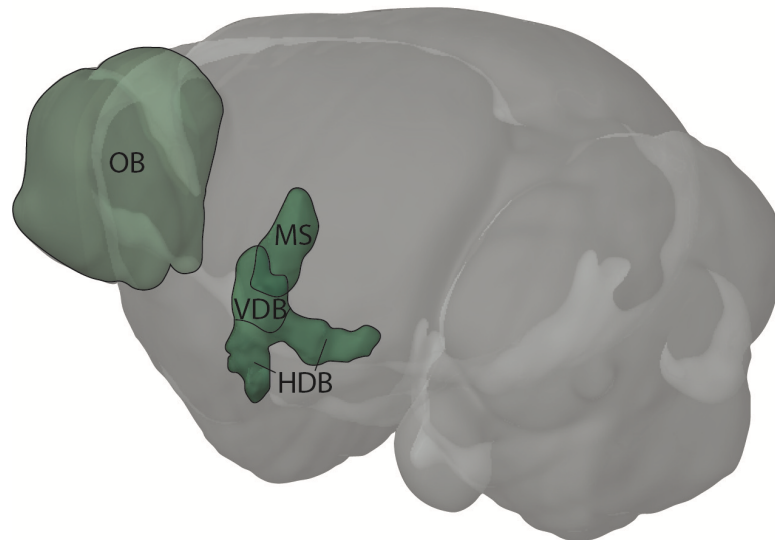


FIGURE 1.5: Anatomical location of the HDB, VDB, MS and OB. Scheme depicting the anatomical shape and location of the horizontal (HDB) and vertical (VDB) limb of the diagonal band of Broca, the medial septum (MS) and the olfactory bulb (OB) within the mouse brain. (Modified from Brain Explorer®)

Besides GABA and ACh, HDB neurons also produce the neurotransmitter glutamate. This synthesis either occurs in a separate solely glutamatergic cell population or accessorially in the GABAergic and cholinergic cells (Manns et al., 2001). Furthermore, HDB neurons express calcium binding proteins like PV, CB, and CR. The majority of PV-positive neurons are GABAergic, whereas CB and CR are found in all principal cell populations (Gritti et al., 2003). Cholinergic neurons in the HDB possibly innervate GABAergic and glutamatergic cells within the nucleus. Cortically projecting GABAergic PV-positive HDB neurons are excited by the ACh receptor agonist carbachol. This effect can be blocked by M_1 and M_2 ACh receptor antagonists (Yang et al., 2014). Also, glutamatergic HDB neurons show excitatory responses after application of carbachol (Yang et al., 2017). This hints towards modulation of GABAergic and glutamatergic HDB neurons through cholinergic HDB or possibly brainstem neurons (Yang et al., 2017; Yang et al., 2014).

1.3.2. Connectivity and functional aspects of the HDB

The HDB is connected to a wide range of brain regions and involved in a plethora of functions of the nervous system. The most prominent afferent connections to the HDB are derived from the ipsilateral hypothalamus and midbrain as well as the contralateral HDB (Price and Powell, 1970a). In recent years, further input and output regions to the HDB were revealed. Modern

rabies virus based monosynaptic tracing techniques exposed different connection modes for the diverse cell populations in the HDB: glutamatergic and SST-positive neurons tend to build reciprocal connections, whereas cholinergic and PV-positive neurons form unidirectional connections (Do et al., 2016). This study also confirmed the nucleus accumbens, lateral hypothalamus and central nucleus of the amygdala as the strongest amongst many input regions for the HDB. Interestingly, the hypothalamus innervates primarily glutamatergic neurons, whereas PV-positive neurons are the predominant recipients of innervations deriving in the nucleus accumbens. The regions receiving the highest percentages of efferents compared to the overall HDB output innervations are the hypothalamus, pallidum, and striatum (Do et al., 2016). Strikingly, the diverse HDB cell populations innervate heterogeneous regions. Cholinergic neurons project predominantly to cortical areas like the piriform cortex, basolateral amygdala, hippocampus and visual cortex. In contrast, glutamatergic, PV-positive and SST-positive HDB neuron populations are, primarily connect to the pallidum, striatum and hypothalamus (Do et al., 2016). The extensive connections of the HDB demonstrate the involvement of this region in various brain functions. For example, neurons in the HDB are activated by baroreceptors and depress blood pressure and heart rate via GABAergic inhibition of vasopressin-secreting neurons in the supraoptic nucleus (Jhamandas and Renaud, 1986a; Jhamandas and Renaud, 1986b; Kirouac and Ciriello, 1997). Also, the involvement of ACh in sleep-wake-cycles is well established. Lee and colleagues could show that cholinergic BF neurons activate cortical regions in bursts during active waking and light sleep phases; the burst firing is thereby synchronized with theta oscillations. The same neurons become silent during slow-wave sleep states. This rhythmic activation of BF neurons probably modulates activation modes in the cortex during the sleep-wake-cycle (Lee et al., 2005). Glutamatergic, cholinergic, and PV-positive HDB neurons are active during wakefulness and light sleep, whereas SST-positive neurons are active during deeper sleep phases. The optogenetic activation of these cell populations induced wakefulness or deep sleep phases, respectively (Xu et al., 2015). The PV positive neurons in the BF are also involved in generating cortical gamma oscillations, which are present during wakeful states (Kim et al., 2015).

The HDB also is involved in the olfactory processing system. Cholinergic and GABAergic neurons of the HDB innervate different layers of the OB and modulate neuronal activity in this area (Niedworok et al., 2012; Price and Powell, 1970c; Záborszky et al., 1986). Furthermore, some HDB neurons show increased firing rates during periods of active odor investigation (Devore et al., 2016). When investigating shorter periods of active sniffing of the odor, Devore and colleagues found that firing rates of 27 % of HDB neurons were modulated. These neurons displayed increased (75 % of modulated HDB neurons) as well as decreased (25 % of modulated HDB neurons) firing rates during phases of active sniffing. This suggests that HDB neurons are odor-responsive and modulate neuronal activity in the OB during the processing of olfactory information.

1.3.3. Modulation of the olfactory system

Acetylcholine (ACh) is a neuromodulator in the central nervous system, which is involved in numerous neuronal circuits in the brain. In the OB cholinergic input is thought to sharpen odor discrimination and detecting weak odors (Ma and Luo, 2012).

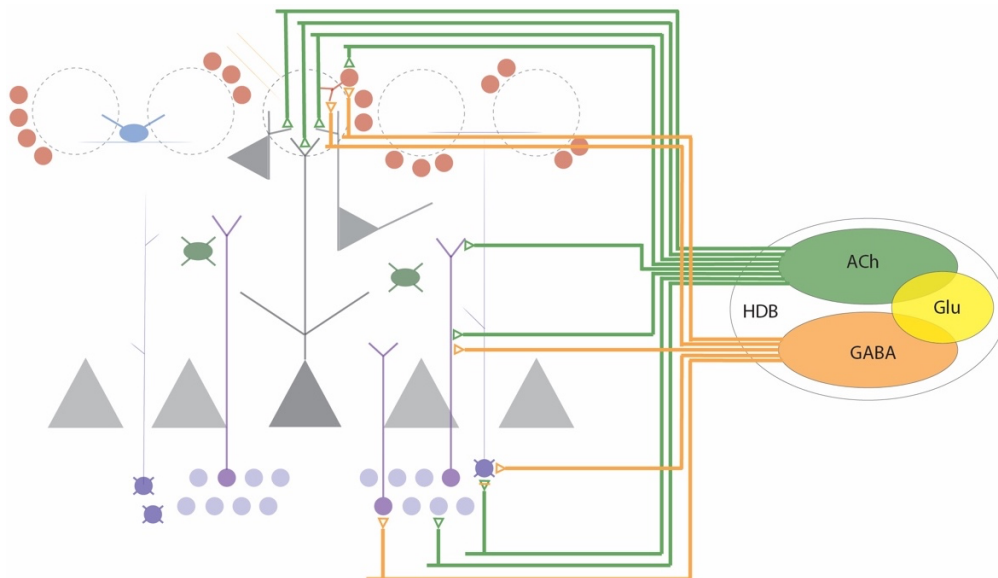


FIGURE 1.6. Cholinergic and GABAergic HDB projections of the OB. Schematic illustration of OB cells innervated by cholinergic and GABAergic fibers from the horizontal limb of the diagonal band of Broca (HDB). Acetylcholine (ACh), Glutamate (Glu), *gamma*-Aminobutyric acid (GABA).

Cholinergic HDB afferents synapse on dendrites of PGCs and GCs in the GL, IPL, and GCL and SACs in the EPL (Kasa et al., 1995) (FIG. 1.6). The effect of ACh is transmitted via nicotinic (nAChR) and muscarinic (mAChR)

acetylcholine receptors. The nAChR is an ion pump without subtypes in the CNS. The group of mAChRs on the contrary, comprises 5 subtypes (M1-5) of G protein-coupled receptors, of which mAChR subtypes M1 and M2 are distributed in all layers of the OB with the highest density in the EPL. Mice lacking the M1 type of AChRs show impaired odor discrimination abilities (Chan et al., 2017). The M1 subtype of mAChRs acts on dendro-dendritic synapses of MCs and GCs in the EPL. Activation of the receptor leads to increased excitability of GCs and consequent GABA release followed by lateral inhibition of MCs (Ghatpande et al., 2006; Pressler et al., 2007). Activating the M2 subtype of mAChRs in the OB directly inhibits MCs and GCs (Smith et al., 2015). Nicotinic AChR are spread through all OB layers, but are most abundant in the GL and MCL (Le Jeune et al., 1995, 1996). Electrophysiological investigations suggest nAChRs are expressed in the glomerular dendritic tuft of MCs (D'Souza and Vijayaraghavan, 2012). Functionally, activation of nAChRs directly excites MCs, but also leads to feedback inhibition through GABAergic interneurons presumably PGCs (Castillo et al., 1999). Consequently, the net effect of nAChRs activation in electrophysiological slice experiments is suppression of MC activity. This effect probably causes the suppression of MC cell firing upon weak OSN stimulation during nAChR activation, a filtering effect only allowing responses to stronger odor input (D'Souza and Vijayaraghavan, 2012). Additionally, the activation of nAChRs directly excites glutamatergic external TCs in the GL. This activation leads to excitation of interneurons releasing GABA back onto ETCs (D'Souza et al., 2013). Raising ACh levels in the OB *in vivo* increases the number of differentially responding MCs after stimulation with similar odors. This effect is dependent on nAChRs and mAChR. After blocking both receptor classes, ACh mediated enhancement of odor discrimination abilities was reversed (Chaudhury et al., 2009; Mandairon et al., 2006). In the glomeruli ACh directly excites M/T cells through nAChR activation, which is followed by GABAergic inhibition mediated by mAChR activation of inhibitory interneurons (Liu et al., 2015). Optogenetic activation of cholinergic neurons in the HDB in anaesthetized mice inhibits spontaneous firing in M/T cells, PGCs, and GCs. Additionally, activation of cholinergic cells sharpens olfactory tuning of M/T cells enhancing responses to optimal odors and suppressing responses to non-

optimal odors (Ma and Luo, 2012). Optogenetic activation of cholinergic HDB axons in the OB increases spontaneous and odor-evoked M/T cell spiking, independent of odor concentration (Rothermel et al., 2014). Axonal stimulation compared to somatic stimulation of cholinergic neurons seems to change the modulation effect. Interestingly, chemogenetic activation of cholinergic neurons in the HDB improves odor discrimination behavior. Chemogenetic silencing of cholinergic HDB neurons reversed this effect and disrupted odor discrimination of similar odors (Smith et al., 2015). *In vivo* Ca²⁺-imaging techniques allow the investigation of numerous cells at the same time. Bendahmane and colleagues combined this technique with electrical HDB stimulation in anaesthetized mice and observed no difference in spontaneous glomerular activity (Bendahmane et al., 2016). Interestingly, odor-evoked glomerular activity was modulated according to odorant concentration with enhanced responses to low, and suppressed responses to high concentrations. This effect could be mimicked by pharmacological AChR activation. The application of pharmacological substances implies intensity-dependent decrease in strong glomerular responses to high odor concentrations after nAChR activation, whereas, mAChR activation promotes activity-invariant increase in glomerular response. These findings suggest an ACh mediated filtering effect, increasing odor sensitivity towards odors with low concentrations and decreasing sensitivity to higher concentrations (Bendahmane et al., 2016). The effect of activity-dependent cholinergic modulation of glomerular activity also plays a role in odor habituation. Decreased activity after prolonged exposure to one odor stimulus can be reversed through mAChR activation through electrical stimulation of the HDB. This is reflected in odor investigation behavior, which is increased after optogenetic activation of cholinergic axons in the OB (Ogg et al., 2018). In summary, ACh modulates activity in distinguished microcircuits in the OB with nAChRs being involved in glomerular activity and mAChRs affecting lateral inhibition of GABAergic interneurons (for review see: (D'Souza and Vijayaraghavan, 2014)). Both receptor types ultimately shape output neuron responses to olfactory stimulation. The current state of research indicates that ACh modulation provides a filtering mechanism for odor sensitivity and thus, increases odor discrimination abilities.

Besides cholinergic fibers, **GABAergic axonal fibers** from the HDB project onto OB neurons (Záborszky et al., 1986) (FIG. 1.6). GABA is the most abundant inhibitory neurotransmitter in the brain. GABAergic inhibition is mediated via ionotropic GABA_A and metabotropic GABA_B receptors at the post-synapse. GABAergic projections from the HDB terminate predominantly in the GL as well as in the IPL and GCL in the OB. They contact dendrites and somata of PGCs and GCs (Gracia-Llanes et al., 2010). In GCs, GABA receptors are found in clusters on the cell somata as well as proximal and apical dendrites. Optogenetic activation of GABAergic HDB fibers in brain slices directly inhibit GCs in the OB. Chemogenetic silencing of GABAergic HDB neurons impairs odor discrimination of chemically similar odors without affecting odor habituation (Nunez-Parra et al., 2013). GABAergic HDB neurons also innervate PGCs in the GL. When optogenetically activated in acute slices, GABAergic projections directly inhibit PGCs (Sanz Diez et al., 2019). An interesting investigation showed that a distinct population of VGlut3-positive cholinergic HDB neurons co-releases GABA onto dSACs in the IPL (Case et al., 2017). This shows that modulation of OB neurons through the HDB is complex and not yet fully understood. The involvement of the HDB in odor processing is very prominent and intensively studied. Nonetheless, an investigation studying odor-evoked activity in neurons of the HDB is still missing.

1.4. Aim of the study

Present research clearly shows the modulatory effect of HDB input to the OB, which promotes odor discrimination through enhancing the signal-to-noise ratio of neuronal activity. However, the response dynamics of different HDB neuron populations to odor stimulation has not been adequately investigated up to now. Investigating the characteristics and quality of odor-driven responses in neurons from the HDB to OB is essential for understanding how the top-down modulation alters cellular activity in the OB and supports odor discrimination. Therefore, this study aims to investigate the following questions:

1. Do HDB axons exhibit odor-evoked activity? And how are these responses characterized?
2. Which neuron types (GABAergic or cholinergic) are implicated in the odor-driven responses?
3. Does silencing of the HDB affect odor-evoked activity in the OB?

To investigate sensory-driven activity in HDB axons, this study employs two-photon *in vivo* Ca^{2+} -imaging in awake head-fixed mice. This technique enables monitoring of axonal activity during odor stimulation in neuronal projections deriving from the HDB and terminating in the GL. Labeling of all neurons and specific neuron types (GABAergic or cholinergic) in the HDB with GCaMP6s allows separate analysis of odor-evoked activity in axon segments providing different types of feedback. Additionally, this study sought to examine the effect of HDB input to M/T cell odor responses. Monitoring and comparing glomerular activity in transgenic *Thy1-GCaMP6f*-mice with and without silencing the HDB gave insight into modulatory effects of the HDB feedback.

2. Methods

2.1. Transgenic mice

B6;129S6-*Chat*^{tm2(cre)Lowl}/J (The Jackson Laboratory Stock No: 006410) mice express Cre recombinase controlled by the *Chat* gene promoter enabling the cell type specific expression in cholinergic neurons. Homozygous mice of this line were used from an age of 2 month and referred to as ChAT-Cre. For specific expression in GABAergic neurons *Gad2*^{tm2(cre)Zjh}/J (The Jackson Laboratory Stock No: 010802) mice were used, which are expressing Cre recombinase controlled by the *Gad2* promoter/enhancer elements. These heterozygous mice referred to as Gad2-Cre were used from an age of 2 months. C57BL/6J-Tg (Thy1-GCaMP6f)GP5.5Dkim/J (The Jackson Laboratory Stock No: 024276) mice express the calcium sensor GCaMP6f in excitatory neurons throughout the brain driven by the *Thy1* promoter. The heterozygous expression is sufficient for the experiments, where mice were used from the age of 2 months. Mice were group housed with a 12/12 day-night-cycle under specific pathogen-free conditions. Cages were ventilated individually (IVCs) and food and water available *ad libitum*.

2.2. Stereotactic injection

For delivery of genetically encoded calcium sensors or fluorescent marker proteins in specific brain regions the technique of Adeno-associated virus (AAV) injections was used as described in the following. Mice were anaesthetized with intraperitoneal (i.p.) injections of ketamine/xylazine mixture (0.13 mg/g bodyweight Ketavet[®] (Pfizer, New York, USA) / 0.01 mg/g bodyweight Rompun[®] (Bayer, Leverkusen, Germany)). Eyes were protected by application of ophthalmic ointment (Bepanthen[®], Bayer, Leverkusen, Germany). Subsequently, mice were fixed in a custom-made surgery frame and anesthesia was consolidated by additional application of isofluran (Actavis, New Jersey, USA) through inhalation. The surgery field was disinfected with 70 % ethanol followed by application of lidocain. Hair was removed with a scissor before the skin was opened with a small incision along the anteroposterior axis. After removal of the periosteum, injections sites were

localized according to bregma (AP: 0 mm, ML: \pm 1.25 mm, DV: - 5.3 mm (from brain surface)). A small craniotomy was performed with a dental drill (Schick, Schemmerhofen, Deutschland) through which the injection needle (NanoFil needle, World Precision Instruments, Sarasota, USA) attached to a microliter syringe (Hamilton, Reno, USA) was slowly lowered into the brain. Upon reaching the indicated depth virus was slowly injected (50 nl/min) into the brain controlled with a four-channel micro controller (SYS-Micro4, World Precision Instruments, Sarasota, USA) and allowed to diffuse for 10 – 15 min. Virus volume was chosen according to conducted experiment (50 nl/hemisphere AAV1-Syn-GCaMP6s (#100843 Addgene, Watertown, USA); 250 nl/hemisphere AAV1/2-TeTn-T2A-KO (kind gift of Martin Schwarz, UKB, Bonn; 250 nl/hemisphere AAV1-Syn-DIO-GCaMP6s, (#100845 Addgene, Watertown, USA)). Injections were conducted bilaterally in the same manner. After finishing the procedure, the skin was closed by stitching and the mice transferred to a heating chamber and allowed to wake up. Post-surgery analgesia consisted of sub-cutaneous injection of burprenophine (Temgesic®, Reckitt Benckiser Healthcare, Kingston Upon Hull, UK) every 8 hours for 3 consecutive days.

2.3. Cranial window implantation

Monitoring neuronal activity in the olfactory bulb was made possible by substituting overlaying parts of the cranium with a coverslip, creating a so-called cranial window. The implantation of the cranial window was conducted one week after intercranial AAV-injection (s. 2.2.) as described in the following. Anesthesia was induced with an intraperitoneal (i.p.) injection of ketamine/xylazine mixture (0.13 mg/g bodyweight Ketavet® (Pfizer, New York, USA) / 0.01 mg/g bodyweight Rompun® (Bayer, Leverkusen, Germany)). Adding the inhalation anesthetic using isoflurane (Actavis, New Jersey, USA) ensured surgical depth of anaesthesia. Subsequently, Dexamethasone 21-phosphate disodium salt, an immunosuppressant drug (0.2 μ g/g bodyweight, Sigma-Aldrich, Darmstadt, Germany) was injected subcutaneously (s.c.) and the eyes were coated with ophthalmic ointment (Bepanthen®, Bayer, Leverkusen, Germany) to protect against drying. After fixing the mice on a surgical frame, the surgery field was disinfected with 70 % ethanol and covered in lidocain. Removal of the dermis in a triangular shape from the interparietal

bone towards the nasal section was performed using surgical scissors. The periosteum was carefully removed followed by dispersion and rinsing after 15 s of Gel Etchant (OptiBond™ FL bottle kit, Kerr, Salerno, Italy) to roughen the cranium. After cleaning and drying the exposed bone, preparations were continued by covering the cranium in a two-component (Primer and Adhesive from the OptiBond™ FL bottle kit, Kerr, Salerno, Italy) light-curable (420 – 480 nm) base (OptiBond™ FL bottle kit, Kerr, Salerno, Italy). This process generates a smooth surface and clean area before starting the craniotomy. For this a circle (Ø 3 mm) above the olfactory bulb was marked and the edges slowly drilled away using a fine dental drill (Schick, Schemmerhofen, Deutschland). The excised bone was carefully removed and the cavity filled with sterile PBS (ROTI®Cell PBS CELLPURE®, Carl Roth GmbH + Co. KG, Karlsruhe, Germany). After stopping all occurring bleedings with an absorbable gelatin sponge (GELITA-SPON®, Gelita Medical GmbH, Eberbach, Deutschland) the dura mater was carefully removed with fine forceps. The craniotomy was thoroughly rinsed with sterile PBS before inserting an appropriate cover slip (Ø 3 mm, thickness 0.14 mm). The cover slip (cranial window) was fixed under slight pressure with a light-curable composite (GRADIA® DIRECT Flo, GC Europe, Leuven, Belgium) covering the edges of the glass and the surrounding bone. For head-fixation a purchased metal bar (Luigs and Neumann, Ratingen, Germany) was fixed on top of the cranium and the whole surgery field covered in the light-curable composite. Finally, the mouse was transferred to a heated wake-up chamber and allowed to recover. Analgesia was carried out by s.c. injection of buprenorphine (Temgesic®, Reckitt Benckiser Healthcare, Kingston Upon Hull, UK) every 8 hours for 3 consecutive days.

2.4. Two-Photon in vivo Ca²⁺-imaging

2.4.1. Two-Photon imaging principles

The underlying effect for multiphoton microscopy was first described by Maria Göppert-Mayer in 1931. In her doctoral thesis, Göppert-Mayer proves the concept of two-photon excitation, where two photons with a frequency sum equivalent to an atom's excitation frequency can excite the atom in a quantum event (Göppert-Mayer, 1931). In two-photon microscopy this effect is used to

excite fluorophores with two photons carrying half the energy than used in single-photon excitation. The probability for the simultaneous absorption of two photons is very low, which makes temporal and spatial focusing of the laser beam to generate sufficient power levels essential. Temporal focusing is attained by concentrating the emitted power in high peaks through pulsing the laser in femtosecond long trains. An objective with a high numerical aperture spatially focuses the laser beam into one spot. With this combination a focal spot with high probability of two-photon absorption in a femtoliter sized volume is generated. Since the probability of the two-photon effect exponentially decays with distance from the focus, only fluorophores within the focal spot are excited, which prevents out-of-focus excitation and out-of-focus fluorescence emission. Since wavelength and energy of a photon are inversely proportional, photons with half the energy level inherit approximately double the wavelength necessary for single photon excitation. Hence, for most fluorophores utilized in biomedical research two-photon excitation falls in the near-infrared spectrum (700 – 1000 nm). Titanium doped sapphire (Ti:Sa) lasers are tunable in this spectral range and can be pulsed, which makes them the preferred light source in two-photon microscopy. The long wavelengths of near-infrared light reduce scattering within organic tissue allowing deeper penetration and thus, imaging of structures in deep tissues. Additionally, the focal volume limited excitation and lower energy of longer wavelengths prevents harmful interaction with out-of-focus structures greatly reducing phototoxicity. Summarizing, two-photon imaging enables the investigation of structures without removing them from the biological context allowing the study of these structures in the living organism, which was first utilized by Denk and colleagues in 1990 (Denk et al., 1990).

2.4.2. Ca²⁺-imaging principles

Neuronal action potential firing is linked to increases in intracellular calcium (Ca²⁺) levels. Visualizing the intracellular Ca²⁺-levels with fluorescent indicators therefore provides an approximation tool for monitoring neuronal activity. Upon binding of Ca²⁺-ions, Ca²⁺-indicators display changes wavelength (e.g., CaMPARI (Fosque et al., 2015)) or in fluorescence intensity. Chemical Ca²⁺-dyes like fluo-4, Calcium Green-1 and Oregon Green BAPTA (OGB)-1 belong to the latter group. These dyes are usually delivered acutely via whole-cell

patch clamp or electroporation potentially damaging the recorded tissue. The addition of acetoxymethyl (AM) groups to chemical Ca^{2+} -dyes create a hydrophobic molecule, which could easily diffuse into cells. This approach proved to be inefficient for *in vivo* experiments due to cleavage of the AM groups by extracellular esterases and consequent insufficient labeling of cells (Jobsis et al., 2007). More commonly used in recent years are genetically encoded Ca^{2+} -indicators (GECIs) like GCaMP, RCaMP and RGeco. GECIs are introduced into cells by viral transduction, *in utero* electroporation and generation of transgenic mouse lines. The advantage of GECIs is their expression and functionality over longer time periods, which enables extended recordings of neuronal activity. Additionally, the usage of genetic tools allows the genetically targeted labeling of specific neuron types and cell compartments (Grienberger and Konnerth, 2012). GECIs consist of a fluorophore fused with the Ca^{2+} -binding protein calmodulin (CaM) and the Ca^{2+} -binding peptide M13 (Nakai et al., 2001). The combination of Ca^{2+} -imaging and two-photon microscopy (Yuste and Denk, 1995) enabled monitoring of neuronal activity in deep tissues *in vivo* in anaesthetized and awake mice driving many discoveries in the field of neuroscience (Dombeck et al., 2009; Svoboda et al., 1997; Wachowiak et al., 2004).

2.5. Two-Photon microscope

Ca^{2+} imaging was performed using a custom made two-photon microscope (Thorlabs, Newton, USA). The Ca^{2+} -sensor GCaMP6 was excited with 920 nm light pulsed by a titanium sapphire (Ti:Sa) 80 MHz Cameleon Ultra II two-photon laser (Coherent, Inc., Santa Clara, USA). The beam was deflected by an 8 kHz galvo-resonant scanner (LSK.GR08/M, Thorlabs, Newton, USA) and focused by a 16x water immersion objective (NA 0.8, N16XLWD-PF, Nikon Corp., Tokio, Japan). Laser power was controlled with a variable laser attenuator (Thorlabs, Newton, USA) and an electro-optic modulator (Thorlabs, Newton, USA), which switched off laser power outside of the imaged field of view to prevent prolonged exposure of the sample. Emission was collected with a GaAsP PMT (Thorlabs, Newton, USA) after passing a 525/50 nm band-pass filter (AHF, Tübingen, Germany). Image collection was carried out employing the ThorImageLS software (Thorlabs, version 2.3).

2.5.1. *Two-Photon imaging, awake*

To employ two-photon Ca^{2+} -imaging in awake behaving mice, animals were head-fixed on a linear treadmill. Therefore, a metal adapter (Luigs and Neumann, Ratingen, Germany) was attached to the head bar installed during window implantation and placed into the headpost holder (Luigs and Neumann, Ratingen, Germany). The headpost holder connected the mice to the adjustable head holder fixed to the microscope. By head-fixing as describe the mice were positioned on the custom-made linear treadmill, which they could move voluntarily. Following this procedure, the cranial window was aligned in parallel with the objective. Fast drying silicon (Kwik-Sil, World Precision Instruments, Sarasota, USA) was spread in a circular shape around the window and immersion (H_2O) applied within the circle. The objective (NA 0.8, N16XLWD-PF, Nikon, Düsseldorf, Germany) was lowered and desired structures brought into focus. After selecting the imaging plane and area ($500.4 \times 500.4 \mu\text{m}$) 2-minute time series (1024×1024 or 512×512 pixel, 1800 or 3600 frames) were acquired at a rate of 15.4 or 30.3 frames per second.

2.5.2. *Odor stimulation*

During image acquisition mice received an odor stimulation with two odorants: rose (undiluted 99% 2-Phenylethanol, 8.2 M, Sigma-Aldrich, Darmstadt, Germany) and vanillin (59 mM in 0.5 % EtOH in H_2O , Sigma-Aldrich, Darmstadt, Germany). Stimulation was delivered through an off-the-shelf two channel dilution olfactometer (Med Associate Inc., Fairfax, USA). The olfactometer was operated with pressurized air, which was first desiccated and rehydrated with distilled water. Outside of odor stimulation air flow was directed to the outlet, which consisted of a modified 10 ml serological pipette (CELLSTAR[®], greiner bio-one, Kremsmünster, Austria) connected to the olfactometer's tubing. This outlet was placed in front of the nostrils with a maximal distance of 0.5 cm and provided a constant flow of clean air. The diameter of the outlet, which exceeded the size of the nose of the animals, ensured the delivery of odor plumes to both nostrils during stimulation. When stimulation was initiated, the olfactometer's airflow was bifurcated to the odor storage vials. The opening of a valve, controlled by the software IGOR PRO Version 6.22a (Python Software Found., USA), allowed for the infiltration of 5 %

odor saturated air into the constant air flow streaming from the outlet. The frame trigger of the microscope was recorded with an ITC-18 board (HEKA, Ludwigshafen/Rhein, Germany) and used to synchronize the olfactometer with the imaging. Odor stimulation onset was at 50 s of imaging and lasted for 5 s. Mice were first stimulated with repeated application of rose followed by repeated stimulation with vanillin. Each stimulation was repeated for a minimum of 8 times and up to 13 times.

2.6. Perfusion

Perfusions were initialized with an i.p. injection of a lethal dose ketamine/xylazine mixture (0.26 mg/g bodyweight Ketavet® (Pfizer, New York, USA) / 0.02 mg/g bodyweight Rompun® (Bayer, Leverkusen, Germany)). After reaching surgical depth of anesthesia, the thorax was opened and a needle inserted in the left heart ventricle. Next, using a roller pump blood was substituted with PBS. For tissue fixation 4 % PFA was introduced into blood system and perfused for 10 minutes. Finally, the brain was dissected and post-fixed in 4% PFA overnight.

2.7. Post-mortem tissue evaluation

2.7.1. Tissue sectioning

Post-mortem brain tissue was sectioned into 100 µm slices employing a vibratome (Leica, VT 1200S, Leica, Nussloch, Germany). For coronal slices, cerebellum was removed and the brain glued with its caudal side to the vibratomes tissue holder. Slices were cut from rostral to caudal. All slices were collected in PBS with 0.01 % of sodium azide (NaN₃) for storage. If acquisition of confocal images was intended, slices were placed on microscope slides and mounted with Dako Fluorescent mounting medium (Agilent, Santa Clara, USA).

2.7.2. Confocal image acquisition

Post-mortem images of tissue sections were acquired using a confocal Laser Scanning Microscope (LSM 900, Zeiss, Jena, Germany). GCaMP6 fluorescence was excited using a 488 nm laser and emission collected with a 490 – 555 nm band pass filter. A bright field image of the surrounding tissue was made using a transmitted light detector (T-PMT). The ZEN black 2012 software was used for image acquisition control. Image size was set to

6.25 $\mu\text{m}/\text{px}$ for overview images and 0.13 $\mu\text{m}/\text{px}$ for detailed images of areas with GCaMP6s positive neurons.

2.7.3. Quantification of GCaMP6s expression

Quantification of expression after stereotactic injection of an AAV carrying the expression cassette for GCaMP6s was conducted in confocal images of post-mortem tissue sections. For each brain four confocal images depicting GCaMP6s positive neurons at different positions anterior and posterior to bregma were analyzed. These brain sections included the HDB (around bregma 0.14 mm and -0.15 mm) as well as brain areas anterior (around bregma 0.50 mm) and posterior (around bregma -0.50 mm). The different brain areas manually marked according to the Allan Mouse Brain Atlas (Lein et al., 2007) with regions of interest (ROIs) in the confocal images using ImageJ/Fiji. The mean gray value of each area was measured as a proxy for the fluorescent intensity, which correlates to the GCaMP6s expression. Additionally, the mean gray value for a small area without GCaMP6s positive cells was measured as the background fluorescence. The background fluorescence was subsequently subtracted from the mean gray values measured for the different brain areas using Excel. The calculated value for each region was then transferred to GraphPad Prism 8 to generate graphs and perform statistical analysis.

2.8. Ca²⁺-imaging data analysis

2.8.1. ROI detection and fluorescence change extraction

Raw data images from Ca²⁺-imaging time-lapses were processed utilizing MATLAB® (Mathworks, Natick, USA) and the Lucas-Kanade method for in frame motion correction (Lucas and Kanade, 1981). Processed images were used to manually draw regions of interest (ROIs) and extract changes in fluorescence over time with ImageJ/Fiji. For this purpose, time-lapses were compressed into average intensity projections and single glomeruli or axon segments selected as ROIs. Employing ImageJ/Fijis measurement function, gray values for each frame of the time-lapse were extracted and data further processed as described below. Mean gray values depict changes in fluorescence during image acquisition.

2.8.2. Trace detection and time-lapse parameter extraction

Analysis was performed using a custom-made MATLAB[®] (Mathworks, Natick, USA) pipeline (created by Dr. Fabrizio Musacchio) executing the following steps. First data was processed by applying a low-pass Butterworth filter removing signal with a frequency higher than 1 Hz. Afterwards, $\Delta F/F$ was calculated by normalizing the fluorescence (F) to baseline fluorescence (F_0): $\Delta F/F = \frac{F-F_0}{F_0}$. Baseline fluorescence was defined as the average value of the 10th percentile of all data points acquired in the time-lapse from 10 – 45 s (Giovannucci, 2019). After detrending the data, trials were averaged, whereby time-lapses comprising severe z-shifts were manually excluded. Following this step, a curve fitting application was conducted and traces fitted to a binomial curve. From this curve amplitude was extracted as the curve maximum occurring between stimulus onset at 50 s and 55 s (axonal Ca²⁺-imaging) or 64 s (glomerular Ca²⁺-imaging). Time to peak was defined as timepoint of amplitude and area under the curve as the integral of the defined curve. For axonal Ca²⁺-imaging the curve fitting range included 50 s after stimulus onset. For glomerular Ca²⁺-imaging only 10 s after stimulus onset were considered for curve fitting. Calculated parameters were extracted in table format and transferred to GraphPad Prism 8 (GraphPad Software Inc., La Jolla, USA) for statistical analysis.

2.9. Statistics

Data values for amplitude, time to peak and area under the curve were transferred to GraphPad Prism 8 and tested for normality distribution with the Shapiro-Wilk normality test. Mean gray values for expression patterns of GCaMP6s were compared using the non-parametric Kruskal-Wallis test with Dunn's multiple comparison (* < 0.03, ** < 0.002, *** < 0.0001, ****p < 0.0001). Data for median comparison of values obtained from axonal Ca²⁺-imaging was compared using the nonparametric Mann-Whitney test (* < 0.05, ** < 0.01, *** < 0.001, ****p < 0.0001). Data for glomerular Ca²⁺-imaging after sham and TeTn treatment were compared applying the nonparametric Kolmogorov-Smirnov test (* < 0.05, ** < 0.01, *** < 0.001, ****p < 0.0001). All data was illustrated as violin plots depicting data distribution as well as median and quartiles and implemented into figures created using Illustrator CS5 Version 15.0.1.

3. Results

3.1. Post-mortem analysis of GCaMP6s expression in brain sections

To determine the transduction of neurons and expression of GCaMP6s after stereotactic AAV-injection, GCaMP6s fluorescence was evaluated after two-photon Ca^{2+} -imaging in post-mortem brain sections. C57BL/6, Gad2-Cre and ChAT-Cre mice were stereotactically injected with an AAV containing an expression cassette for the Ca^{2+} -sensor GCaMP6s under the synapsin promoter. The fluorescent indicator was consequently expressed in neurons in close proximity to the injection site and transported into the axon. This enabled the investigation of odor-evoked activity changes of HDB axons in the glomerular layer utilizing *in vivo* two-photon Ca^{2+} -imaging. Brains exposed to two-photon Ca^{2+} -imaging were extracted after perfusion and sectioned into 100 μm slices. Brain sections including the HDB (around 0.14 mm anterior and -0.15 mm posterior to bregma) as well as anterior (around bregma 0.50 mm) and posterior (around bregma -0.70 mm) sections were mounted and imaged using a laser-scanning microscope. The acquired images revealed that HDB neurons throughout the whole HDB were GCaMP6s positive (FIG 3.1). Additionally, some GCaMP6s positive neurons were detected in surrounding brain areas adjoining the HDB. Those brain areas were the olfactory tubercle (OT), hypothalamus (Hy), substantia innominate (SI), nucleus of the lateral olfactory tract (NLOT), anterior amygdala area (AAA), medial amygdala nucleus (MeA) and cortical amygdala area (CoA). The described results suggest that transduced neurons in C57BL/6, Gad2-Cre, as well as ChAT-Cre mice resided mainly in the HDB. However, few neurons in the OT, Hy, SI, NLOT, AAA, MeA and CoA were also transduced by the AAV-GCaMP6s-injection. Thus, GCaMP6s-positive axons in the OB recorded during Ca^{2+} -imaging primarily derived from the HDB. In support of this conclusion, all recorded axons were localized in the GL of the OB, which receives direct centrifugal input from the anterior piriform cortex (APC), the anterior olfactory nucleus (AON) and the HDB (Wen et al., 2019). However, the AON and APC were not containing any GCaMP6s positive neurons. In conclusion, these data suggest that GCaMP6s positive axons indeed derive from the HDB.

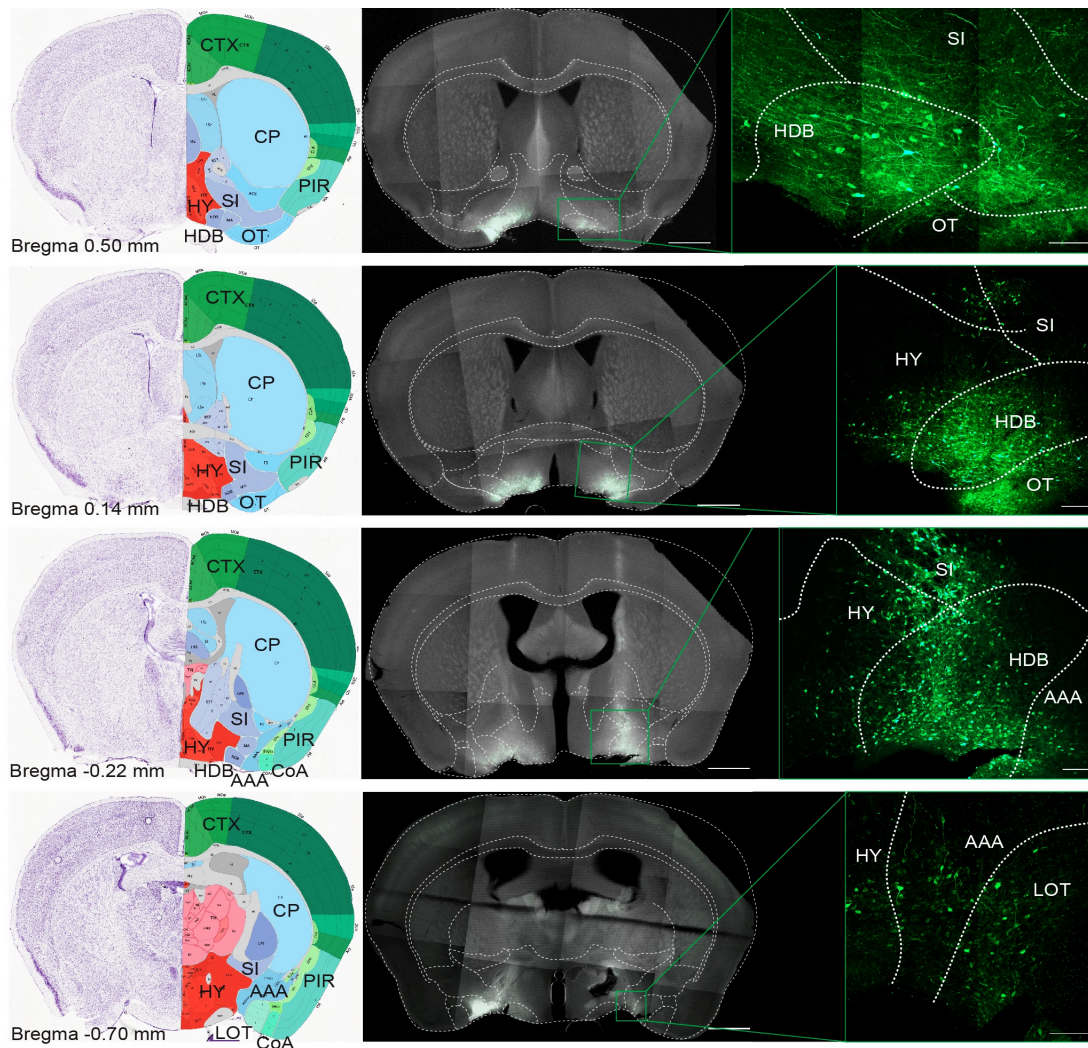


FIGURE 3.1. GCaMP6s expression after stereotactic AAV-injection. Left: Images from Allan Mouse Brain Atlas (Lein et al., 2007) depicting brain areas in coronal brain sections. Middle: Exemplary overview images of brain sections from C57BL/6 mice stereotactically injected with AAV-Syn-GCaMP6s in the same anteroposterior location relative to Bregma as images from Allan Mouse Brain Atlas. Left: maximum intensity projections of z-stacks depicting brain slices with GCaMP6s positive neurons after AAV-injection. Horizontal limb of the diagonal band of broca (HDB), olfactory tubercle (OT), hypothalamus (Hy), substantia innominate (SI), nucleus of the lateral olfactory tract (NLOT), anterior amygdala area (AAA), medial amygdala nucleus (MeA) and cortical amygdala area (CoA). Scale bars 100 μ m.

3.2. Cell type-unspecific odor-tuned HDB axons in the OB

To investigate odor-evoked responses in HDB axons in the OB, Ca^{2+} -responses upon olfactory input in HDB axons terminating in the GL were recorded and characterized. HDB axons were labelled by injecting an AAV caring the expression cassette for GCaMP6s into the HDB of C57BL/6 mice. Employing two-Photon *in vivo* Ca^{2+} -imaging in awake head-fixed mice after labeling HDB neurons with GCaMP6s and implanting a cranial window above

the OB allowed the investigation of Ca^{2+} -changes of HDB projections in the GL during odor stimulation. The same axon segments were monitored during repetitive stimulation with two consecutively applied odorants. Recordings were conducted during repeated rose odor stimulation followed by recordings carried out during repeated stimulation with vanillin odorant (8-13 repetitions per odor) (FIG. 3.2 A, B, C).

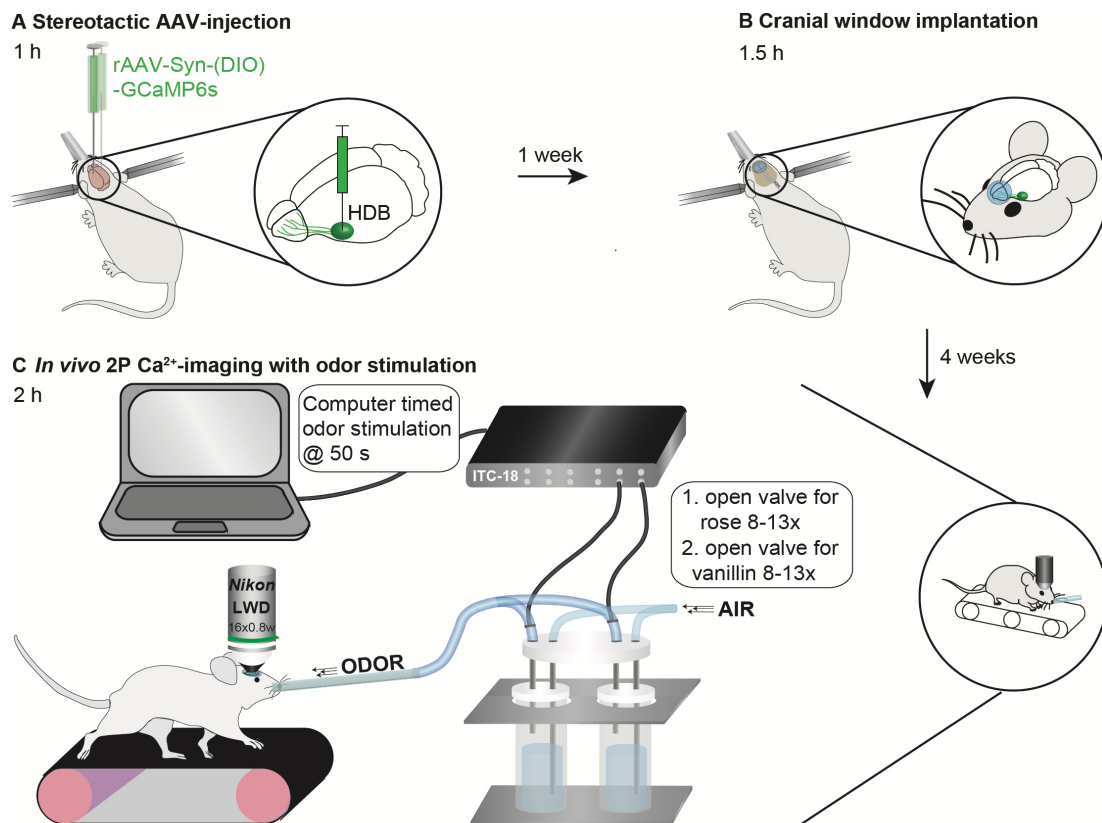


FIGURE 3.2. Experimental procedure of monitoring of Ca^{2+} -levels in HDB axons. (A) Schematic illustration of the bilateral AAV-syn-GCaMP6s (or AAV-syn-DIO-GCaMP6s in *Gad2-Cre* and *ChAT-Cre* mice (s. 3.3 and 3.4) injection into the HDB. **(B)** Schematic illustration of the OB window implantation. **(C)** Schematic illustration of awake head-fixed recording of Ca^{2+} -changes in the olfactory bulb during odor stimulation. Depicted are the mouse running voluntarily on a linear treadmill while receiving repeated rose odor stimulation followed by repeated vanillin odor stimulation using a computer controlled.

After evaluating the expression of GCaMP6s in post-mortem tissue sections, Ca^{2+} -imaging data obtained from brains with reliable expression of GCaMP6s in the HDB were analyzed. During the analysis process, recordings were corrected for motion artefacts in the x,y-direction using the Lucas-Kanade method (Lucas and Kanade, 1981). Afterwards the recorded axon segments were analyzed for their odor response characteristics. For this purpose, time-lapses without z-shifts were selected and the depicted axons manually selected

in Fiji. Following, the mean gray values of every ROI for each frame of the time-lapse were measured to obtain the change in fluorescent intensity over time for all ROIs. The extracted values for individual ROIs or axon segments from all selected time-lapses recorded during either rose or vanillin stimulation were subsequently pooled and an average was calculated. The obtained Ca^{2+} -fluorescence transients were further processed using a custom-made MATLAB® script. This method generated trial-averaged Ca^{2+} -transients for each analyzed axon segment recorded during repeated stimulation with one odor (either rose or vanillin). After preprocessing the Ca^{2+} -transients and applying a curve fitting, the characteristic values amplitude, time to peak, and area under the curve (AUC) for each axon segment were measured.

Analysis

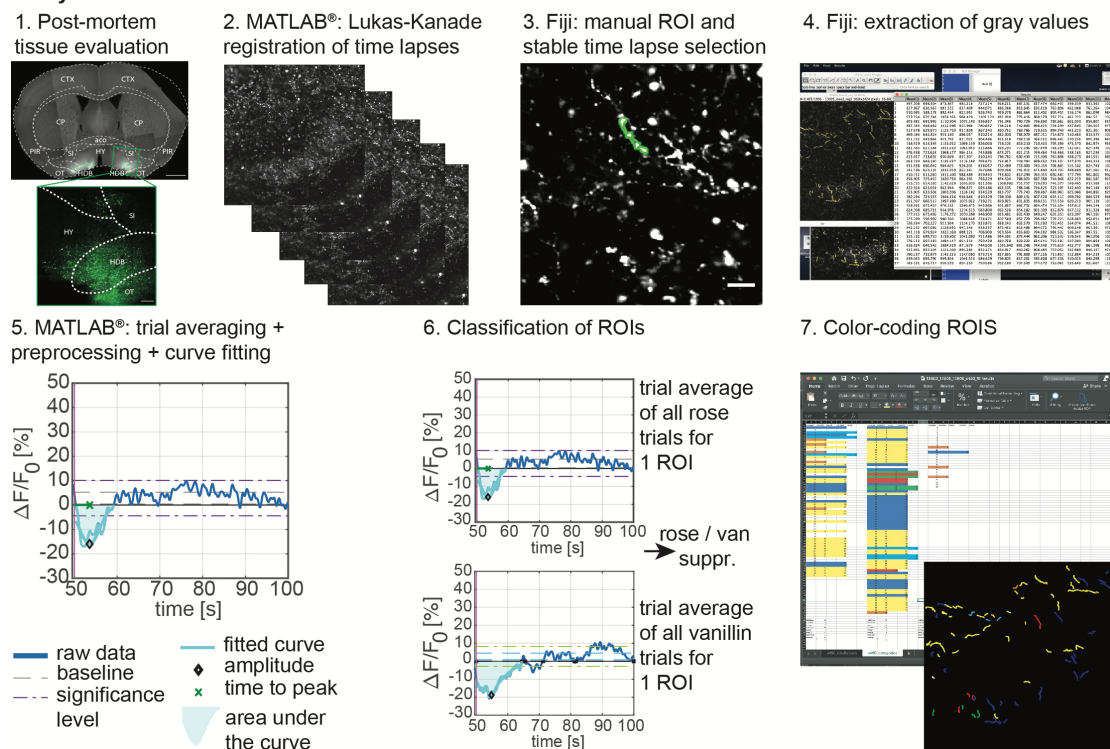


FIGURE 3.3. Analytical procedure for data obtained during recording of Ca^{2+} -levels in HDB axons. Illustration of the analysis conducted for data obtained during the experiments illustrated in FIG. 3.2. **(1.)** tissue was evaluated post-mortem to select data derived from brains with thorough GCaMP6s expression in the HDB. **(2.)** Ca^{2+} -imaging time-lapses were corrected in the x,y-direction. **(3.)** axon segments were selected manually with the ImageJ/Fiji ROI selection tool and time-lapses with z-shifts from the analysis excluded. **(4.)** For each ROI mean gray values were extracted for each frame over one time-lapse. **(5.)** Measuring characteristics of the Ca^{2+} -transients after trial-averaging, filtering and curve fitting using MATLAB®. **(6.)** Classification of axon fragments according their Ca^{2+} -transients' characteristics. **(7.)** Color-coding of ROIs according to their classification determined in the previous step. This color code was transferred to the respective ROIs of an average intensity projection of one time-lapse.

The analyzed axon segments displayed positive or negative amplitudes of the Ca^{2+} -transients in response to odor stimulation with either one or both of the separately applied odorants rose and vanillin. These characteristics were then used to classify the Ca^{2+} -responses of the axon segments. Consequently, each class of Ca^{2+} -responses was assigned a color. Lastly, each ROI in an average intensity projection of one time-lapse representing an axon segment was labeled according to the color code (FIG. 3.3).

To investigate odor-evoked Ca^{2+} -changes of HDB axons irrespective of their neuron subtype (GABAergic, cholinergic), C57BL/6 mice were injected with AAV-Syn-GCaMP6s into the HDB and a cranial window was implanted above the OB. Consequent awake Ca^{2+} -imaging of HDB axons in the GL was performed during repeated odor stimulation with rose followed by vanillin as described above (FIG. 3.4 A). This experiment revealed HDB axon segments displaying reliable changes in Ca^{2+} -levels upon odor stimulation with either one or both consecutively applied odorants (FIG. 3.4 B, C). Averaging all trials of all Ca^{2+} -transients (grand average) recorded during stimulation with one odorant, uncovered a strong net decrease in fluorescence in axon segments upon separate presentation of both odorants (FIG. 3.4 D). Response properties for individual axons were determined by analyzing their trial-averaged Ca^{2+} -transients. A negative peak minimum in the trial-averaged Ca^{2+} -transients displayed by individual axon segments recorded during odor application reflected the net decrease in the grand average Ca^{2+} -levels (amplitude median: $-9.4 \pm 7.7 \% \Delta F/F$ rose and $-8.7 \pm 6.0 \% \Delta F/F$ vanillin) (FIG. 3.4 E). The rise time of Ca^{2+} -transients was fast for both odorants. However, the time to peak medians measured upon rose or vanillin stimulation did show significant difference (time to peak median: 3.7 ± 2.1 s rose vs. 4.3 ± 3.0 s vanillin; * $p = 0.0285$) (FIG. 3.4 F). The area under the curve values demonstrate similarities for stimulation with the two odorants (AUC median: $55.6 \pm 59.1 \% \Delta F/F \cdot s$ rose and $54.0 \pm 78.6 \% \Delta F/F \cdot s$ vanillin) (FIG. 3.4 G). The described odor-evoked changes in fluorescence were displayed by 77 % of all analyzed ROIs. The remaining 23 % were not responsive to the used odorants. Interestingly, the observed odor-tuned axon segments displayed varying response properties to rose or vanillin. The monitored axon segments were sensitive to either one or

both of the presented odors. Moreover, the responses fell into one of two modes: suppressed and enhanced odor-evoked response patterns (FIG. 3.4 H). 69 % of investigated axon segments reacted with suppressed Ca^{2+} -levels to an odor stimulation. The most prevalent class of suppressed axon segments displayed a decrease in fluorescence following consecutive stimulation with both odors (Rose / Vanillin suppr., 40 %). 23 % of axon segments responded with suppressed Ca^{2+} -levels only upon stimulation with vanillin, but were not responsive to rose odor stimulation (Vanillin suppr.). Another subset of axon segments showed suppressed Ca^{2+} -transients only in response to rose odor stimulation, but did not display changes in Ca^{2+} -levels when stimulated with vanillin (Rose suppr., 6 %). Furthermore, one class of axon segments displayed enhanced Ca^{2+} -transients upon consecutive stimulation with rose and vanillin odor (Rose / Vanillin enh., 2 %). Axon segments reacting with enhanced Ca^{2+} -levels solely upon stimulation with the rose odorant, but were unaffected by vanillin stimulation (Rose enh.) accounted for 2 % of all analyzed segments. The last class of 4 % of all analyzed axon segments displayed enhanced response patterns exclusively when exposed to vanillin, but were not responsive to rose stimulation (Vanillin enh.) (FIG. 3.4 I).

To determine if odor-tuned HDB axon segments with the same response properties are located in proximity to each other possibly adhering to an odortopic distribution, the spatial innervation pattern of the HDB afferents in the recorded sections was investigated corresponding to their different response characterizations. First, the analyzed axon segments were classified and color-coded according to their response properties. The color-code was transferred to the axon segments depicted in the average intensity projection of their respective acquired time-lapses (FIG. 3.3). This technique revealed an intermingled spatial distribution of odor-tuned HDB axons within the GL (FIG. 3.4 J). These observations suggest, that HDB afferents in the GL exhibit odor-evoked activity with selective response properties for different odors. Furthermore, axon segments with different response properties are spatially intermingled.

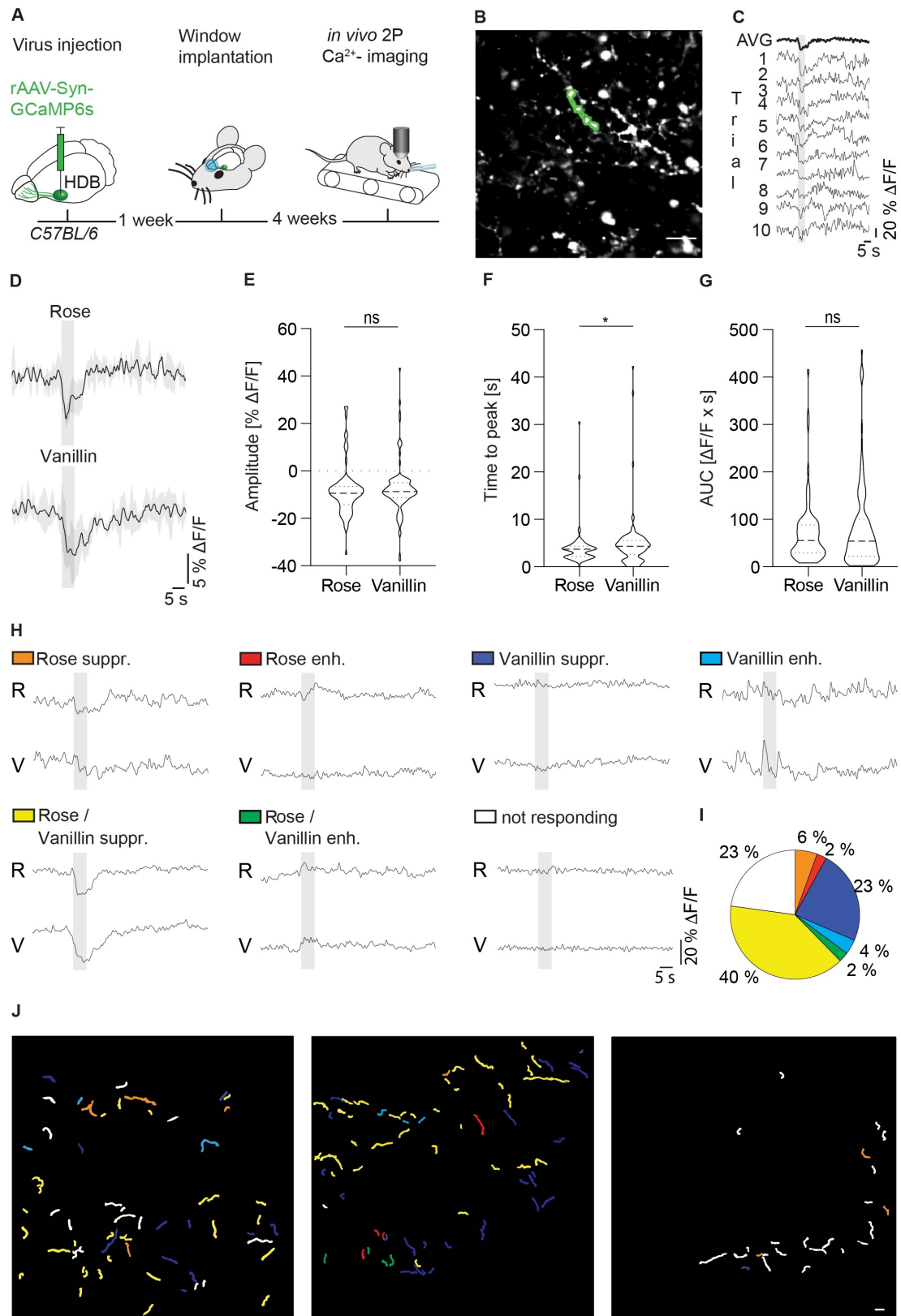


FIGURE 3.4. Cell type-unspecific odor-tuned projections from the HDB. (A) Schematic illustration of experimental timeline with AAV-syn-GCaMP6s injection into the HDB, OB window implantation and awake head-fixed recording of Ca²⁺-changes in the olfactory bulb during odor stimulation. (B) Exemplary average intensity projection of *in vivo* time-lapse of afferent HDB-projection in the OB expressing GCaMP6s approx. 100 μm below brain surface. (C) Ca²⁺-transients in presented ROI in response to rose odor stimulation (gray bar) over 10 individual trials and average (AVG). (D) Grand average of all Ca²⁺-transients from 162 ROIs in 3 mice

upon rose or vanillin odor stimulation. **(E-G)** amplitude **(E)**, time to peak **(F)** and area under the curve (AUC) **(G)** of all ROIs representing odor-tuned HDB axons (n=81 ROIs for rose and n=115 ROIs for vanillin in 3 mice). **(H)** Exemplary 8-trial average Ca^{2+} -transients with response classification according to their Ca^{2+} -responses to rose (R) and vanillin (V) odor. Classes are: rose suppr. (orange), enh. (red), not responding (white), vanillin suppr. (blue), enh. (cyan), rose & vanillin suppr. (yellow), rose & vanillin enh. (green). **(I)** Fraction of axons according to their classification. **(J)** Spatial distribution of ROIs according to their classification. All data represented as mean \pm SEM (transients) or median \pm quartiles (violin plots). Scale bar 20 μm .

3.3. Cholinergic odor-tuned HDB axons in the OB

The recording and analysis of cell type-unspecific GCaMP6s labeled HDB afferents in the GL revealed odor-tuned axon segments, which are responsive to one or both applied odorants. Furthermore, the HDB axon segments showed either enhanced or suppressed Ca^{2+} -levels in response to odor stimulation. The HDB comprises two neuron population known to innervate the OB: cholinergic and GABAergic neurons. The two HDB neuron populations potentially correspond to the two response modes, with cholinergic axons constituting the group of HDB axon segments with enhanced response patterns and GABAergic axons displaying suppressed Ca^{2+} -transients. To test this hypothesis, odor-driven responses in different neuron populations of the HDB were analyzed using mouse lines with cell type-specific expression of the Cre-recombinase. Combining these mouse lines with the injection of an AAV containing a loxP-flanked expression cassette enables labeling of specific cell types. The ChAT-Cre mouse line expresses the Cre-recombinase specifically in cholinergic neurons under the *ChAT*-promotor. Stereotactic AAV-injection into this mouse line was used to specifically label cholinergic HDB neurons with GCaMP6s (FIG. 3.5 A). After implantation of a cranial window over the OB, axon segments were monitored during odor stimulation with repeated rose odor followed by repeated vanillin stimulation as described in the previous paragraph 3.2 (FIG 3.2). The obtained information about odor-evoked changes in Ca^{2+} -levels in cholinergic HDB axon segments were analyzed for their response characteristics as described in paragraph 3.2 (FIG. 3.3). GCaMP6s positive cholinergic HDB axons in the GL of the OB of ChAT-Cre mice (FIG. 3.5 B) displayed reliable changes in fluorescence upon repetitive odor stimulation with rose or vanillin (FIG. 3.5 C). Interestingly, responding cholinergic axon segments exclusively displayed enhanced GCaMP6s fluorescence upon stimulation with either vanillin or rose odor (FIG. 3.5 D). Consequently,

amplitude maxima of cholinergic axons were positive (amplitude median: 10.0 ± 8.0 % $\Delta F/F$ rose and 11.8 ± 8.1 % $\Delta F/F$ vanillin) (FIG. 3.5 E). The time to peak of Ca^{2+} -transients in cholinergic axon segments measured during rose or vanillin odor stimulation were significantly different (median: 5.4 ± 12.6 s rose vs. 2.0 ± 5.7 s vanillin; **** $p < 0.0001$) (FIG. 3.5 F). Furthermore, the area under the curve values significantly differed between Ca^{2+} -transients acquired during rose or vanillin stimulation (median: 258.7 ± 215.6 % $\Delta F/F*s$ rose vs. 175.0 ± 192.4 % $\Delta F/F*s$ vanillin; **** $p < 0.0001$) (FIG. 3.5 G). The cholinergic axon segments exhibited, similar to the cell type-unspecific odor-tuned HDB axons presented in the previous paragraph 3.2, odor-evoked responses to either one, both or neither of the two applied odorants rose and vanillin. 13 % of cholinergic axon segments were enhanced exclusively by vanillin odor stimulation (Vanillin enh.) and 22 % solely by rose odor stimulation (Rose enh.) (FIG. 3.5 H, I). The majority of axon segments displayed enhanced responses to both independently applied odors (Rose + Vanillin enh., 45 %). 19 % of analyzed axon segments did not respond to the used odorants (FIG. 3.5 J). The spatial distribution of cholinergic axons in the GL with different response properties was analyzed as shown for the cell type-unspecific axon population in paragraph 3.2. Also, the cholinergic HDB axons with different response properties are spatially intermingled within the GL diverting from an odotopic structure. The presented results indicate that cholinergic HDB axons are odor-sensitive with exclusively enhanced response patterns. Furthermore, the responses exhibited upon rose odor stimulation are faster and have higher AUC values in comparison to responses upon vanillin odor stimulation. The spatial distribution of odor-sensitive HDB axons in the GL does not follow an odotopic structure but shows to be intermingled. Moreover, 46 % of cholinergic axons displayed odor-tuning to both applied odors, whereas 36 % respond to only rose or vanillin. The observed odor-evoked response characteristic of exclusively enhanced GCaMP6s fluorescence in cholinergic HDB axons was similar in a subset of cell type-unspecific axons of the previous experiment (paragraph 3.2, FIG. 3.4 H red, blue, green). This similarity in the response mode suggests that the enhanced subset of cell type-unspecific axons might be indeed partially cholinergic HDB afferents.

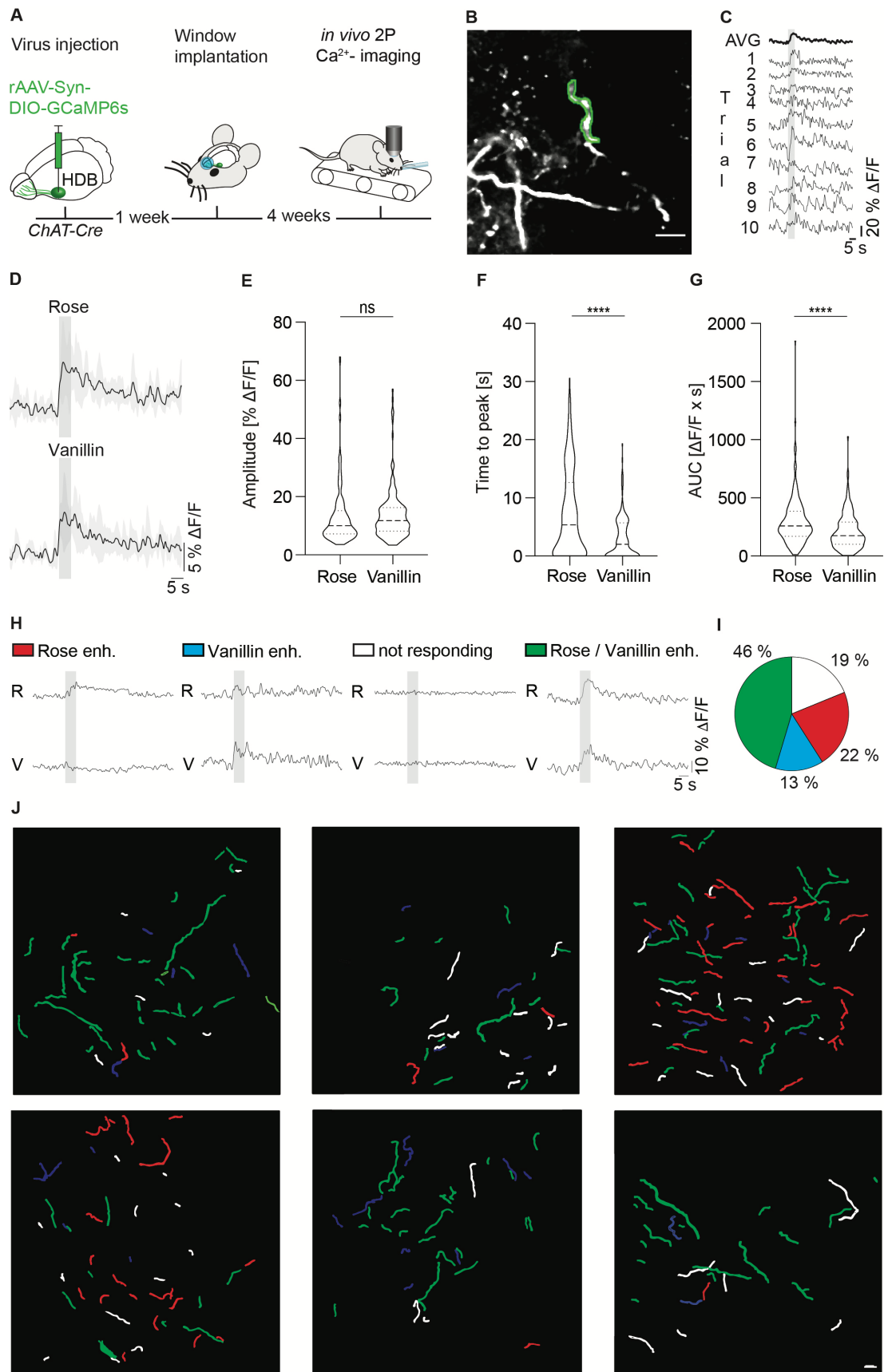


FIGURE 3.5. Cholinergic odor-tuned projections from the HDB. (A) Schematic illustration of experimental timeline with AAV-syn-GCaMP6s injection into the HDB, OB window implantation and awake head-fixed recording of Ca^{2+} -changes in the olfactory bulb during odor

stimulation. **(B)** Exemplary average intensity projection of *in vivo* time-lapse of afferent HDB-projection in the OB expressing GCaMP6s approx. 100 μm below brain surface. **(C)** Ca^{2+} -transients recorded from the green ROI in (B) in response to rose odor stimulation (gray bar) and 10-trial average (AVG). **(D)** Grand average of all Ca^{2+} -transients in all 317 ROIs from $n=6$ mice upon rose or vanillin odor stimulation. **(E-G)** amplitude **(E)**, time to peak **(F)** and area under the curve (AUC) **(G)** of ROIs representing odor-tuned axons ($n=183$ for rose and $n=164$ ROIs in 6 mice). **(H)** Exemplary 8-trial average Ca^{2+} -transients with response classification according to their Ca^{2+} -responses to rose (R) or vanillin (V) odor. Classes are: rose enh. (red), not responding (white), vanillin enh. (cyan), rose & vanillin enh. (green). **(I)** Fraction of axons according to their classification. **(J)** Spatial distribution of ROIs according to their classification. All data represented as mean \pm SEM (transients) or median \pm quartiles (violin plots). Scale bar 20 μm .

3.4. GABAergic odor-tuned HDB axons in the OB

Another HDB neuron population innervating the OB are GABAergic neurons. Cell type-specific expression of GCaMP6s was achieved using the Gad2-Cre mouse line. This mouse line expresses the Cre-recombinase specifically in GABAergic neurons under the *Gad2*-promotor. Stereotactic injection into the HDB of Gad2-Cre mice with an AAV containing a loxP-flanked expression cassette for GCaMP6s enabled the targeted labeling of GABAergic HDB neurons (FIG. 3.6 A). After implantation of a cranial window above the OB, GABAergic HDB axons within the OB were recorded during repeated odor stimulation (FIG. 3.6 B, C). During each recording session axons were stimulated with repeated rose odorant application followed by repeated presentation with vanillin odorant. The recorded GABAergic axon segments were analyzed with regard to their response properties to the applied odorants as described in paragraph 3.2 (FIG. 3.2, 3.3). This approach facilitated the identification of odor-sensitive GABAergic axons in the GL (FIG. 3.6 A, B). GABAergic HDB axons, similar to cholinergic axons showed a reliable change in fluorescence upon odor stimulation (FIG. 3.6 C). Remarkably, the majority of GABAergic axon segments exhibited suppressed Ca^{2+} -transients when stimulated with rose or vanillin odor. The grand average of all analyzed axon segments was a suppressed Ca^{2+} -transient for rose or vanillin odor stimulation (FIG. 3.6 D). In accordance with this, the trial-averaged Ca^{2+} -transients exhibited by individual GABAergic axons also show a negative median for amplitude maxima. The amplitude minima measured in trial-averaged Ca^{2+} -transients in response to rose stimulation were significantly different to amplitude values measured upon vanillin stimulation (median -8.2 ± 6.9 % $\Delta\text{F}/\text{F}$ rose vs -6.6 ± 5.3 % $\Delta\text{F}/\text{F}$ vanillin, $**p = 0.0055$) (FIG. 3.6 E). The time to peak

of Ca^{2+} -transients measured upon vanillin stimulation was significantly faster compared to rose stimulation (median: 4.9 ± 3.1 s rose and 3.1 ± 3.5 s vanillin; *** $p = 0.0002$) (FIG. 3.6 F). Also, the area under the curve values (AUC) measured upon rose compared to vanillin differed significantly (median: 48.2 ± 69.5 % $\Delta F/F^*s$ rose and 33.5 ± 55.6 % $\Delta F/F^*s$ vanillin; *** $p = 0.0005$) (FIG. 3.6 G).

The GABAergic HDB axons exhibited odor-evoked responses, which fell into the same categories as described for cholinergic and cell type-unspecific HDB axons in the previous paragraphs 3.2 and 3.3. Thus, GABAergic HDB axon segments displayed changes in Ca^{2+} -levels in response to either rose or vanillin, consecutively to both odors or none of the used odorants. Furthermore, the odor-evoked responses of GABAergic HDB axons displayed the two response modes of enhanced and suppressed Ca^{2+} -transients as were shown for the cell type-unspecific HDB axons in paragraph 3.2. Interestingly, 85 % of GABAergic HDB axons exhibited suppressed Ca^{2+} -transients upon odor stimulation. 16 % of GABAergic axon segments displayed a decrease in fluorescence upon rose odor stimulation, while not showing a response to vanillin (Rose suppr). A smaller subset of 1 % of GABAergic axon segments fall into the category of suppressed vanillin odor responders, which do not respond to rose odor stimulation (Vanillin suppr). Decrease in fluorescence upon consecutive stimulation with rose followed by vanillin odor stimulation was detected in 68 % of axon segments (Rose / Vanillin suppr.). Very few axon segments were enhanced upon odor stimulation. 2 % of GABAergic axon segments showed increase in fluorescence upon consecutive rose and vanillin odor stimulation (Rose / Vanillin enh.). GABAergic axon segments displaying enhanced Ca^{2+} -transients solely upon stimulation with rose, but not vanillin, constitute 3 % of analyzed axon segments (Rose enh.). 2 % of GABAergic axon segments had increased Ca^{2+} -levels in response to vanillin odor stimulation, while their Ca^{2+} -levels were unchanged by stimulation with rose (Vanillin enh.). Only 9 % of GABAergic axon segments were unaffected by odor stimulation with either rose or vanillin odor (FIG. 3.6 H, I).

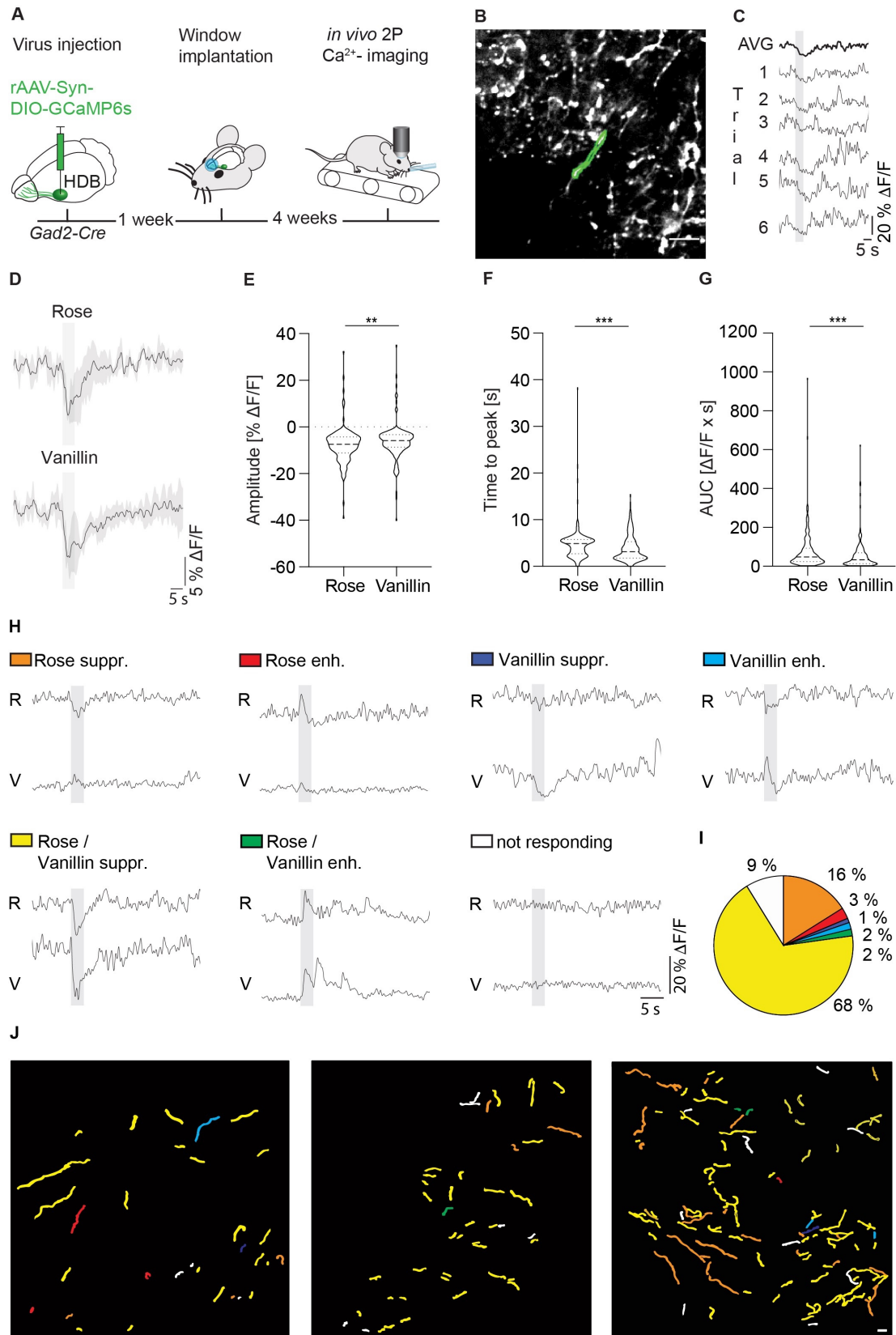


FIGURE 3.6. GABAergic odor-tuned projections from the HDB. (A) Schematic illustration of experimental timeline with AAV-Syn-DIO-GCaMP6s injection into the HDB, OB window implantation and awake head-fixed recording of Ca²⁺-changes in the olfactory bulb during odor stimulation. **(B)** Exemplary average intensity projection of *in vivo* timelapse of afferent HDB-projection in the OB expressing GCaMP6s approx. 100 μm below brain surface. **(C)** Exemplary individual Ca²⁺-transients of the green ROI in response to rose odor stimulation (gray bar) and

6-trial average (AVG). **(D)** Grand average of all Ca^{2+} -transients in 193 ROIs from $n=3$ mice upon rose or vanillin odor stimulation. **(E-G)** Amplitude **(E)**, Time to Peak **(F)** and Area under the curve (AUC) **(G)** of all ROIs representing odor-tuned HDB axons ($n=169$ ROIs for rose and $n=149$ ROIs for vanillin in 3 mice). **(H)** Exemplary 8-trial average Ca^{2+} -transients with response classification according to their Ca^{2+} -responses to rose (R) or vanillin (V) odor ($n=193$ ROIs in 3 mice). Classes are: rose up (red), not responding (white), vanillin up (cyan), rose & vanillin up (green). **(I)** Fraction of axons according to their classification. **(J)** Spatial distribution of ROIs according to their classification. All data represented as mean \pm SEM (transients) or median \pm quartiles (violin plots). Scale bar 20 μm .

The spatial distribution of GABAergic axon segments with different response properties again showed an intermingled pattern (FIG. 3.6 J). These results demonstrate that GABAergic HDB afferents are odor-tuned with 70 % of axon segments responding to both odors, while 22 % respond to only one of the applied odorants. The majority (85 %) of GABAergic HDB axons showed odor-evoked suppressed responses and only a small subset (7 %) of axon segments displayed enhanced responses. As demonstrated by the described experiments, the GABAergic population predominantly displays the characteristic decrease in fluorescence suggesting these fibers might be part of the suppressed population identified in the cell type-unspecific experiment described in 3.2.

3.5. Reduced glomerular activity upon HDB silencing with tetanus toxin

Parts of the following results have been published in:

Schwarz, I.*, Müller, M.*, Pavlova, I., Schweihoff, J., Musacchio, F., Mittag, M., Fuhrmann, M.*, and Schwarz, M.K.* (2020). The diagonal band of Broca continually regulates olfactory-mediated behaviors by modulating odor-evoked responses within the olfactory bulb. *bioRxiv*, 2020.2011.2007.372649.

*equal contribution of first and last authors.

The results outlined in the previous paragraphs (3.2-3.4) show the odor-tuning of cell type-unspecific, cholinergic and GABAergic HDB neurons innervating the GL. Thus, the disruption of HDB input to bulbar neurons probably effects odor-evoked activity in the glomeruli. To gain insights into how the lack of HDB innervation changes glomerular activity, Ca^{2+} -levels in glomeruli were

compared in mice with silenced HDB to glomerular activity in mice with unaffected HDB input. Glomerular activity was recorded in awake head-fixed *Thy1-GCaMP6f.GP5.5* expressing GCaMP6f in subsets of M/T cells in the OB including their dendrites reaching into the GL and forming glomeruli (FIG. 3.7 B). Silencing of the HDB was mediated through stereotactic injection with an AAV containing an expression cassette for the tetanus toxin (TeTn) light chain. Using two-photon *in vivo* Ca²⁺-imaging in Sham- and TeTn-treated *Thy1-GCaMP6f.GP5.5* mice enabled the analysis of glomerular activity in response to repeated odor stimulation. The mice were first stimulated with repeated application of rose followed by repeated presentation of vanillin odor as described in paragraph 3.2 (FIG. 3.2). Odor stimulation with rose or vanillin odor enhanced glomerular fluorescence in both Sham- and TeTn-treated animals. Interestingly, odor-evoked glomerular activity was reduced in mice after TeTn-treatment compared to sham-treated mice (FIG. 3.7 C, D, I). Comparing amplitude, time to peak and area under the curve measured in trial-averaged Ca²⁺-transients of individual glomeruli revealed significant decrease in these values upon rose odor stimulation in TeTn-treated compared to Sham-injected mice (amplitude median: 7.0 ± 15.8 % $\Delta F/F$ sham vs 5.1 ± 4.2 % $\Delta F/F$ TeTn, time to peak median: 4.3 ± 6.1 s sham vs 2.6 ± 2.7 s TeTn, AUC median: 41.00 ± 122.1 % $\Delta F/F*s$ veh vs 33.2 ± 28.5 % $\Delta F/F*s$ TeTn). Similar results were observed for time to peak and area under the curve measurements after vanillin odor stimulation (time to peak median: 5.0 ± 3.6 s sham vs 2.7 ± 3.5 s TeTn, AUC median: 43.30 ± 50.2 % $\Delta F/F*s$ veh vs 34.1 ± 31.6 % $\Delta F/F*s$ TeTn). Whereas, the amplitude measured upon vanillin odor stimulation was not significantly different in TeTn-treated mice compared to sham-treated mice (amplitude median: 6.50 ± 6.1 % $\Delta F/F$ sham vs 5.90 ± 4.4 % $\Delta F/F$ TeTn) (FIG. 3.7 D-L). Comparing the fraction of responding glomeruli when stimulated with rose or vanillin odor was not significantly different between sham- and TeTn-treated mice. However, the trend of reduced percentage of responding glomeruli after TeTn-treatment is obvious (FIG. 3.7 H, M). Summarizing, silencing the HDB impairs glomerular activity upon odor stimulation suggesting the enhancement of Mitral/Tufted cell activity through odor-tuned HDB input.

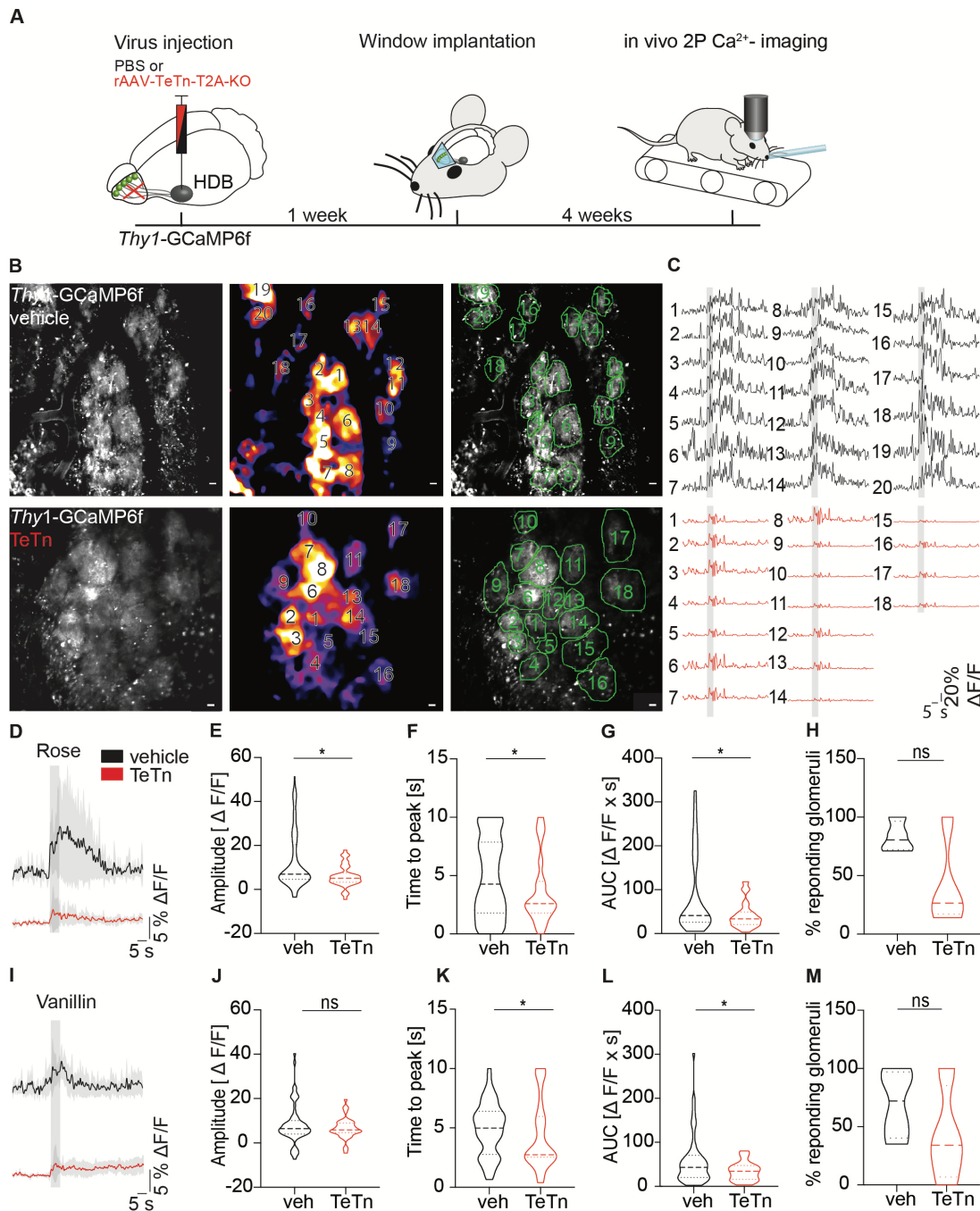


FIGURE 3.7. HDB silencing with tetanus toxin affects odor-evoked Ca²⁺-response in the OB. (A) Schematic illustration of experimental timeline with AAV-TeTn-T2A-KO injection into the HDB, OB window implantation and awake head-fixed recording of Ca²⁺-changes in the olfactory bulb during odor stimulation. (B) left: exemplary average intensity projection of a recorded time-lapse of GCaMP6f expressing glomeruli; middle: the same average intensity projection as in the left panel color-coded according to fluorescence intensity/pixel; right: the same average intensity projection as in the left with indicated ROIs identifying individual glomeruli. (C) Exemplary Ca²⁺-transients of ROIs indicated in B in response to rose odor stimulation in vehicle or TeTn-injected mice. (D) Grand average of all ROIs from n=4 vehicle and n=4 TeTn-injected mice upon rose odor stimulation. (E-H) Amplitude (E), Time to peak (F), Area under the curve (G) and percentage of responding glomeruli of vehicle-injected (n=103 ROIs in 4 mice) compared with TeTn-injected mice (n=107 ROIs in 4 mice). (I-M) Analog to (D-H) stimulated with vanillin odor. All data represented as mean \pm SEM and percentiles; Kolmogorov-Smirnov test (*p < 0.05); scale bars 20 μ m. (Parts of this figure have been published in (Schwarz et al., 2020)).

4. Discussion

Interpreting sensory information emanating from surrounding objects secures an organism's survival by allowing adequate reactions to food sources and mates, but also potentially hazardous threads. Important cues about the environment are encoded in olfactory information, which is received and processed initially in the olfactory bulb (OB), before being transferred to higher brain regions. The information processing performed in circuits of different OB neurons is modulated by centrifugal input originating from a variety of brain areas. One of those regions is the horizontal limb of the diagonal band of broca (HDB), which provides strong cholinergic, GABAergic and potentially glutamatergic innervation to diverse cell types in the OB. To understand the provided top-down modulation it is crucial to investigate odor-evoked activity in neurons of the HDB and its influence on activity of bulbar neurons. Few *in vivo* studies investigate the effect of manipulation of activity in HDB neurons on neuronal activity in the OB. Bendahmane and colleagues studied the effect of electrical HDB stimulation on glomerular Ca^{2+} -levels in a Ca^{2+} -imaging study in anesthetized mice. They revealed the odor concentration-dependent modulation of odor-evoked glomerular responses. The pharmacological activation of acetylcholine receptors (AChR) had a similar effect as electrical HDB stimulation implicating that the concentration-dependent modulation is mediated by cholinergic HDB input (Bendahmane et al., 2016). In a later study, the same group discovered that electrical HDB stimulation reverses habituation to an odor after continuing exposition. Prolonged odor presentation led to a rapid increase in GCaMP3 fluorescence followed by a steady decrease over the course of the odor stimulation. This decrease in Ca^{2+} -levels could be reversed by electrical HDB stimulation (Ogg et al., 2018). Also, the cell type-specific activation of HDB neurons modulates M/T cell activity. Activation of cholinergic HDB neuron somata sharpens odor-evoked M/T cell responses to certain odors (Ma and Luo, 2012). While the optogenetic activation of cholinergic HDB axons in the OB leads to overall increase of odor-driven M/T cell activity (Böhm et al., 2020; Rothermel et al., 2014). The optogenetic activation of GABAergic HDB axons in the OB enhances as well as suppresses

odor-evoked M/T cell activity. The majority of M/T cells increase odor-evoked firing rates during optogenetic stimulation of GABAergic HDB axons while a smaller group of M/T cells decrease odor-evoked firing (Böhm et al., 2020). These studies imply that the HDB is involved in processing of odor information in the OB. Thus, the question arises if HDB activity is tuned to odor input. Indeed, Devore and colleagues could show that HDB neurons increase firing rates on the population and single neuron level during active odor investigation (Devore et al., 2016). These studies suggest, that a subset of HDB neurons is responsive to odor input and modulates neuronal activity in the OB. However, the responses of HDB axons to odor-stimulation were so far never investigated. Since the optogenetic stimulation of cholinergic HDB somata compared to axons result in different modulation of M/T cell firing (Böhm et al., 2020; Ma and Luo, 2012; Rothermel et al., 2014), odor-evoked activity in HDB axons could differ from odor-evoked activity in HDB somata. This question is addressed in the presented study by investigating axonal Ca^{2+} -levels in awake, head-fixed mice. Furthermore, the presented study investigates odor-evoked axonal response characteristics of different HDB neuron/axon populations.

Additionally, the presented study for the very first-time reports changed odor-evoked glomerular activity after HDB manipulation compared to sham-treated mice in awake animals. Previous studies reporting changes in odor-evoked M/T cell and glomerular activity upon manipulation of the HDB were conducted in anesthetized mice (Bendahmane et al., 2016; Ogg et al., 2018). However, anesthesia reduces odor-evoked responses in periglomerular cells (PGCs), superficial short-axon cells (sSACs) and granule cells (GCs) and consequently enhances sensory-evoked responses in M/T cells in an inhalation independent manner. Furthermore, temporal dynamics of odor-driven activity in these cells are changed. The anesthesia related alteration in neuronal activity leads to inaccurate odor representation (Kato et al., 2012; Wachowiak et al., 2013). Therefore, odor-evoked neuronal activity is only accurately represented without anesthesia.

Monitoring axonal activity in different cell type-specific HDB axons in the OB was achieved in the presented study by employing *in vivo* two-photon Ca^{2+} -imaging in head-fixed, awake behaving mice. This approach offers further insight into odor-evoked responses in the HDB and allows conclusions about

the resulting effect on neurons in the OB. This approach enabled the simultaneous recording and subsequent analysis of multiple HDB axon segments within the glomerular layer (GL) of each mouse. Furthermore, the application of Ca^{2+} -imaging in head-fixed, awake mice ensures recording of axonal Ca^{2+} -levels without effects of anesthesia on neuronal activity. Taking advantage of this technique, the presented results for the very first-time revealed odor-evoked activity changes in HDB axons in the GL upon presentation of two different odorants (FIG. 3.4 C; FIG. 3.5 C; FIG. 3.6 C). These changes depended on the applied odorant molecules with HDB axons responding to consecutive stimulation with both odorants and other HDB axons responding specifically to either rose or vanillin. In the investigated cell type-unspecific, cholinergic and GABAergic HDB neuron populations the largest group of odor-tuned axon segments were responsive to both consecutively applied odorants (42 % of cell type-unspecific, 46 % of cholinergic and 70 % of GABAergic axon segments). HDB axon segments responding odor-specifically to only one of the applied odorants constituted 35 % of cell type-unspecific, 35 % of cholinergic and 22 % of GABAergic axon segments. Interestingly, a larger subset within these either rose- or vanillin-sensitive HDB axons in the cell type-unspecific population responded exclusively to vanillin (27 % vanillin responding segments vs. 8 % rose responding segments). Whereas a larger subset of HDB axons tuned to either rose or vanillin in the cholinergic and especially the GABAergic HDB neuron population was responsive to only rose, but not vanillin. In the cholinergic population 22 % of analyzed axon segments responded to rose, but not vanillin. Whereas 13 % of the cholinergic axon segments were vanillin- but not rose-sensitive. In the GABAergic axon population, 19 % of axon segments displayed changes in Ca^{2+} -levels exclusively upon rose stimulation. In contrast, 3 % of the GABAergic axon segments showed Ca^{2+} -responses to vanillin, but not rose odor stimulation (FIG. 3.4 H, I; FIG. 3.5 H, I; FIG. 3.5 H, I). Interestingly, the odor-evoked responses recorded in HDB axon segments showed both enhanced and suppressed response patterns. Thus, the same axon segments consistently displayed either positive or negative changes relative to baseline Ca^{2+} -levels upon stimulation with different odors (FIG. 3.4 H, I; FIG. 3.5 H, I; FIG. 3.6 H, I). Different subsets of the axon segments showed suppressed or enhanced Ca^{2+} -

transients in response to either rose or vanillin or consecutively to both odors. The investigation of different neuron populations revealed that HDB axons deriving from the same population exhibited predominantly the same response pattern (either suppressed or enhanced) (FIG. 3.4 D; FIG. 3.5 D; FIG. 3.6 D): cholinergic axons persistently displayed enhanced activity upon odor stimulation (FIG. 3.5 I), whereas GABAergic (FIG. 3.6 I) and cell type-unspecific (FIG. 3.4 I) HDB axons primarily showed suppressed odor responses. In the cell type-unspecific neuron population 69 % of analyzed axon segments displayed suppressed odor-evoked responses. Whereas 8 % showed enhanced Ca^{2+} -levels upon odor stimulation. The majority (85 %) of analyzed axon segments in the GABAergic HDB neuron population displayed suppressed odor-evoked responses upon odor stimulation and only 7 % showed enhanced responses. The high percentage of suppressed axons in the cell type-unspecific population suggests that HDB feedback fibers in the GL are mostly GABAergic with only a small percentage of cholinergic axons (FIG. 3.5 H, I; 3.6 H, I). As described above, a subset of HDB axons in all neuron populations were responsive upon consecutive stimulation with both odorants. These axon segments expressed either suppressed or enhanced responses to the two odorants. There was no subset of axon segments detected showing enhanced Ca^{2+} -transients in response to one odor and suppressed Ca^{2+} -transients upon stimulation with the other odor. This suggests a consistency in response patterns within one axon over different odors. HDB axon segments within the cell type-unspecific, cholinergic or GABAergic population expressing suppressed and enhanced odor-responsive activity were spatially intermingled in the recoded areas of the GL (FIG. 3.4 J; FIG. 3.5 J; FIG. 3.6 J). This implies that axons of different cell types have a diffuse innervation pattern in the OB. In the last experiment described, silencing HDB transmission with a stereotactic injection with an AAV containing an expression cassette for the tetanus toxin (TeTn) light chain resulted in significant attenuation of glomerular activity (FIG. 3.7). This finding revealed for the very first time the impairment of odor-evoked glomerular activity in absence of HDB input in awake mice. This suggest that the odor-driven input provided by the HDB is crucial for odor representation in the glomeruli.

4.1. GCaMP6s expression after stereotactic AAV-injection

Odor-evoked changes in axonal activity can be indirectly approximated by monitoring changes in cytosolic Ca^{2+} -levels. An action potential leads to increased Ca^{2+} -levels in the cytosol of neurons, which can be detected by Ca^{2+} -indicators. If the Ca^{2+} -indicators are linked to fluorescent proteins, the changes in Ca^{2+} -levels can be monitored using fluorescence microscopy. This technique is called Ca^{2+} -imaging. The application of two-photon-microscopy enabled Ca^{2+} -imaging in living tissue (Yuste and Denk, 1995). A popular class of Ca^{2+} -indicators are the very sensitive GCaMP6 proteins (Chen et al., 2013), which are also used in this study. For monitoring Ca^{2+} -levels in axon segments the highly sensitive variant GCaMP6s was chosen here. HDB-specific expression of GCaMP6s was achieved by stereotactic injection of an AAV containing an expression cassette for GCaMP6s. This specific transduction of neurons in the HDB was targeted to prevent contamination of the monitored axon population in the OB by projections deriving from other brain regions than the HDB. The GCaMP6s expression was examined in post-mortem brain slices imaged with a confocal microscope. When analyzing GCaMP6s expression after AAV injection, it was indeed observed that neurons throughout the whole HDB were transduced. Additionally, a few neurons in the adjoining brain regions olfactory tubercle (OT), hypothalamus (Hy), substantia innominate (SI), nucleus of the lateral olfactory tract (NLOT), anterior amygdala area (AAA), medial amygdala nucleus (MeA) and cortical amygdala area (CoA) were GCaMP6s positive (FIG. 3.1). This suggests that not only the HDB but also the OT, Hy, SI, NLOT, AAA, MeA and CoA were partially transduced after injection with an AAV containing an expression cassette for GCaMP6s. All of these regions extend projections into the granule cell layer (GCL) of the OB (MohedanoMorianio et al., 2012). Whereas the glomerular layer (GL) is only innervated directly by the anterior piriform cortex (APC), the anterior olfactory nucleus (AON) and the HDB (Wen et al., 2019). This suggests that the GCaMP6s positive axon segments detected and analyzed in the GL are indeed axon segments deriving from HDB neurons as was intended in this study. Summarizing, the stereotactic AAV injection despite a minor expression of GCaMP6s in the OT, Hy, SI, NLOT, AAA, MeA and CoA mainly infected HDB neurons. Furthermore, since the investigated GL does not receive input from

those erroneously injected regions, the monitored odor-sensitive axons derive from neurons in the HDB.

4.2. Odor-evoked activity in HDB axons

The HDB is a nucleus in the basal forebrain, whose neurons project to several layers in the OB and innervate various cell types. This top-down modulation regulates both spontaneous and odor-driven activity in neurons of the OB (Bendahmane et al., 2016; Böhm et al., 2020; Gracia-Llanes et al., 2010; Ma and Luo, 2012; Ogg et al., 2018; Rothermel et al., 2014; Sanz Diez et al., 2019). However, axonal responses to olfactory input in neurons of the HDB are only inadequately studied. One previous study recorded neuronal activity from somata in the HDB during active odor investigation (Devore et al., 2016). Devore and colleagues found that 14 out of 45 recorded HDB neurons show significant increase in firing rates. Further analysis revealed that 27 % of HDB neurons displayed changes in firing rate during short bouts of active sniffing. 75 % of these neurons increased firing rate during bouts of active sniffing. Whereas the remaining 25 % showed decreased activity (Devore et al., 2016). This electrophysiological study does not allow conclusions about odor-evoked activity changes in HDB axons and differences in responses of different cell types (GABAergic or cholinergic). The relevance of odor-evoked responses in HDB feedback axons in the OB becomes apparent by the different modulation of OB neurons after optogenetic stimulation of cholinergic HDB somata or axons: activation of cholinergic HDB somata sharpens M/T cell responses to different odors (Ma and Luo, 2012), whereas activation of cholinergic HDB axon within the OB increases odor-evoked M/T cell firing (Böhm et al., 2020; Rothermel et al., 2014). Thus, the presented experiments investigated HDB axon activity in the OB in correspondence with olfactory input utilizing *in vivo* two-photon Ca^{2+} -imaging. Moreover, the technique of *in vivo* two-photon Ca^{2+} -imaging in combination with cell type-specific labelling of HDB neurons allowed for the first time the analysis of odor-evoked activity in specific HDB neuron populations. It was found that a high proportion (78 % of all analyzed axon segments) of cell type-unspecific HDB fibers in the GL display reliable responses upon odor stimulation (FIG. 3.4 C, D). These odor-evoked responses in axon segments can be separated into two distinct response

modes: axon segments with suppressed or negative Ca^{2+} -transients and axon segments with enhanced or positive Ca^{2+} -transients (FIG. 3.4 H). Axons displayed consistently either suppressed or enhanced Ca^{2+} -transients upon stimulation with different odors. There was no group of axon segments observed changing between enhanced and suppressed Ca^{2+} -transients in response to different odors. This implies the existence of two separate groups of HDB feedback axons in the OB, one with suppressed odor-evoked changes in Ca^{2+} -levels and one with enhanced odor-evoked changes in Ca^{2+} -levels (FIG. 3.4 H). The sensitivity to different odors varied for individual HDB axons with axon segments responding to only one or both separately applied odors. The two response modes (enhanced or suppressed) in combination with different odor-sensitivities to rose or vanillin creates six observed subsets of odor-tuned HDB axons. The first subset of HDB axon segments responded with enhanced Ca^{2+} -transients to rose, but not vanillin odor stimulation (Rose enh.). This subset constituted 2 % of cell type-unspecifically labeled HDB axon segments. The second subset of axon segments responded with enhanced Ca^{2+} -transients to vanillin, but not rose stimulation (Vanillin enh.). Within the cell type-unspecifically labeled HDB neuron population 4 % of axon segments are part of the second subset. The third subset of axon segments responded with enhanced Ca^{2+} -transients consecutively to rose followed by vanillin stimulation (Rose/ Vanillin enh.). 2 % of cell type-unspecifically labeled HDB axon segments were classified as this third subset. The fourth subset of axon segments responded with suppressed Ca^{2+} -transients to rose, but not vanillin stimulation (Rose suppr.), which constituted 6 % of cell type-unspecifically labeled HDB axon segments. The fifth subset of axon segments responded with suppressed Ca^{2+} -transients to vanillin, but not rose stimulation (Vanillin suppr.). 23 % of axon segments within the cell type-unspecific HDB neuron population were classified as this fifth subset. The sixth subset of axon segments responded with suppressed Ca^{2+} -transients consecutively to rose followed by vanillin stimulation (Rose/ Vanillin suppr.) and constituted 40 % of cell type-unspecifically labeled HDB axon segments (FIG. 3.4 H, I). The odor-sensitive response modes are similar to those described for axonal boutons in the GL and GCL deriving from the anterior piriform cortex (APC) (Otazu et al., 2015). APC boutons in the OB exhibit the same distinct suppressed and enhanced

response modes while being odor-specific. In the OB approx. 55 % of responding boutons deriving from the APC exhibit suppressed and approx. 40 % enhanced response patterns. In the present study, a majority of 69 % of the analyzed cell type-unspecific HDB axons tuned to the presented odors fell into the suppressed group, while 8 % fell into the enhanced group (FIG. 3.4 J). Both studies report that the majority of recorded feedback axons exhibit suppressed response patterns. Thus, in HDB as well as APC boutons exhibited reduced activity in response to olfactory input. As the GABAergic HDB axons also exhibited this characteristic suppression of Ca^{2+} -levels upon odor stimulation (FIG. 3.6), it can be assumed that the suppressed HDB and possibly APC boutons are GABAergic. Consequently, olfactory input reduces inhibitory feedback to the OB. It can be excluded that the reduction in GCaMP fluorescence is caused by an experimental artifact known as z-shift, where movement of the specimen causes a disruption of the time-lapse and displacement of the focus plane. All imaging series including movement artifacts were excluded from the analysis (see 2. Methods). Additionally, Otazu and colleagues proofed the ability of suppressed boutons to exhibit increased fluorescence (Otazu et al., 2015). Electrical stimulation in the APC paired with odor stimulation induced a switch in response modality to enhancement in otherwise suppressed boutons. Subsequently, decreasing fluorescence is not a consequence of indicator saturation, but visualizes real suppressed activity in certain odor responding cells (Otazu et al., 2015).

Otazu and colleagues describe that approx. 95 % of APC boutons are odor-tuned (Otazu et al., 2015), while the presented dissertation detects 77 % of axon segments in the cell type-unspecific HDB neuron population as odor-tuned. This dissimilarity could result from different odor sets used in the two studies. Otazu and colleagues applied 20 different odors, which could activate a larger group of boutons. In the present study, only two odors were tested, presumably activating a smaller set of axons. However, the bimodal modulation of bulbar odor responses described in the present work for the HDB appears to have some similarities to the bimodal APC modulation. Otazu and colleagues surmise that the duality of enhancement and suppression in odor-evoked responses of APC boutons facilitates increased flexibility in cortical feedback to the OB. This feedback might modulate specific subsets of OB interneurons to

emphasize behaviorally relevant odors (Otazu et al., 2015). This mechanism might also be employed by HDB feedback axons to the OB. The enhanced and suppressed odor-evoked responses in HDB axons reported in this study might differentially modulate odor-driven activity in bulbar neurons. This modulation might result in enhancement and suppression of odor-evoked glomerular activity. The pattern of glomerular activity encodes odor identity and also shows the duality of enhanced and suppressed activity in responses to olfactory input. Contrary to boutons, dendritic mitral cell (MC) tufts interchange the two response modalities in an odor-specific manner (Economo et al., 2016). Economo and colleagues hypothesized that inhibitory glomerular interneurons shape the suppression of some glomeruli upon stimulation with specific odors. Many adjacent glomeruli exhibited the same response modality to odorants, which could be influenced by a network of short-axon cells (SACs) connecting these glomeruli and inhibiting external tufted cells (ETCs) (Economo et al., 2016). The inhibition of glutamatergic ETCs would lead to lack of excitation throughout innervated glomeruli and thus, accounts for the suppression of spontaneous and sensory-evoked activity. Cholinergic HDB projections directly innervate ETCs (D'Souza et al., 2013) and reflect the odor-sensitive and highly selective response characteristics in glomeruli (FIG. 3.4). Furthermore, previous studies showed that centrifugal input from the HDB modulates odor-evoked M/T cell and glomerular activity (Bendahmane et al., 2016; Böhm et al., 2020; D'Souza et al., 2013; D'Souza and Vijayaraghavan, 2012; Ma and Luo, 2012; Ogg et al., 2018; Rothermel et al., 2014). Therefore, HDB input could be involved in odor-specific suppression and enhancement of sensory-evoked glomerular responses. The odor-evoked activity in HDB axons could drive further excitation of ETCs and Mitral- and Tufted cell (M/T) dendritic tufts and subsequently enhance activity in the glomeruli. Furthermore, cholinergic HDB neurons directly innervate PGCs, which drive inhibition in the glomeruli. Hence, odor-selective suppression of glomerular activity could be driven by top-down modulation activating inhibitory interneurons. Odor identity is encoded in glomerular activity. Shaping this response pattern through suppression and enhancement of glomerular and M/T cell activity could be one mechanism for the increase of HDB mediated odor discrimination abilities described before (Nunez-Parra et al., 2013; Smith et al., 2015). The odor-evoked enhanced and

suppressed responses in HDB axons possibly bimodally modulates glomerular responses in an odor-specific manner and thereby heightens the differences in odor representation of different odors. The information relayed to cortical regions processing the information about odor identity will be refined in this model. Consequently, odor discrimination would be improved. However, the exact involvement of HDB feedback innervation in suppression and enhancement of odor-evoked glomerular activity needs to be further investigated. This could be achieved by additional monitoring of OB cell activity in parallel to monitoring of HDB axons.

The recorded changes in Ca^{2+} -transients displayed by cell type-unspecifically labeled HDB axons did show similar amplitudes and area under the curve values upon stimulation with both tested odorants. While the time to peak values measured upon rose or vanillin stimulation did show significant difference. This suggests, that axons of the cell type-unspecific HDB neuron population respond with similar intensity but varying time scales to different odors. The difference in time to peak values measured upon rose compared to vanillin stimulation could represent odor-specific response characteristics displayed by cell type-unspecifically labeled HDB axons. Another reason could be that odor-evoked responses in HDB axons are shaped by odor-concentration. The rose odorant solution used for stimulation in the presented experiments had a concentration of 8.2 M. The vanillin solution however had a concentration of 59 mM. These different odor concentrations might be reflected by the diverging time to peak values. However, to further investigate this question, additional experiments with more varying odor concentrations would be necessary.

77 % of all analyzed axon segments of the cell type-unspecific HDB neuron population were responsive to either rose or vanillin or both odors (FIG. 3.4 M). Thus, most HDB axons seem to be odor-sensitive. Since the presented study only tested for two odors, it cannot account for the not responding axons. These axons might be unresponsive to odor stimulation. Another possibility is that those HDB axons are sensitive for not tested odors. Hence, there is the possibility that all HDB axons are odor-responsive. 42 % of all analyzed HDB axon segments of the cell type-unspecific HDB neuron population are responsive to both odors (FIG. 3.4 I). This suggests that almost half of all HDB

axons of the cell type-unspecific HDB neuron population in the OB are broadly tuned to more than one odor, possibly even to a varied set of odorants.

The presented study also investigated the spatial distribution of cell type-unspecifically labeled HDB axon segments according to their different odor-evoked response properties. This analysis aimed to evaluate if axon segments with the same response properties are located in proximity to each other possibly adhering to an odotopic distribution. For this purpose, the HDB axon segments depicted in the average intensity projection of their respective acquired time-lapses were color-coded according to their response specifications. Interestingly, the axons of the cell type-unspecific HDB neuron population showing diverse response modalities and specificity for different odors were spatially intermingled seemingly deviating from the usual odotopic structure of glomeruli. Several facts could account for this distribution. On the one hand, the HDB feedback axons could be responsive to a variety of odors. In the presented results, 42 % of analyzed axon segments were responsive to both applied odorants (FIG. 3.4 H, I). These axons possibly are responsive to more than two odors, which could not be determined with the limited set of used odorants. HDB projections responding to various odors would innervate several glomeruli responding to the different odors. Thus, the projections would be spread out throughout a diverse set of glomeruli and within the GL. The categorization after stimulation with only two odors neglects all other odorants the analyzed axons could respond to. Thus, a possible odotopic structure of HDB axons innervating the glomeruli would not be detected. Additionally, a single odor can activate a range of glomeruli distributed in the dorsal OB (Soucy et al., 2009). The glomeruli activated by one specific odor are not necessarily adjacent. If the innervating HDB fibers were distributed according to odor specificity within those glomeruli, their location would be rather distant from axons responding to the same odor. Thus, the axon segments with different response classes would be intermingled.

On the other hand, as explained before, HDB projections appear to be involved in enhancement, but also in suppression of odor-evoked activity in glomeruli. Therefore, the projections need to innervate not only glomeruli showing enhanced activity patterns after sensory input, but also those exhibiting suppressed activity patterns. The odotopic structure postulated for the GL is

based on odor-evoked increases in glomerular activity and consequently does not account for suppressed glomeruli. Thus, HDB axons facilitating suppression of glomerular activity will spatially diverge from the odotopic structure, which is reflected in the presented results.

The odor information input necessary for sensory-evoked neuronal responses in HDB neurons needs to be relayed through other olfactory structures. A closed feedback loop involving the OB, piriform cortex (PC), and HDB was proposed to regulate ACh input to the olfactory system (de Almeida et al., 2016). This is supported by anatomical studies showing direct connectivity from PC and OB cells to the HDB (Do et al., 2016; Hu et al., 2016). And indeed, electrical stimulation of principal neurons in the PC and the lateral olfactory tract (LOT), which contains M/T cell projections, induces responses in neurons in the medial HDB (Linster and Hasselmo, 2000). These finding suggests transmission of odor related information to the HDB from the PC and OB. This circuit possibly transmits odor-driven activity to HDB neurons and subsequently induces the odor-evoked responses in HDB axons in the OB (FIG. 3.4). In this model, olfactory information is relayed from the OB is either directly or indirectly through the PC to the HDB, which in turn modulates odor processing within the OB.

Newer findings suggest, the innervation of OB projecting HDB neurons by the paraventricular nucleus (PVN) and the supraoptic nucleus of the hypothalamus (Schwarz et al., 2020). These nuclei of the hypothalamus in turn receive direct sensory input from the OB (Bader et al., 2012). This feedback loop involving the OB, PVN and HDB seems to be important for social behavior. Thus the HDB seems to be important in the recognition of social odors and their effect on behavioral output interacting with conspecifics (Schwarz et al., 2020). It is tempting to speculate that socially related odors account for HDB axon activity in the same way as observed for rose and vanillin in this study, however this needs to be further investigated. Nevertheless, the presented results proof odor responsiveness of HDB neurons, which implies that those neurons are part of one or both of the described feedback loops.

4.3. Neuron type-specific innervation and differences in activity patterns

The previously discussed experiment verifies suppressed and enhanced odor-specific responses in cell type-unspecific populations of HDB axons in the OB (FIG. 3.4). It remains an open question, which neuron types in the HDB constitute the odor-tuned axons within the OB. The HDB is composed of cholinergic (Armstrong et al., 1983), GABAergic (Panula et al., 1984) and glutamatergic neurons (Manns et al., 2001). The cholinergic (Price and Powell, 1970c) and GABAergic (Záborszky et al., 1986) neuron populations are shown to not only project to the OB, but also modulate odor-driven behavior (Nunez-Parra et al., 2013; Smith et al., 2015). To investigate the influence of different neuron types on activity within the OB, it is important to examine these populations individually. This goal was achieved by employing cell type-specific Chat-Cre and GAD2-Cre mouse lines and by monitoring odor-driven axonal activity changes in the different populations. The presented results demonstrate odor-tuning of cholinergic and GABAergic HDB axons (FIG. 3.4, 7, 8) with similar response characteristics as the cell type-unspecific axon segments.

In the cholinergic population 81 % of axons showed reliable odor-driven activity changes. Remarkably, all responding axons exhibited an enhanced response pattern (FIG. 3.5 D, H). This suggests that some of the 8 % axon segments with an enhanced response in the cell type-unspecific population of odor-tuned HDB axons (FIG. 3.4 I) might in fact represent cholinergic axons releasing ACh in the OB. Cell type-unspecifically labeled axon segments could not be simultaneously labeled according to their neuron type as well as odor-evoked response characteristics. Thus, it is not possible to determine the exact proportion of cholinergic neurons within the odor-tuned cell type-unspecifically labeled HDB axons displaying enhanced Ca^{2+} -transients. Since glutamatergic HDB projections to the OB were not analyzed, it cannot be excluded that they also contribute to the observed fraction of axons exhibiting enhanced response patterns. However, since the majority of excitatory neurons in the HDB are cholinergic (Brashear et al., 1986; Kiss et al., 1990), it is reasonable to assume that the majority of axons with enhanced Ca^{2+} -transients derive from cholinergic HDB neurons.

The amplitude in Ca^{2+} -transients in cholinergic axons upon stimulation with rose or vanillin odor did not show significant difference, suggesting similar strength

in odor-evoked activity (FIG. 3.5 E). The significant difference in time to peak and AUC median values (FIG. 3.5 F, G) might depict odor-specific or concentration-dependent response characteristics of HDB axons. The odor-tuned axons might discriminate different odors by displaying the described dissimilarity in response characteristics. However, the dissimilarities could also arise from different concentrations of the used odorant concentrations (8.2 M rose vs. 59 mM vanillin solution). The HDB axons might display Ca^{2+} -transient with diverging characteristics in a concentration-dependent manner. However, as described above these questions cannot be definitely answered without further investigation of the concentration dependency of odor-evoked responses of cholinergic HDB neurons and axons.

The majority (46 %) of odor-sensitive cholinergic axons responded to both applied odors (FIG. 3.5 H, I). This suggests a sensitivity to a variety of odorants as already discussed for the cell type-unspecific axon population. The spatial distribution of cholinergic axons with enhanced and suppressed odor-specific response patterns was intermingled (FIG. 3.5 J) as shown for the cell type-unspecific axon population (FIG. 3.4 J). This argues that cholinergic HDB innervations target a variety of glomeruli driven by a mixture of different odorants similar to cell type-unspecific projections.

These cholinergic projections terminate in the GL, external plexiform layer (EPL), mitral cell layer (MCL) and granule cell layer (GCL) in the OB innervating principal cells as well as a variety of interneurons. In the GL, cholinergic input excites ETCs and the dendritic tufts of MCs through the activation of nAChRs. Subsequent GABAergic PGC activation leads to feedforward inhibition of ETCs and MCs (Castillo et al., 1999; D'Souza et al., 2013). Ultimately, nAChR activation reduces MC firing, probably suppressing MC responses to weak sensory input (D'Souza and Vijayaraghavan, 2012). In the EPL, the activation of the M1 subtype of mAChRs inhibits MC firing through excitation of GABAergic GCs (Ghatpande et al., 2006; Pressler et al., 2007). Contrarily, the M2 subtype inhibits both GCs and MCs (Smith et al., 2015). *In vivo* activation of cholinergic HDB axons in the OB leads to increased odor-evoked M/T cell activity (Rothermel et al., 2014). The odor-sensitive activation of cholinergic axons shown in this study likely drives direct excitation of M/T cells to certain odors facilitating increase in odor-evoked responses (FIG. 3.5). Another *in vivo*

study shows, that the activation of cholinergic neurons in the HDB sharpens olfactory tuning of M/T cells (Bendahmane et al., 2016; Ma and Luo, 2012). The activation of AChR following odor-specific activity in cholinergic axons could play a role in enhancing or suppressing M/T cell responses to certain odors by either direct excitation of M/T cells or PGC and GC mediated feedforward inhibition of M/T cells. Either way, odor-specific responses in cholinergic axons shape odor-specific activity in M/T cells. Consequently, responses to certain odorants are more distinct and separated from each other. This neuromodulatory effect probably leads to improvement of odor discrimination abilities (Smith et al., 2015).

The investigation of HDB fibers in the OB of GAD2-Cre mice revealed GABAergic HDB axons to be odor-sensitive with predominantly suppressed, but also enhanced response pattern (FIG. 3.6) similar to cell type-unspecific axons (FIG. 3.4). In contrast to cholinergic fibers GABAergic axons primarily exhibited suppressed odor responses. As this group of neurons is unique in displaying suppressed response patterns, it can be assumed that they correspond to axons with suppressed Ca^{2+} -transients observed in the experiment with cell type-unspecific axon labeling. This is consistent with the finding that the majority of OB projecting HDB neurons are GABAergic (Záborszky et al., 1986). The current study identified a small subset of GABAergic axons with enhanced Ca^{2+} -transients among the large majority of axons with suppressed Ca^{2+} -transients. This result is in line with a recent study finding that the optogenetic activation of GABAergic HDB axons in the OB leads to a bimodal increase and decreased in M/T cell firing (Böhm et al., 2020). Enhanced GABAergic HDB projections in the GL inhibit PGCs (Gracia-Llanes et al., 2010; Sanz Diez et al., 2019) and drive disinhibition of M/T cells. On the other hand, the suppression of this mechanism leads to feedforward inhibition and decrease of M/T responses. Böhm and colleagues find the majority of M/T cells exhibit increased odor-evoked activity (28 % of units) and only a smaller group of cells show decreased odor-evoked (10 % of units) activity during optogenetic stimulation of GABAergic HDB axons (Böhm et al., 2020). The odor-specific bimodal modulation of GABAergic HDB axons could shape M/T cell activity to emphasize one odor over the other. This process would sharpen the odor responses and could account for increased odor discrimination

abilities observed after chemogenetic activation of GABAergic HDB cells (Nunez-Parra et al., 2013).

Furthermore, the presented results revealed that GABAergic HDB axon segments in the OB were responsive to either rose or vanillin odor or to consecutive stimulation with both odors. To further characterize the Ca^{2+} -transients displayed by GABAergic axon segments, the amplitude, time to peak and area under the curve were measured. All measured values did show significant difference when comparing values measured upon rose or vanillin stimulation (FIG. 3.6 E, F, G). As described for the cell type-unspecifically labeled and cholinergic HDB axons, these diverging Ca^{2+} -transient characteristics could depict odor-specific response properties or concentration dependency of responses displayed by odor-sensitive HDB axons. Odor-evoked responses displayed by GABAergic HDB neurons could be shaped by odor identity and thus show differences in the measurements characterizing the responses. On the other side, the differences in characteristics measured in the Ca^{2+} -transients could arise from variances in odor concentration. The odorant solutions used in this study were concentrated at 8.2 M for the rose odorant and 59 mM for the vanillin odorant. This dissimilarity in concentration might be depicted in varying response characteristics displayed by odor-sensitive GABAergic HDB axons.

The odor-tuned GABAergic HDB axons in the OB showed to be sensitive to one or both presented odors as described for the other investigated neuronal populations (FIG. 3.6 H, I). The most striking similarity to the cholinergic and cell type-unspecific axon populations is the responsiveness to both applied odors of a majority of axons (69 % of all axon segments). This again implies the sensitivity of GABAergic HDB axons to a variety of odors. The spatially intermingled distribution of axon segments with different response properties reflects the broad sensitivity. Since only two odors were used in this study, odor-evoked activity in GABAergic HDB axons to other odorants cannot be excluded. The GABAergic HDB axons are possibly responsive to a variety of odorants and consequently innervate glomeruli specific for different odorants. Thus, the axons only tested for their sensitivity to rose and vanillin do not depict the odotopic structure. The intermingled spatial distribution also suggests, the innervation of a variety of glomeruli responding to different odorants. The

modulation of a large number of glomeruli is indispensable for shaping the response to odor input and emphasize the activity pattern evoked by a certain odor.

The presented results suggest the involvement of both cholinergic and GABAergic HDB projections in promoting distinction of different odorants. The data presented in this dissertation implies an interplay of both innervations in shaping cellular activity in the OB to accentuate specific odors by contrasting effects on odor-evoked responses in different cell types. The odor-tuned axons releasing different neurotransmitters probably act within the same glomerular network to modulate M/T cell activity according to preferred odor output information. The cell type-unspecific axons with suppressed and enhanced odor-evoked activity were spatially intermingled in the recoded OB segments. The association of axons releasing a specific neurotransmitter with the two response modalities (enhanced cholinergic axons and predominantly suppressed GABAergic axons) suggests, that the distribution of acetylcholine and GABA releasing HDB axons in the OB is spatially intermingled. This implies the termination of the different neuron populations in the same and also neighboring glomerular microcircuits. Odor-driven ACh release from cholinergic HDB axons in the olfactory bulb on the one hand increases odor-evoked M/T cell firing by direct nAChR mediated excitation in the glomerular tuft and inhibition of GABAergic PGCs and sSACs (Rothermel et al., 2014). The dopaminergic sSACs, which provide interglomerular excitation to ETCs leading to reduction of glomerular firing, are inhibited directly through mAChR activation (Pignatelli and Belluzzi, 2008). This process drives excitation in connected glomeruli. On the other hand, nAChR mediated firing in dSACs, reaching into the GL inhibits TC activity (Case et al., 2017). Additionally, the activation of M1-type AChR increases GCs excitability and consequently lateral inhibition among M/T cells (Ghatpande et al., 2006) (FIG. 4.1 A). The enhanced lateral inhibition in itself could enhance odor-tuning of M/T cells (Ma and Luo, 2012). The GABAergic HDB projections target inhibitory PGCs, dSACs and GCs and putatively provide disinhibition to M/T cells (Gracia-Llanes et al., 2010; Sanz Diez et al., 2019). Odor-evoked suppression of Ca²⁺-levels in GABAergic HDB axons as described in the presented study might disrupt this disinhibition and lead to reduced M/T cell firing (FIG. 4.3 C). Most GABAergic axon segments

analyzed in this study exhibited suppressed response patterns upon odor stimulation. Thus, the GABAergic HDB input might predominantly reduce M/T cell activity. However, a small percentage of GABAergic axons exhibited enhanced odor responses. These axons possibly increase disinhibition and thus odor-driven M/T dendritic tuft activity (FIG. 4.3 B). Ultimately, the combined effect of odor-driven activity in cholinergic and GABAergic HDB axons could result in heightened activity in few M/T cells and attenuated activity in a broad range of M/T cells. Hence, divergence in activity patterns in response to different odors could be increased. The OB output neurons would relay the more divergent information to higher brain regions and facilitate odor discrimination.

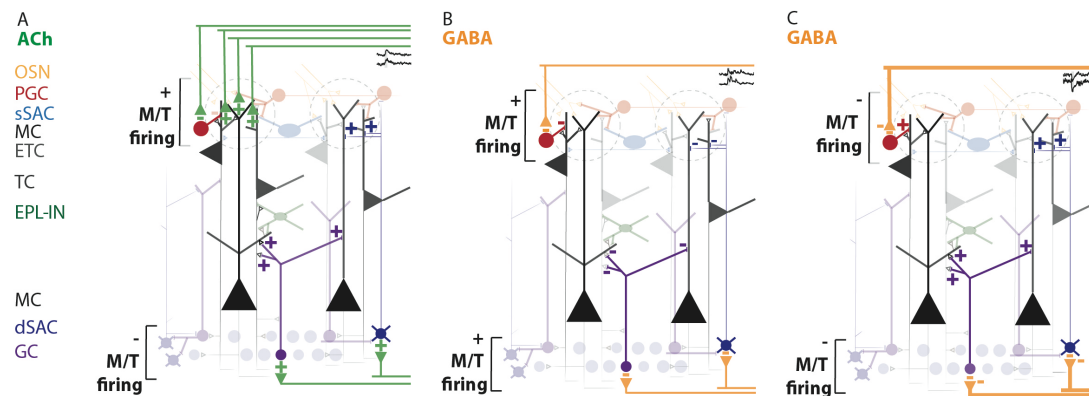


FIGURE 4.1. Hypothesized bimodal HDB modulation of M/T cell activity. (A) Effects of enhanced odor-evoked responses of cholinergic HDB input. (B) Effects of enhanced odor-evoked responses of GABAergic HDB input. (C) Effects of suppressed odor-evoked responses of GABAergic HDB input. Olfactory sensory neurons (OSN); periglomerular cells (PGC); superficial short-axon cells (sSAC); external tufted cells (ETC); tufted cells (TC); external plexiform layer interneurons (EPL-IN); mitral cells (MC); deep short-axon cells (dSAC); granule cells (GC).

4.4. HDB mediated modulation of glomerular activity

The composition and response patterns of different HDB neuron populations shaping the odor-evoked modulation of OB output neurons supposedly has a predominantly inhibiting effect on M/T cell activity. To further investigate the effect of HDB innervation on M/T cell activity, *in vivo* two-photon Ca^{2+} -imaging in awake head-fixed mice was employed to monitor odor-evoked glomerular responses after silencing the HDB. Silencing HDB transmission with stereotactic injection with an AAV containing an expression cassette for the tetanus toxin (TeTn) light chain resulted in significant attenuation of glomerular activity upon stimulation with both applied odors compared to glomerular activity in mice with intact HDB innervation (FIG. 3.7). The expression of the

Ca²⁺-indicator GCaMP6f in transgenic *Thy1-GCaMP6f* mice visualized glomerular activity in the presented experiment. These mice express GCaMP6f in neurons throughout the brain including M/T cells (Dana et al., 2014). Consistent with previous studies (Chaigneau et al., 2007; Fletcher et al., 2009; Wachowiak et al., 2013), consecutive stimulation with highly concentrated rose and vanillin odorants led to increase in fluorescence in glomeruli (FIG. 3.7 C). The odor stimulation activated numerous glomeruli, which is consistent with a correlation between numbers of recruited glomeruli and odor concentrations (Fried et al., 2002). When averaging Ca²⁺-transients of all recorded glomeruli the difference between sham- and TeTn-treatment became apparent (FIG. 3.7 D, I). This was confirmed by statistical analysis verifying the significant reduction in amplitude of Ca²⁺-transients during rose stimulation as well as differences in time to peak and area under the curve of Ca²⁺-transients upon stimulation with both odors. Amplitude values measured during vanillin stimulation did not show a significant difference in median, variance or distribution. The vanillin solution used in these experiments had a concentration of 59 mM, which is considerably lower compared to the undiluted 99% 2-Phenylethanol solution used for rose odor stimulation with a concentration of 8.2 M. Intensity of odor-evoked glomerular responses are directly correlated to odor concentration (Fried et al., 2002). Lower vanillin concentration could lead to weaker odor-evoked glomerular activity compared to rose stimulation. This could result in less pronounced differences between the sham- and TeTn-condition, that are not detected by the statistical tests used.

Interestingly, the percentage amount of responding glomeruli showed reduction in animals treated with TeTn compared to sham, even if not significant. The group sizes of 4 data points lower the power of statistical tests to detect significant differences. Nevertheless, the trend towards reduction in animals after HDB silencing is distinct (median: 81 % sham vs 27 % TeTn for rose, 72 % sham vs 34 TeTn % for vanillin). This comparison shows a less pronounced percentage reduction of responding glomeruli upon stimulation with vanillin odor. Since the number of activated glomeruli also positively correlates with odor concentration (Fried et al., 2002), the reduced number of activated glomeruli upon vanillin stimulation possibly again results from the less concentrated vanillin solution. Nevertheless, the reduced amount of responding

glomeruli after TeTn-silencing compared to sham-treatment seems to be a result of interrupted HDB innervation.

As described above, cholinergic HDB axons increase M/T cell and respectively glomerular activity (Böhm et al., 2020; Rothermel et al., 2014). The abolishment of HDB transmission through TeTn treatment prevents this enhancement of glomerular activity mediated by cholinergic HDB input. The presented results further indicate that the glomerular layer is predominantly innervated by GABAergic from the HDB. This feedback mainly terminates on inhibitory PGCs, dSACs, and GCs (Gracia-Llanes et al., 2010; Sanz Diez et al., 2019), and thus disinhibits M/T cells (Böhm et al., 2020). The elimination of HDB input possibly disrupts disinhibition. Thus, the GABAergic interneurons would drive stronger inhibition on glomeruli, which could induce further depletion of glomerular activity. Summarizing, silencing the HDB leads to impaired glomerular excitation and increased inhibition by inhibitory interneurons in the OB. Interference with M/T cell activity disrupts information about odor identity, which induces decrease in odor discrimination abilities shown after chemogenetic silencing of GABAergic HDB neurons (Nunez-Parra et al., 2013; Schwarz et al., 2020).

The expression of the light chain of tetanus toxin eliminates synaptic transmission from the targeted neurons (Sweeney et al., 1995). Consequently, injection into the HDB abolished innervation of all connected brain regions. The HDB projects to a variety of brain regions like the nucleus accumbens, lateral hypothalamus, central nucleus of the amygdala and PC (Do et al., 2016; Záborszky et al., 1986). The APC (Price and Powell, 1970b, c) and the lateral hypothalamus (Peyron et al., 1998) in turn directly innervate the OB. Hence, these brain regions could also be involved in the effect of TeTn mediated HDB silencing.

The optogenetic activation of pyramidal cells in the piriform cortex (PC) facilitates reduction of sensory-evoked M/T cell activity by activation of GCs, PGCs and sSAC (Balu et al., 2007; Boyd et al., 2012; Matsutani, 2010). Therefore, the reduced glomerular activity could be caused by activity of PC pyramidal neurons attenuating sensory-driven M/T cell activity. HDB innervation complexly modulates PC activity: Electrical stimulation of the HDB increases excitability in pyramidal neurons of the PC probably through

disinhibition within the cortical region (Zimmer et al., 1999). Furthermore, stimulation of the HDB increases di-synaptic EPSPs in APC neurons caused by activation of fibers within the PC after LOT stimulation while suppressing EPSPs in APC neurons evoked by stimulation of the posterior PC (Linster et al., 1999). Simultaneous electrical stimulation of the HDB and OB in the contrary decreases PC responses to OB input (Rosin et al., 1999). Silencing HDB transmission could cause disruption of odor-evoked activity in the PC and consequently effect bulbar excitation. Taking this information into account, it is possible that the lack of direct HDB innervation of OB cells in cooperation with the lack of modulation of PC neurons could cause the described attenuation of glomerular activity. However, the extensive innervation of the GL by odor-tuned HDB fibers (FIG. 2, 3, 4, 5) indicates a not negligible impact of M/T cell activity modulation provided by HDB axons. Our recent study investigating odor-driven behavior after selective light-mediated silencing of HDB axons in the OB. This investigation revealed impairment of odor habituation/ discrimination abilities as well as social behavior (Schwarz et al., 2020).

4.5. Conclusion and future experiments

In conclusion, the presented experiments reveal odor-evoked activity in axons deriving from neurons of the HDB and terminating in the GL. These axons are either broadly-tuned to both consecutively presented odors or specifically to one of the used odors. The HDB axon responses show both enhanced and suppressed activity patterns. This bimodal response pattern determined by the different neuron populations of the HDB characterizes the feedback to the OB. The majority of GABAergic HDB axons exhibited suppressed activity upon odor stimulation and only a small percentage of GABAergic showed enhanced odor-evoked response patterns. In contrast, cholinergic HDB axons exclusively showed enhanced response patterns upon odor stimulation. Thus, GABAergic neurons possibly account for the majority of the predominantly suppressed axons in the cell type-unspecifically labeled axon population. This work for the first time directly shows that GABAergic HDB axons predominantly display suppressed activity, whereas cholinergic HDB axons are responding with enhanced activity upon odor stimulation. Hence, the distinct HDB neuron

population innervating the OB have different modulatory effects on bulbar activity.

Interestingly, the majority of axons investigated in the different HDB neuron populations showed odor-evoked responses either to only one of the presented odors or to consecutive stimulation with both odors. These odor-tuned projections probably innervate a broad set of bulbar microcircuits and modulate their odor-evoked activity in a bimodal fashion. This generates a spatially intermingled pattern of suppressed and enhanced axons with specificity towards different odors. The bimodal HDB modulation of odor-evoked M/T cell and GABAergic bulbar interneuron activity potentially enhances the response to certain odors and suppresses responses to other odors. On the one hand, cholinergic and enhanced GABAergic HDB innervations described here drive increased M/T activity (FIG. 4.1 A). Activation of nAChRs directly excites M/T cells. In contrast, mAChR activation inhibits sSAC as well as PGC driving disinhibition of ETCs and thus activation of M/T cells (Pignatelli and Belluzzi, 2008; Rothermel et al., 2014). GABA release from enhanced GABAergic HDB axons identified in the present study further disinhibit M/T cell activity through inhibition of PGCs, dSACs, and GCs (FIG. 4.1 B) (Gracia-Llanes et al., 2010; Sanz Diez et al., 2019). On the other hand, ACh and GABA release from HDB fibers in the OB also have a decreasing effect on M/T cell activity (FIG. 4.1 A, B). Hereby, activation of nAChRs on dSACs leads to inhibition of TCs (Case et al., 2017), while mAChR activation increases GC excitability, which potentiates lateral inhibition of M/T cells (Ghatpande et al., 2006; Ma and Luo, 2012). The odor-evoked suppression of GABAergic HDB input shown above disrupts the disinhibition of M/T cells (FIG. 4.1 C). Bulbar GABAergic PGCs, dSACs and GCs are no longer inhibited and therefore further suppress activity in M/T cells (Gracia-Llanes et al., 2010; Sanz Diez et al., 2019). Thus, the combination of odor-sensitive cholinergic and GABAergic HDB feedback innervation to the OB presented in this dissertation, modulate neuronal activity in bulbar neurons in a complex manner resulting in mixed suppression and enhancement of M/T cell activity. This mechanism of bimodal modulation presumably enhances the representation of certain odors while suppressing others and thus, promotes odor detection and discrimination.

The presented results indicate that a predominant proportion of OB innervating HDB projections are GABAergic with suppressed response patterns to odor input. As described above, the suppression of GABAergic HDB input disrupts disinhibition of M/T cells. Consequently, glomerular activity would be reduced by HDB feedback after receiving olfactory input. The suppression of GABAergic HDB input and consequent disruption of disinhibition mediated by GABAergic HDB feedback is modelled by silencing the HDB. This silencing of the HDB furthermore disrupts cholinergic transmission, which leads to lack of enhancement odor-evoked glomerular activity. These effects led to the observed overall reduction of glomerular activity upon odor stimulation after HDB silencing. However, the effect of modulatory HDB input on cellular activity in bulbar neurons is not directly measured in the presented results and can only be speculated on. The parallel monitoring of activity in HDB axons and OB neurons with Ca^{2+} -sensors of different colors could give direct insights into the effect of sensory-evoked odor-specific activity in HDB axons on bulbar neurons. The usage of optogenetic and chemogenetic manipulation of axonal activity in HDB neurons in combination with monitoring of bulbar neurons could provide further conclusions on the impact of activation or inactivation of HDB neurons on neuronal activity in the OB. Since these manipulations are reversible, a direct comparison between manipulation and normal state could be obtained. Uncovering the neuronal circuit driving odor-evoked responses in the HDB could provide further knowledge about the modulation of odor processing. This could be achieved by studying odor-evoked activity in the HDB and possible connected areas. The utilization of GRIN lenses in combination with microscopy or fiber photometry could enable the monitoring of cellular activity in those brain areas. These possible experiments could further advance our knowledge about the modulatory effect of the HDB on olfactory processing and corroborate the introduced hypothesis about bimodal modulation emphasizing certain odors.

5. Appendix

5.1. Abbreviations

5-HT	Serotonin
5-HT _{2A}	Serotonin receptor 2A
5-HT _{2C}	Serotonin receptor 2C
AAA	Anterior amygdala area
AAV	Adeno-associated virus
ACh	Acetylcholine
AChR	Acetylcholine receptor
aCoA	Anterior cortical amygdala
AMPA	α -amino-3-hydroxy-5-methyl-4-isoxazolepropionic acid
AON	Anterior olfactory nucleus
AONpe	Anterior olfactory nucleus pars externa
AP	Anterio-posterior
APC	Anterior piriform cortex
AUC	Area under the curve
AVG	Average
BF	Basal forebrain
Ca ²⁺	Calcium
CB	Calbindin
ChAT	Choline acetyltransferase
CoA	The cortical nucleus of the amygdala
CR	Calretinin
CRH	corticotropin-releasing hormone
DA	Dopamine
DA-D ₁ -like receptor	D1-like family of dopamine receptors
dAON	Dorsal anterior olfactory nucleus
DBB	Diagonal band of Broca
dSAC	Deep short-axon cell
DV	Dorso-ventral
EC	Entorhinal cortex

EPL	External plexiform layer
EPL-dSAC	External plexiform layer innervating deep short-axon cell
EPL-IN	External plexiform layer interneurons
ETC	External tufted cells
GaAsP PMT	Gallium arsenide phosphide photomultiplier tube
GABA	γ -aminobutyric acid
GABA _A receptors	γ -aminobutyric acid receptor A
GABA _B receptors	γ -aminobutyric acid receptor B
Gad2	Glutamate decarboxylase 2
GC	Granule cell
GCL	Granule cell layer
GCL-dSACs	Granule cell layer innervating deep short-axon cell
GECI	Genetically encoded calcium indicator
GL	Glomerular layer
GL-dSAC	Glomerular layer innervating deep short-axon cell
Glu	Glutamate
HDB	Horizontal limb of the diagonal band of Broca
Hy	Hypothalamus
i.p.	Intraperitoneal
IPL	Internal plexiform layer
iSAC	Intermediate short-axon cell
JGC	Juxtaglomerular cells
LC	Locus coeruleus
LEC	Lateral entorhinal cortex
LOT	Lateral olfactory tract
M/T cells	Mitral- and Tufted cells
M ₁ ACh receptor	Muscarinic acetylcholine receptor M1
M ₂ ACh receptor	Muscarinic acetylcholine receptor M2
mAChR	Muscarinic acetylcholine receptor
MC	Mitral cell
MCL	Mitral cell layer
MeA	Medial amygdala nucleus
ML	Medio-lateral

MSDB	Medial septum diagonal band
NA	Numeric aperture
nAChR	Nicotinic acetylcholine receptor
NaN ₃	Sodium azide
NE	Noradrenergic
NE β -receptor	Adrenergic receptor group beta
NLOT	Nucleus of the lateral olfactory tract
NMDA	N-methyl-D-aspartate
OB	Olfactory bulb
ORN	Olfactory receptor neuron
OT	Olfactory tubercle
PBS	Phosphate buffered saline
PC	Piriform cortex
pCoA	Posterolateral cortical amygdala
PFA	Paraformaldehyde
PGC	Periglomerular cells
PPC	Posterior piriform cortex
PV	Parvalbumin
ROI	Region of interest
s.c.	Subcutaneously
SEM	Standard error of the mean
sSAC	Superficial short-axon cells
SST	Somatostatin
Syn	Synapsin1
TC	Tufted cell
TeTn	Tetanus toxin
Thy1	thymus cell antigen 1
TT	Tenia tecta
VDB	Vertical limb of the diagonal band of Broca
veh	Vehicle
VGlut3	Vesicular glutamate transporter 3
VIP	Vasoactive intestinal peptide

5.2. Material

5.2.1. Consumables for surgeries

<i>Product</i>	<i>Product No.</i>	<i>Manufacturer</i>
<i>Disposable scalpels, sterile</i>	0505	Swann-Morton, Sheffield, UK
<i>Drill head</i>	H71 104 003	Gebr. Basseler, Lemgo, Germany
<i>Gel Etchant</i>	26684 E	Kerr, Salerno, Italy
<i>Gelatin sponge (GELITA-SPON®)</i>	GS-110	Gelita Medical GmbH, Eberbach, Germany
<i>Light-curable composite (GRADIA® DIRECT Flo)</i>	2358	GC Europe, Leuven, Belgium
<i>Sterile collection swabs (EUROTUBO®)</i>	300202	DeltaLab, Barcelona, Spain
<i>Sugi®Eyespear</i>	30601	Kettenbach, Eschenburg, Germany
<i>Two-component bonding agent (OptiBond™ FL)</i>	26684 E	Kerr, Salerno, Italy

5.2.2. Equipment for surgeries

<i>Product</i>	<i>Product No.</i>	<i>Manufacturer</i>
Dental drill	A755983	Schick, Schemmerhofen, Germany
Heating pad for mice (Rodent Warner X2)	53851	Stoelting Co., Wood Dale, USA
Injection needle (NanoFil™ syringe)	NF35BV-2	World Precision Instruments, Sarasota, USA
Isoflurane evaporator (UniVet-Porta T-8)	UV 170001-T8	Groppler Medizintechnik, Deggendorf, Germany
Injection system (NanoFil™)	NANOFIL	World Precision Instruments, Sarasota, USA
LED light source	CL 1500 ECO	Carl Zeiss AG, Oberkochen, Germany
Light-curing device, LED LN Junior RE/LE (3 axes)	210-1000000070-RE/LE	Luigs and Neumann, Ratingen, Germany
Micro Syringe Pump Controller (Micro4)	SYS-MICRO4	World Precision Instruments, Sarasota, USA
Microliter syringe		Hamilton, Reno, USA
Remote Control SM-7	200-100 900 9050	Luigs and Neumann, Ratingen, Germany
Stereomicroscope SZ 51	19320	Olympus, Tokyo, Japan
Stereotactic frame for mice	-	Custom build

Sterilizer, Steri 250	031100	Keller, Burgdorf, Switzerland
-----------------------	--------	-------------------------------

5.2.3. Equipment for tissue sectioning

<i>Product</i>	<i>Product No.</i>	<i>Manufacturer</i>
Automated Vibatome	VT1200 S	Leica, Nussloch, Germany

5.2.4. Equipment for in vivo imaging

<i>Product</i>	<i>Product No.</i>	<i>Manufacturer</i>
ITC-18 board	-	HEKA, Ludwigshafen/Rhein, Germany
Head bar	200-200 500 2135	Luigs and Neumann, Ratingen, Germany
Head bar adapter	200-200 500 2111	Luigs and Neumann, Ratingen, Germany
Head bar holder	200-200 500 2105-M	Luigs and Neumann, Ratingen, Germany
Head holding adapter for mice	MA-6N	Narishige Group, Tokyo, Japan
Linear treadmill	-	Custom build
Olfactometer	PHM-275	Med Associate Inc., Fairfax, USA

5.2.5. Microscopes

<i>Product</i>	<i>Product No.</i>	<i>Manufacturer</i>
Two-photon microscope parts	-	Thorlabs, Newton, USA
Titanium sapphire laser	-	Coherent, Inc., Santa Clara, USA
Galvo-Resonant Scanner	LSK-GR08/M	Thorlabs, Newton, USA
Electro-optic modulator	M350-105 + 302RM	ConOptics, Inc., Danbury, USA
Objective	CFI75 LWD 16XW	Nikon, Tokyo, Japan
Laser attenuator	-	Thorlabs, Newton, USA
GaAsP PMT	H7422-40, H6780-20	Thorlabs, Newton, USA
UMP3 Ultra Micro Pump	UMP3	World Precision Instruments, Sarasota, USA
LSM 900	-	Carl Zeiss AG, Oberkochen, Germany

5.2.6. Reagents

<i>Product</i>	<i>Product No.</i>	<i>Manufacturer</i>
2-Phenylethanol	P6134	Sigma-Aldrich, Darmstadt, Germany
Glucose 5%	11383011	B Braun, Melsungen, Germany
PFA (ROTI®-Histofix 10 %)	A146.3	Carl Roth GmbH + Co. KG, Karlsruhe, Germany
Phosphate buffered saline, PBS	A0964	AppliChem, Darmstadt, Germany
Sterile PBS (ROTI®Cell PBS CELLPURE®)	9143.1	Carl Roth GmbH + Co. KG, Karlsruhe, Germany
Vanillin	V1104	Sigma-Aldrich, Darmstadt, Germany

5.2.7. Anesthesia and medication

<i>Product</i>	<i>Product No.</i>	<i>Manufacturer</i>
Bepanthen®	-	Bayer, Lerverkusen, Germany
Dexamethasone 21-phosphate disodium salt	D1159-500MG	Sigma, Darmstadt, Germany
Isoflurane	07253744	Actavis, New Jersey, USA
Ketamin 10 % (Ketaminhydrochlorid)	-	Serumwerk Bernburg AG, Bernburg, Germany
Xylocain® (Lidocaine)	-	Aspen Pharma Trading Limited, Dublin, Ireland
Rompun® (Xylazinhydrochloride) 2%	KP09X0L	Bayer, Leverkusen, Germany
Temgesic® (Buprenorphinhydrochloride, 0.324 mg)	-	Reckitt Benckiser Healthcare, Kingston Upon Hull, UK
Metamizole (Metapyrin®)	-	Serumwerk Bernburg AG, Bernburg, Germany

5.2.8. AAVs

<i>Product</i>	<i>Product No.</i>	<i>Manufacturer</i>
AAV1-Syn-GCaMP6s	#100843	Addgene, Watertown, USA
AAV1-Syn-DIO-GCaMP6s	#100845	Addgene, Watertown, USA
AAV1/2-TeTn-T2A-KO	-	kind gift of Martin Schwarz, UKB, Bonn

5.2.9. Software

<i>Product</i>	<i>Manufacturer</i>
BioRender	BioRender, Toronto, Canada
Brain Explorer [®] 2	Allan Institute for Brain Science, Seattle, USA
GraphPad Prism 8	GraphPad Software, Inc., San Diego, USA
IGOR PRO Version 6.22a	WaveMetrics, Inc., Portland, USA
Illustrator CS5 Version 15.0.1	Adobe Systems Inc., San Jose, USA
ImageJ/FIJI	Wayne Rasband, NIH, Bethesda, USA
MATLAB [®]	Mathworks, Natick, USA
Microsoft [®] Excel Mac 2019	Microsoft Corp., Redmond, USA
Microsoft [®] Word Mac 2019	Microsoft Corp., Redmond, USA
ThorImageLS software	Thorlabs, Newton, USA
ZEN 2010	Carl Zeiss AG, Oberkochen, Germany

5.3. Contributions

Julia Steffen, Andrea Baral and Olga Sharma conducted genotyping for the used transgenic mouse lines ChAT-Cre, Gad2-Cre and *Thy1*-GCaMP6f. Furthermore, they executed perfusions and tissue sectioning for post-mortem tissue analysis. Fabrizio Musacchio created the MATLAB® analysis pipeline for analysis of Ca²⁺-imaging data. Manuel Mittag offered support for the categorization of axonal Ca²⁺-responses. Martin Schwarz and Inna Schwarz provided the AAV1/2-Tetn-T2A-KO as well as insights into stereotactic injections targeting the HDB. Falko Fuhrmann and Daniel Justus constructed the linear treadmill and provided technical advice.

6. References

Armstrong, D.M., Saper, C.B., Levey, A.I., Wainer, B.H., and Terry, R.D. (1983). Distribution of cholinergic neurons in rat brain: demonstrated by the immunocytochemical localization of choline acetyltransferase. *J Comp Neurol* 216, 53-68.

Astic, L., and Saucier, D. (1986). Anatomical mapping of the neuroepithelial projection to the olfactory bulb in the rat. *Brain Res Bull* 16, 445-454.

Aungst, J.L., Heyward, P.M., Puche, A.C., Karnup, S.V., Hayar, A., Szabo, G., and Shipley, M.T. (2003). Centre-surround inhibition among olfactory bulb glomeruli. *Nature* 426, 623-629.

Bader, A., Klein, B., Breer, H., and Strotmann, J. (2012). Connectivity from OR37 expressing olfactory sensory neurons to distinct cell types in the hypothalamus. *Frontiers in Neural Circuits* 6.

Balu, R., Pressler, R.T., and Strowbridge, B.W. (2007). Multiple Modes of Synaptic Excitation of Olfactory Bulb Granule Cells. *The Journal of Neuroscience* 27, 5621-5632.

Banerjee, A., Marbach, F., Anselmi, F., Koh, M.S., Davis, M.B., Garcia da Silva, P., Delevich, K., Oyibo, H.K., Gupta, P., Li, B., *et al.* (2015). An Interglomerular Circuit Gates Glomerular Output and Implements Gain Control in the Mouse Olfactory Bulb. *Neuron* 87, 193-207.

Bendahmane, M., Ogg, M.C., Ennis, M., and Fletcher, M.L. (2016). Increased olfactory bulb acetylcholine bi-directionally modulates glomerular odor sensitivity. *Sci Rep* 6, 25808.

Böhm, E., Brunert, D., and Rothermel, M. (2020). Input dependent modulation of olfactory bulb activity by HDB GABAergic projections. *Scientific Reports* 10, 10696.

Bonino, M., Cantino, D., and Sasso-Pognetto, M. (1999). Cellular and subcellular localization of gamma-aminobutyric acidB receptors in the rat olfactory bulb. *Neurosci Lett* 274, 195-198.

Boyd, A.M., Sturgill, J.F., Poo, C., and Isaacson, J.S. (2012). Cortical feedback control of olfactory bulb circuits. *Neuron* 76, 1161-1174.

Brashear, H.R., Zaborszky, L., and Heimer, L. (1986). Distribution of GABAergic and cholinergic neurons in the rat diagonal band. *Neuroscience* 17, 439-451.

- Brill, J., Shao, Z., Puche, A.C., Wachowiak, M., and Shipley, M.T. (2016). Serotonin increases synaptic activity in olfactory bulb glomeruli. *J Neurophysiol* 115, 1208-1219.
- Brinon, J.G., Alonso, J.R., Arevalo, R., Garcia-Ojeda, E., Lara, J., and Aijon, J. (1992). Calbindin D-28k-positive neurons in the rat olfactory bulb. An immunohistochemical study. *Cell Tissue Res* 269, 289-297.
- Brunert, D., Tsuno, Y., Rothermel, M., Shipley, M.T., and Wachowiak, M. (2016). Cell-Type-Specific Modulation of Sensory Responses in Olfactory Bulb Circuits by Serotonergic Projections from the Raphe Nuclei. *The Journal of Neuroscience* 36, 6820-6835.
- Burton, S.D. (2017). Inhibitory circuits of the mammalian main olfactory bulb. *J Neurophysiol* 118, 2034-2051.
- Burton, S.D., LaRocca, G., Liu, A., Cheetham, C.E.J., and Urban, N.N. (2017). Olfactory Bulb Deep Short-Axon Cells Mediate Widespread Inhibition of Tufted Cell Apical Dendrites. *The Journal of Neuroscience* 37, 1117-1138.
- Burton, S.D., and Urban, N.N. (2014). Greater excitability and firing irregularity of tufted cells underlies distinct afferent-evoked activity of olfactory bulb mitral and tufted cells. *The Journal of Physiology* 592, 2097-2118.
- Burton, S.D., and Urban, N.N. (2015). Rapid Feedforward Inhibition and Asynchronous Excitation Regulate Granule Cell Activity in the Mammalian Main Olfactory Bulb. *The Journal of Neuroscience* 35, 14103-14122.
- Cang, J., and Isaacson, J.S. (2003). In Vivo Whole-Cell Recording of Odor-Evoked Synaptic Transmission in the Rat Olfactory Bulb. *The Journal of Neuroscience* 23, 4108-4116.
- Case, D.T., Burton, S.D., Gedeon, J.Y., Williams, S.G., Urban, N.N., and Seal, R.P. (2017). Layer- and cell type-selective co-transmission by a basal forebrain cholinergic projection to the olfactory bulb. *Nat Commun* 8, 652.
- Castillo, P.E., Carleton, A., Vincent, J.-D., and Lledo, P.-M. (1999). Multiple and Opposing Roles of Cholinergic Transmission in the Main Olfactory Bulb. *The Journal of Neuroscience* 19, 9180-9191.
- Chaigneau, E., Tiret, P., Lecoq, J., Ducros, M., Knöpfel, T., and Charpak, S. (2007). The relationship between blood flow and neuronal activity in the rodent olfactory bulb. *The Journal of neuroscience : the official journal of the Society for Neuroscience* 27, 6452-6460.
- Chan, W., Singh, S., Keshav, T., Dewan, R., Eberly, C., Maurer, R., Nunez-Parra, A., and Araneda, R.C. (2017). Mice Lacking M1 and M3 Muscarinic

Acetylcholine Receptors Have Impaired Odor Discrimination and Learning. *Front Synaptic Neurosci* 9, 4.

Chaudhury, D., Escanilla, O., and Linster, C. (2009). Bulbar Acetylcholine Enhances Neural and Perceptual Odor Discrimination. *The Journal of Neuroscience* 29, 52-60.

Chen, T.-W., Wardill, T.J., Sun, Y., Pulver, S.R., Renninger, S.L., Baohan, A., Schreiter, E.R., Kerr, R.A., Orger, M.B., Jayaraman, V., *et al.* (2013). Ultrasensitive fluorescent proteins for imaging neuronal activity. *Nature* 499, 295-300.

Christie, J.M., Bark, C., Hormuzdi, S.G., Helbig, I., Monyer, H., and Westbrook, G.L. (2005). Connexin36 Mediates Spike Synchrony in Olfactory Bulb Glomeruli. *Neuron* 46, 761-772.

Clark, W.E. (1951). The projection of the olfactory epithelium on the olfactory bulb in the rabbit. *J Neurol Neurosurg Psychiatry* 14, 1-10.

Crespo, C., Blasco-Ibanez, J.M., Marques-Mari, A.I., Alonso, J.R., Brinon, J.G., and Martinez-Guijarro, F.J. (2002). Vasoactive intestinal polypeptide-containing elements in the olfactory bulb of the hedgehog (*Erinaceus europaeus*). *J Chem Neuroanat* 24, 49-63.

D'Souza, R.D., Parsa, P.V., and Vijayaraghavan, S. (2013). Nicotinic receptors modulate olfactory bulb external tufted cells via an excitation-dependent inhibitory mechanism. *Journal of Neurophysiology* 110, 1544-1553.

D'Souza, R.D., and Vijayaraghavan, S. (2012). Nicotinic Receptor-Mediated Filtering of Mitral Cell Responses to Olfactory Nerve Inputs Involves the $\alpha 3\beta 4$ Subtype. *The Journal of Neuroscience* 32, 3261-3266.

D'Souza, R.D., and Vijayaraghavan, S. (2014). Paying attention to smell: cholinergic signaling in the olfactory bulb. *Front Synaptic Neurosci* 6, 21.

Dana, H., Chen, T.-W., Hu, A., Shields, B.C., Guo, C., Looger, L.L., Kim, D.S., and Svoboda, K. (2014). Thy1-GCaMP6 transgenic mice for neuronal population imaging in vivo. *PloS one* 9, e108697-e108697.

de Almeida, L., Idiart, M., Dean, O., Devore, S., Smith, D.M., and Linster, C. (2016). Internal Cholinergic Regulation of Learning and Recall in a Model of Olfactory Processing. *Frontiers in Cellular Neuroscience* 10.

de Olmos, J., Hardy, H., and Heimer, L. (1978). The afferent connections of the main and the accessory olfactory bulb formations in the rat: an experimental HRP-study. *J Comp Neurol* 181, 213-244.

De Saint Jan, D., Hirnet, D., Westbrook, G.L., and Charpak, S. (2009). External tufted cells drive the output of olfactory bulb glomeruli. *J Neurosci* 29, 2043-2052.

Denk, W., Strickler, J., and Webb, W. (1990). Two-photon laser scanning fluorescence microscopy. *Science* 248, 73-76.

Devore, S., Pender-Morris, N., Dean, O., Smith, D., and Linster, C. (2016). Basal forebrain dynamics during nonassociative and associative olfactory learning. *Journal of Neurophysiology* 115, 423-433.

Do, J.P., Xu, M., Lee, S.H., Chang, W.C., Zhang, S., Chung, S., Yung, T.J., Fan, J.L., Miyamichi, K., Luo, L., *et al.* (2016). Cell type-specific long-range connections of basal forebrain circuit. *Elife* 5.

Dombeck, D.A., Graziano, M.S., and Tank, D.W. (2009). Functional clustering of neurons in motor cortex determined by cellular resolution imaging in awake behaving mice. *J Neurosci* 29, 13751-13760.

Economo, M.N., Hansen, K.R., and Wachowiak, M. (2016). Control of Mitral/Tufted Cell Output by Selective Inhibition among Olfactory Bulb Glomeruli. *Neuron* 91, 397-411.

Escanilla, O., Arrellanos, A., Karnow, A., Ennis, M., and Linster, C. (2010). Noradrenergic modulation of behavioral odor detection and discrimination thresholds in the olfactory bulb. *European Journal of Neuroscience* 32, 458-468.

Eyre, M.D., Antal, M., and Nusser, Z. (2008). Distinct Deep Short-Axon Cell Subtypes of the Main Olfactory Bulb Provide Novel Intrabulbar and Extrabulbar GABAergic Connections. *The Journal of Neuroscience* 28, 8217-8229.

Fletcher, M.L., Masurkar, A.V., Xing, J., Imamura, F., Xiong, W., Nagayama, S., Mutoh, H., Greer, C.A., Knöpfel, T., and Chen, W.R. (2009). Optical imaging of postsynaptic odor representation in the glomerular layer of the mouse olfactory bulb. *Journal of neurophysiology* 102, 817-830.

Fosque, B.F., Sun, Y., Dana, H., Yang, C.-T., Ohya, T., Tadross, M.R., Patel, R., Zlatic, M., Kim, D.S., Ahrens, M.B., *et al.* (2015). Labeling of active neural circuits in vivo with designed calcium integrators. *Science* 347, 755-760.

Fried, H.U., Fuss, S.H., and Korsching, S.I. (2002). Selective imaging of presynaptic activity in the mouse olfactory bulb shows concentration and structure dependence of odor responses in identified glomeruli. *Proceedings of the National Academy of Sciences* 99, 3222-3227.

Fukunaga, I., Berning, M., Kollo, M., Schmaltz, A., and Schaefer, A.T. (2012). Two distinct channels of olfactory bulb output. *Neuron* 75, 320-329.

Ghatpande, A.S., Sivaraaman, K., and Vijayaraghavan, S. (2006). Store Calcium Mediates Cholinergic Effects on mIPSCs in the Rat Main Olfactory Bulb. *Journal of Neurophysiology* 95, 1345-1355.

Gire, D.H., Franks, K.M., Zak, J.D., Tanaka, K.F., Whitesell, J.D., Mulligan, A.A., Hen, R., and Schoppa, N.E. (2012). Mitral cells in the olfactory bulb are mainly excited through a multistep signaling path. *J Neurosci* 32, 2964-2975.

Göppert-Mayer, M. (1931). Über Elementarakte mit zwei Quantensprüngen. *Annalen der Physik* 401, 273-294.

Gracia-Llanes, F.J., Crespo, C., Blasco-Ibanez, J.M., Nacher, J., Varea, E., Rovira-Esteban, L., and Martinez-Guijarro, F.J. (2010). GABAergic basal forebrain afferents innervate selectively GABAergic targets in the main olfactory bulb. *Neuroscience* 170, 913-922.

Grienberger, C., and Konnerth, A. (2012). Imaging calcium in neurons. *Neuron* 73, 862-885.

Gritti, I., Manns, I.D., Mainville, L., and Jones, B.E. (2003). Parvalbumin, calbindin, or calretinin in cortically projecting and GABAergic, cholinergic, or glutamatergic basal forebrain neurons of the rat. *Journal of Comparative Neurology* 458, 11-31.

Haberly, L.B., and Price, J.L. (1977). The axonal projection patterns of the mitral and tufted cells of the olfactory bulb in the rat. *Brain Res* 129, 152-157.

Hamilton, K.A., Heinbockel, T., Ennis, M., Szabo, G., Erdelyi, F., and Hayar, A. (2005). Properties of external plexiform layer interneurons in mouse olfactory bulb slices. *Neuroscience* 133, 819-829.

Hayar, A., Karnup, S., Ennis, M., and Shipley, M.T. (2004). External tufted cells: a major excitatory element that coordinates glomerular activity. *J Neurosci* 24, 6676-6685.

Hayar, A., Shipley, M.T., and Ennis, M. (2005). Olfactory bulb external tufted cells are synchronized by multiple intraglomerular mechanisms. *J Neurosci* 25, 8197-8208.

Hu, R., Jin, S., He, X., Xu, F., and Hu, J. (2016). Whole-Brain Monosynaptic Afferent Inputs to Basal Forebrain Cholinergic System. *Frontiers in Neuroanatomy* 10.

Huang, L., Garcia, I., Jen, H.-I., and Arenkiel, B. (2013). Reciprocal connectivity between mitral cells and external plexiform layer interneurons in the mouse olfactory bulb. *Frontiers in Neural Circuits* 7.

Huang, Z., Thiebaud, N., and Fadool, D.A. (2017). Differential serotonergic modulation across the main and accessory olfactory bulbs. *The Journal of Physiology* 595, 3515-3533.

Igarashi, K.M., Ieki, N., An, M., Yamaguchi, Y., Nagayama, S., Kobayakawa, K., Kobayakawa, R., Tanifuji, M., Sakano, H., Chen, W.R., *et al.* (2012). Parallel Mitral and Tufted Cell Pathways Route Distinct Odor Information to Different Targets in the Olfactory Cortex. *The Journal of Neuroscience* 32, 7970-7985.

Isaacson, J.S., and Strowbridge, B.W. (1998). Olfactory reciprocal synapses: dendritic signaling in the CNS. *Neuron* 20, 749-761.

Jacobowitz, D.M., and Winsky, L. (1991). Immunocytochemical localization of calretinin in the forebrain of the rat. *J Comp Neurol* 304, 198-218.

Jhamandas, J.H., and Renaud, L.P. (1986a). Diagonal band neurons may mediate arterial baroreceptor input to hypothalamic vasopressin-secreting neurons. *Neurosci Lett* 65, 214-218.

Jhamandas, J.H., and Renaud, L.P. (1986b). A gamma-aminobutyric-acid-mediated baroreceptor input to supraoptic vasopressin neurones in the rat. *The Journal of Physiology* 381, 595-606.

Jobsis, P.D., Rothstein, E.C., and Balaban, R.S. (2007). Limited utility of acetoxymethyl (AM)-based intracellular delivery systems, in vivo: interference by extracellular esterases. *J Microsc* 226, 74-81.

Kapoor, V., Provost, A.C., Agarwal, P., and Murthy, V.N. (2016). Activation of raphe nuclei triggers rapid and distinct effects on parallel olfactory bulb output channels. *Nature Neuroscience* 19, 271-282.

Kasa, P., Hlavati, I., Dobo, E., Wolff, A., Joo, F., and Wolff, J.R. (1995). Synaptic and non-synaptic cholinergic innervation of the various types of neurons in the main olfactory bulb of adult rat: immunocytochemistry of choline acetyltransferase. *Neuroscience* 67, 667-677.

Kato, Hiroyuki K., Chu, Monica W., Isaacson, Jeffrey S., and Komiyama, T. (2012). Dynamic Sensory Representations in the Olfactory Bulb: Modulation by Wakefulness and Experience. *Neuron* 76, 962-975.

Kato, H.K., Gillet, S.N., Peters, A.J., Isaacson, J.S., and Komiyama, T. (2013). Parvalbumin-expressing interneurons linearly control olfactory bulb output. *Neuron* 80, 1218-1231.

Kauer, J.S. (1991). Contributions of topography and parallel processing to odor coding in the vertebrate olfactory pathway. *Trends Neurosci* 14, 79-85.

Keller, A., Yagodin, S., Aroniadou-Anderjaska, V., Zimmer, L.A., Ennis, M., Sheppard, N.F., Jr., and Shipley, M.T. (1998). Functional organization of rat olfactory bulb glomeruli revealed by optical imaging. *J Neurosci* 18, 2602-2612.

Kikuta, S., Fletcher, M.L., Homma, R., Yamasoba, T., and Nagayama, S. (2013). Odorant response properties of individual neurons in an olfactory glomerular module. *Neuron* 77, 1122-1135.

Kikuta, S., Sato, K., Kashiwadani, H., Tsunoda, K., Yamasoba, T., and Mori, K. (2010). Neurons in the anterior olfactory nucleus pars externa detect right or left localization of odor sources. *Proceedings of the National Academy of Sciences* 107, 12363-12368.

Kim, T., Thankachan, S., McKenna, J.T., McNally, J.M., Yang, C., Choi, J.H., Chen, L., Kocsis, B., Deisseroth, K., Strecker, R.E., *et al.* (2015). Cortically projecting basal forebrain parvalbumin neurons regulate cortical gamma band oscillations. *Proceedings of the National Academy of Sciences* 112, 3535-3540.

Kirouac, G.J., and Ciriello, J. (1997). Cardiovascular responses to glutamate stimulation of diagonal band of Broca. *American Journal of Physiology-Heart and Circulatory Physiology* 273, H540-H545.

Kiss, J., Patel, A.J., Baimbridge, K.G., and Freund, T.F. (1990). Topographical localization of neurons containing parvalbumin and choline acetyltransferase in the medial septum-diagonal band region of the rat. *Neuroscience* 36, 61-72.

Kiyokage, E., Pan, Y.Z., Shao, Z., Kobayashi, K., Szabo, G., Yanagawa, Y., Obata, K., Okano, H., Toida, K., Puche, A.C., *et al.* (2010). Molecular identity of periglomerular and short axon cells. *J Neurosci* 30, 1185-1196.

Kosaka, K., Heizmann, C.W., and Kosaka, T. (1994). Calcium-binding protein parvalbumin-immunoreactive neurons in the rat olfactory bulb. 1. Distribution and structural features in adult rat. *Exp Brain Res* 99, 191-204.

Kosaka, T., Hataguchi, Y., Hama, K., Nagatsu, I., and Wu, J.Y. (1985). Coexistence of immunoreactivities for glutamate decarboxylase and tyrosine hydroxylase in some neurons in the periglomerular region of the rat main olfactory bulb: possible coexistence of gamma-aminobutyric acid (GABA) and dopamine. *Brain Res* 343, 166-171.

Kosaka, T., and Kosaka, K. (2008). Heterogeneity of parvalbumin-containing neurons in the mouse main olfactory bulb, with special reference to short-axon cells and betaIV-spectrin positive dendritic segments. *Neurosci Res* 60, 56-72.

- Kosaka, T., and Kosaka, K. (2010). Heterogeneity of calbindin-containing neurons in the mouse main olfactory bulb: I. General description. *Neurosci Res* 67, 275-292.
- Le Jeune, H., Aubert, I., Jourdan, F., and Quirion, R. (1995). Comparative laminar distribution of various autoradiographic cholinergic markers in adult rat main olfactory bulb. *J Chem Neuroanat* 9, 99-112.
- Le Jeune, H., Aubert, I., Jourdan, F., and Quirion, R. (1996). Developmental profiles of various cholinergic markers in the rat main olfactory bulb using quantitative autoradiography. *J Comp Neurol* 373, 433-450.
- Lee, M.G., Hassani, O.K., Alonso, A., and Jones, B.E. (2005). Cholinergic Basal Forebrain Neurons Burst with Theta during Waking and Paradoxical Sleep. *The Journal of Neuroscience* 25, 4365-4369.
- Lein, E.S., Hawrylycz, M.J., Ao, N., Ayres, M., Bensinger, A., Bernard, A., Boe, A.F., Boguski, M.S., Brockway, K.S., Byrnes, E.J., *et al.* (2007). Genome-wide atlas of gene expression in the adult mouse brain. *Nature* 445, 168-176.
- Lepousez, G., Csaba, Z., Bernard, V., Loudes, C., Videau, C., Lacombe, J., Epelbaum, J., and Viollet, C. (2010). Somatostatin interneurons delineate the inner part of the external plexiform layer in the mouse main olfactory bulb. *Journal of Comparative Neurology* 518, 1976-1994.
- Leveteau, J., and MacLeod, P. (1966). Olfactory discrimination in the rabbit olfactory glomerulus. *Science* 153, 175-176.
- Li, A., Rao, X., Zhou, Y., and Restrepo, D. (2019). Complex neural representation of odour information in the olfactory bulb. *Acta Physiol (Oxf)* 228, e13333.
- Linster, C., and Hasselmo, M.E. (2000). Neural activity in the horizontal limb of the diagonal band of Broca can be modulated by electrical stimulation of the olfactory bulb and cortex in rats. *Neurosci Lett* 282, 157-160.
- Linster, C., Wyble, B.P., and Hasselmo, M.E. (1999). Electrical Stimulation of the Horizontal Limb of the Diagonal Band of Broca Modulates Population EPSPs in Piriform Cortex. *Journal of Neurophysiology* 81, 2737-2742.
- Liu, S., Aungst, J.L., Puche, A.C., and Shipley, M.T. (2012). Serotonin modulates the population activity profile of olfactory bulb external tufted cells. *Journal of Neurophysiology* 107, 473-483.
- Liu, S., Plachez, C., Shao, Z., Puche, A., and Shipley, M.T. (2013). Olfactory bulb short axon cell release of GABA and dopamine produces a temporally

biphasic inhibition-excitation response in external tufted cells. *J Neurosci* 33, 2916-2926.

Liu, S., Puche, A.C., and Shipley, M.T. (2016). The Interglomerular Circuit Potently Inhibits Olfactory Bulb Output Neurons by Both Direct and Indirect Pathways. *The Journal of Neuroscience* 36, 9604-9617.

Liu, S., Shao, Z., Puche, A., Wachowiak, M., Rothermel, M., and Shipley, M.T. (2015). Muscarinic Receptors Modulate Dendrodendritic Inhibitory Synapses to Sculpt Glomerular Output. *The Journal of Neuroscience* 35, 5680-5692.

Lucas, B., and Kanade, T. (1981). An Iterative Image Registration Technique with an Application to Stereo Vision (IJCAI), Vol 81.

Ma, M., and Luo, M. (2012). Optogenetic Activation of Basal Forebrain Cholinergic Neurons Modulates Neuronal Excitability and Sensory Responses in the Main Olfactory Bulb. *The Journal of Neuroscience* 32, 10105-10116.

Macrides, F., Eichenbaum, H.B., and Forbes, W.B. (1982). Temporal relationship between sniffing and the limbic theta rhythm during odor discrimination reversal learning. *J Neurosci* 2, 1705-1717.

Mandairon, N., Ferretti, C.J., Stack, C.M., Rubin, D.B., Cleland, T.A., and Linstner, C. (2006). Cholinergic modulation in the olfactory bulb influences spontaneous olfactory discrimination in adult rats. *European Journal of Neuroscience* 24, 3234-3244.

Manella, L.C., Petersen, N., and Linstner, C. (2017). Stimulation of the Locus Ceruleus Modulates Signal-to-Noise Ratio in the Olfactory Bulb. *The Journal of Neuroscience* 37, 11605-11615.

Manns, I.D., Mainville, L., and Jones, B.E. (2001). Evidence for glutamate, in addition to acetylcholine and GABA, neurotransmitter synthesis in basal forebrain neurons projecting to the entorhinal cortex. *Neuroscience* 107, 249-263.

Markopoulos, F., Rokni, D., Gire, D.H., and Murthy, V.N. (2012). Functional properties of cortical feedback projections to the olfactory bulb. *Neuron* 76, 1175-1188.

Matsutani, S. (2010). Trajectory and terminal distribution of single centrifugal axons from olfactory cortical areas in the rat olfactory bulb. *Neuroscience* 169, 436-448.

McLean, J.H., Shipley, M.T., Nickell, W.T., Aston-Jones, G., and Reyher, C.K.H. (1989). Chemoanatomical organization of the noradrenergic input from

locus coeruleus to the olfactory bulb of the adult rat. *Journal of Comparative Neurology* 285, 339-349.

MohedanoMorian, A., de la Rosa-Prieto, C., Saiz-Sanchez, D., Ubeda-Banon, I., Pro-Sistiaga, P., de Moya-Pinilla, M., and Martinez-Marcos, A. (2012). Centrifugal telencephalic afferent connections to the main and accessory olfactory bulbs. *Frontiers in Neuroanatomy* 6.

Mombaerts, P., Wang, F., Dulac, C., Chao, S.K., Nemes, A., Mendelsohn, M., Edmondson, J., and Axel, R. (1996). Visualizing an olfactory sensory map. *Cell* 87, 675-686.

Mori, K., Kishi, K., and Ojima, H. (1983). Distribution of dendrites of mitral, displaced mitral, tufted, and granule cells in the rabbit olfactory bulb. *Journal of Comparative Neurology* 219, 339-355.

Nagayama, S., Enerva, A., Fletcher, M.L., Masurkar, A.V., Igarashi, K.M., Mori, K., and Chen, W.R. (2010). Differential axonal projection of mitral and tufted cells in the mouse main olfactory system. *Front Neural Circuits* 4.

Najac, M., De Saint Jan, D., Reguero, L., Grandes, P., and Charpak, S. (2011). Monosynaptic and polysynaptic feed-forward inputs to mitral cells from olfactory sensory neurons. *J Neurosci* 31, 8722-8729.

Nakai, J., Ohkura, M., and Imoto, K. (2001). A high signal-to-noise Ca²⁺ probe composed of a single green fluorescent protein. *Nature Biotechnology* 19, 137-141.

Nickell, W.T., Behbehani, M.M., and Shipley, M.T. (1994). Evidence for GABAB-mediated inhibition of transmission from the olfactory nerve to mitral cells in the rat olfactory bulb. *Brain Res Bull* 35, 119-123.

Niedworok, C.J., Schwarz, I., Ledderose, J., Giese, G., Conzelmann, K.K., and Schwarz, M.K. (2012). Charting monosynaptic connectivity maps by two-color light-sheet fluorescence microscopy. *Cell Rep* 2, 1375-1386.

Nunez-Parra, A., Maurer, R.K., Krahe, K., Smith, R.S., and Araneda, R.C. (2013). Disruption of centrifugal inhibition to olfactory bulb granule cells impairs olfactory discrimination. *Proc Natl Acad Sci U S A* 110, 14777-14782.

Ogg, M.C., Ross, J.M., Bendahmane, M., and Fletcher, M.L. (2018). Olfactory bulb acetylcholine release dishabituates odor responses and reinstates odor investigation. *Nature Communications* 9, 1868.

Orona, E., Rainer, E.C., and Scott, J.W. (1984). Dendritic and axonal organization of mitral and tufted cells in the rat olfactory bulb. *Journal of Comparative Neurology* 226, 346-356.

- Oswald, A.M., and Urban, N.N. (2012). There and back again: the corticobulbar loop. *Neuron* 76, 1045-1047.
- Otazu, G.H., Chae, H., Davis, M.B., and Albeanu, D.F. (2015). Cortical Feedback Decorrelates Olfactory Bulb Output in Awake Mice. *Neuron* 86, 1461-1477.
- Pandipati, S., Gire, D.H., and Schoppa, N.E. (2010). Adrenergic Receptor-Mediated Disinhibition of Mitral Cells Triggers Long-Term Enhancement of Synchronized Oscillations in the Olfactory Bulb. *Journal of Neurophysiology* 104, 665-674.
- Panula, P., Revuelta, A.V., Cheney, D.L., Wu, J.-Y., and Costa, E. (1984). An immunohistochemical study on the location of GABAergic neurons in rat septum. *Journal of Comparative Neurology* 222, 69-80.
- Parrish-Aungst, S., Shipley, M.T., Erdelyi, F., Szabo, G., and Puche, A.C. (2007). Quantitative analysis of neuronal diversity in the mouse olfactory bulb. *J Comp Neurol* 501, 825-836.
- Petzold, G.C., Hagiwara, A., and Murthy, V.N. (2009). Serotonergic modulation of odor input to the mammalian olfactory bulb. *Nature Neuroscience* 12, 784-791.
- Peyron, C., Tighe, D.K., van den Pol, A.N., de Lecea, L., Heller, H.C., Sutcliffe, J.G., and Kilduff, T.S. (1998). Neurons containing hypocretin (orexin) project to multiple neuronal systems. *J Neurosci* 18, 9996-10015.
- Pignatelli, A., and Belluzzi, O. (2008). Cholinergic Modulation of Dopaminergic Neurons in the Mouse Olfactory Bulb. *Chemical Senses* 33, 331-338.
- Pinching, A.J., and Powell, T.P. (1971a). The neuron types of the glomerular layer of the olfactory bulb. *J Cell Sci* 9, 305-345.
- Pinching, A.J., and Powell, T.P. (1971b). The neuropil of the periglomerular region of the olfactory bulb. *J Cell Sci* 9, 379-409.
- Pressler, R.T., Inoue, T., and Strowbridge, B.W. (2007). Muscarinic Receptor Activation Modulates Granule Cell Excitability and Potentiates Inhibition onto Mitral Cells in the Rat Olfactory Bulb. *The Journal of Neuroscience* 27, 10969-10981.
- Price, J.L., and Powell, T.P. (1970a). The afferent connexions of the nucleus of the horizontal limb of the diagonal band. *J Anat* 107, 239-256.

Price, J.L., and Powell, T.P. (1970b). An Electron-Microscopic Study of the Termination of the Afferent Fibres to the Olfactory Bulb from the Cerebral Hemisphere. *Journal of Cell Science* 7, 157-187.

Price, J.L., and Powell, T.P. (1970c). An experimental study of the origin and the course of the centrifugal fibres to the olfactory bulb in the rat. *J Anat* 107, 215-237.

Price, J.L., and Powell, T.P. (1970d). The morphology of the granule cells of the olfactory bulb. *J Cell Sci* 7, 91-123.

Price, J.L., and Powell, T.P. (1970e). The synaptology of the granule cells of the olfactory bulb. *J Cell Sci* 7, 125-155.

Rall, W., Shepherd, G.M., Reese, T.S., and Brightman, M.W. (1966). Dendrodendritic synaptic pathway for inhibition in the olfactory bulb. *Exp Neurol* 14, 44-56.

Ribak, C.E., Vaughn, J.E., Saito, K., Barber, R., and Roberts, E. (1977). Glutamate decarboxylase localization in neurons of the olfactory bulb. *Brain Res* 126, 1-18.

Roland, B., Deneux, T., Franks, K.M., Bathellier, B., and Fleischmann, A. (2017). Odor identity coding by distributed ensembles of neurons in the mouse olfactory cortex. *Elife* 6.

Rosin, J.-F., Datiche, F., and Cattarelli, M. (1999). Modulation of the piriform cortex activity by the basal forebrain: an optical recording study in the rat. *Brain Research* 820, 105-111.

Rothermel, M., Carey, R.M., Puche, A., Shipley, M.T., and Wachowiak, M. (2014). Cholinergic Inputs from Basal Forebrain Add an Excitatory Bias to Odor Coding in the Olfactory Bulb. *The Journal of Neuroscience* 34, 4654-4664.

Rubin, B.D., and Katz, L.C. (1999). Optical imaging of odorant representations in the mammalian olfactory bulb. *Neuron* 23, 499-511.

Sanz Diez, A., Najac, M., and De Saint Jan, D. (2019). Basal forebrain GABAergic innervation of olfactory bulb periglomerular interneurons. *J Physiol* 597, 2547-2563.

Schneider, S.P., and Macrides, F. (1978). Laminar distributions of interneurons in the main olfactory bulb of the adult hamster. *Brain Res Bull* 3, 73-82.

Schoenfeld, T.A., Marchand, J.E., and Macrides, F. (1985). Topographic organization of tufted cell axonal projections in the hamster main olfactory bulb: an intrabulbar associational system. *J Comp Neurol* 235, 503-518.

Schoppa, N.E. (2006). Synchronization of Olfactory Bulb Mitral Cells by Precisely Timed Inhibitory Inputs. *Neuron* 49, 271-283.

Schoppa, N.E., Kinzie, J.M., Sahara, Y., Segerson, T.P., and Westbrook, G.L. (1998). Dendrodendritic Inhibition in the Olfactory Bulb Is Driven by NMDA Receptors. *The Journal of Neuroscience* 18, 6790-6802.

Schoppa, N.E., and Westbrook, G.L. (2002). AMPA autoreceptors drive correlated spiking in olfactory bulb glomeruli. *Nature Neuroscience* 5, 1194-1202.

Schwarz, I., Müller, M., Pavlova, I., Schweihoff, J., Musacchio, F., Mittag, M., Fuhrmann, M., and Schwarz, M.K. (2020). The diagonal band of broca continually regulates olfactory-mediated behaviors by modulating odor-evoked responses within the olfactory bulb. *bioRxiv*, 2020.2011.2007.372649.

Shiple, M.T., and Adamek, G.D. (1984). The connections of the mouse olfactory bulb: a study using orthograde and retrograde transport of wheat germ agglutinin conjugated to horseradish peroxidase. *Brain Res Bull* 12, 669-688.

Smith, R.S., Hu, R., DeSouza, A., Eberly, C.L., Krahe, K., Chan, W., and Araneda, R.C. (2015). Differential Muscarinic Modulation in the Olfactory Bulb. *J Neurosci* 35, 10773-10785.

Soucy, E.R., Albeanu, D.F., Fantana, A.L., Murthy, V.N., and Meister, M. (2009). Precision and diversity in an odor map on the olfactory bulb. *Nat Neurosci* 12, 210-220.

Svoboda, K., Denk, W., Kleinfeld, D., and Tank, D.W. (1997). In vivo dendritic calcium dynamics in neocortical pyramidal neurons. *Nature* 385, 161-165.

Sweeney, S.T., Broadie, K., Keane, J., Niemann, H., and O'Kane, C.J. (1995). Targeted expression of tetanus toxin light chain in *Drosophila* specifically eliminates synaptic transmission and causes behavioral defects. *Neuron* 14, 341-351.

Toida, K., Kosaka, K., Heizmann, C.W., and Kosaka, T. (1994). Synaptic contacts between mitral/tufted cells and GABAergic neurons containing calcium-binding protein parvalbumin in the rat olfactory bulb, with special reference to reciprocal synapses between them. *Brain Res* 650, 347-352.

Wachowiak, M., and Cohen, L.B. (2001). Representation of odorants by receptor neuron input to the mouse olfactory bulb. *Neuron* 32, 723-735.

Wachowiak, M., Denk, W., and Friedrich, R.W. (2004). Functional organization of sensory input to the olfactory bulb glomerulus analyzed by two-photon calcium imaging. *Proc Natl Acad Sci U S A* 101, 9097-9102.

Wachowiak, M., Economo, M.N., Díaz-Quesada, M., Brunert, D., Wesson, D.W., White, J.A., and Rothermel, M. (2013). Optical dissection of odor information processing in vivo using GCaMPs expressed in specified cell types of the olfactory bulb. *The Journal of neuroscience : the official journal of the Society for Neuroscience* 33, 5285-5300.

Wen, P., Rao, X., Xu, L., Zhang, Z., Jia, F., He, X., and Xu, F. (2019). Cortical Organization of Centrifugal Afferents to the Olfactory Bulb: Mono- and Trans-synaptic Tracing with Recombinant Neurotropic Viral Tracers. *Neuroscience Bulletin* 35, 709-723.

Xu, M., Chung, S., Zhang, S., Zhong, P., Ma, C., Chang, W.-C., Weissbourd, B., Sakai, N., Luo, L., Nishino, S., *et al.* (2015). Basal forebrain circuit for sleep-wake control. *Nature Neuroscience* 18, 1641-1647.

Yang, C., McKenna, J.T., and Brown, R.E. (2017). Intrinsic membrane properties and cholinergic modulation of mouse basal forebrain glutamatergic neurons in vitro. *Neuroscience* 352, 249-261.

Yang, C., McKenna, J.T., Zant, J.C., Winston, S., Basheer, R., and Brown, R.E. (2014). Cholinergic Neurons Excite Cortically Projecting Basal Forebrain GABAergic Neurons. *The Journal of Neuroscience* 34, 2832-2844.

Yuste, R., and Denk, W. (1995). Dendritic spines as basic functional units of neuronal integration. *Nature* 375, 682-684.

Záborszky, L., Carlsen, J., Brashear, H.R., and Heimer, L. (1986). Cholinergic and GABAergic afferents to the olfactory bulb in the rat with special emphasis on the projection neurons in the nucleus of the horizontal limb of the diagonal band. *Journal of Comparative Neurology* 243, 488-509.

Zhou, F.W., Dong, H.W., and Ennis, M. (2016). Activation of beta-noradrenergic receptors enhances rhythmic bursting in mouse olfactory bulb external tufted cells. *J Neurophysiol* 116, 2604-2614.

Zimmer, L.A., Ennis, M., and Shipley, M.T. (1999). Diagonal band stimulation increases piriform cortex neuronal excitability in vivo. *Neuroreport* 10, 2101-2105.

CONFERENCE PRESENTATIONS

Müller M.*, Schwarz I.*, Pavlova I.*, Mittag M., Musacchio F., Fuhrmann M.* & Schwarz M.K.*. Odor-driven modulation of olfactory perception by basal forebrain nuclei. Bonn Brain³ Abstracts. Presentation delivered at the Bonn Brain³ meeting, Bonn, Germany, March 2019.

Müller M.*, Schwarz I.*, Pavlova I.*, Mittag M., Musacchio F., Fuhrmann M.* & Schwarz M.K.*. Odor-driven modulation of olfactory perception by basal forebrain nuclei. Bonn Brain³ Abstracts. Presentation delivered at the 13th Göttingen Meeting of the German Neuroscience Society, Göttingen, Germany, March 2019.

Müller M.*, Schwarz I.*, Pavlova I.*, Mittag M., Fuhrmann M.* & Schwarz M.K.*. Functional characterization of odor-driven modulation of olfactory perception by basal forebrain nuclei. Society for Neuroscience Abstracts. Poster presentation delivered at the Society for Neuroscience meeting, San Diego, USA, November 2018.

Müller M.*, Schwarz I.*, Pavlova I.*, Mittag M., Fuhrmann M.* & Schwarz M.K.*. Functional characterization of odor-driven modulation of olfactory perception by basal forebrain nuclei. Federation of European Neuroscience Society Abstracts. Poster Presentation delivered at the Federation of European Neuroscience Society meeting, Berlin, Germany, July 2018.

Müller M.*, Schwarz I.*, Pavlova I.*, Mittag M., Fuhrmann M.* & Schwarz M.K.*. Odor-driven modulation of olfactory perception by basal forebrain nuclei. Bonn Brain³ Abstracts. Presentation delivered at the Bonn Brain³ meeting, Bonn, Germany, March 2018.

Müller M.*, Schwarz I.*, Fuhrmann M.* & Schwarz M.K.*. Odor-driven modulation of olfactory perception by basal forebrain nuclei. Society for Neuroscience Abstracts. Poster presentation delivered at the Society for Neuroscience meeting, Washington, DC., USA, November 2017.

Müller M.*, Schwarz I.*, Fuhrmann M.* & Schwarz M.K.*. Odor-driven modulation of olfactory perception by basal forebrain nuclei. Bonn Brain³ Abstracts. Presentation delivered at the Bonn Brain³ meeting, Bonn, Germany, March 2017.

Müller M., Tavosanis G.*, Fuhrmann M.*. A genetic screen to identify novel molecular pathways involved in early dendritic spine loss in Alzheimer's Disease: a cross species approach in Drosophila and mice. Federation of European Neuroscience Society Abstracts. Poster Presentation delivered at the Federation of European Neuroscience Society meeting, Copenhagen, Denmark, July 2016.

*first and last authors contributed equally

PREPRINT PUBLICATIONS

Schwarz, I.*, **Müller, M.***, Pavlova, I., Schweihoff, J., Musacchio, F., Mittag, M., Fuhrmann, M.*, and Schwarz, M.K.* (2020). The diagonal band of broca continually regulates olfactory-mediated behaviors by modulating odor-evoked responses within the olfactory bulb. bioRxiv, doi: <https://doi.org/10.1101/2020.11.07.372649>.

*first and last authors contributed equally